SLOVAK UNIVERSITY OF TECHNOLOGY
IN BRATISLAVA

FACULTY OF CHEMICAL AND FOOD TECHNOLOGY

Reg. No.: FCHPT-12838-76098

Predictive Control and Economic Optimization for Energy Management Systems

DISSERTATION THESIS

2026

Ing. Tereza Ábelová

**SLOVAK UNIVERSITY OF TECHNOLOGY
IN BRATISLAVA**

FACULTY OF CHEMICAL AND FOOD TECHNOLOGY

Reg. No.: FCHPT-12838-76098

Predictive Control and Economic Optimization for Energy Management Systems

DISSERTATION THESIS

Study programme:	Process Control
Study field:	Cybernetics
Training workspace:	Institute of Information Engineering, Automation, and Mathematics
Thesis supervisor:	prof. Ing. Michal Kvasnica, PhD.

2026

Ing. Tereza Ábelová

Slovak University of Technology in Bratislava
Department of Information Engineering and Process Control

Faculty of Chemical and Food Technology
Academic year: 2025/2026
Reg. No.: FCHPT-12838-76098

DISSERTATION THESIS TOPIC

Student:	**Ing. Tereza Ábelová**
Student's ID:	76098
Study programme:	Process Control
Study field:	Cybernetics
Thesis supervisor:	prof. Ing. Michal Kvasnica, PhD.
Head of department:	prof. Ing. Miroslav Fikar, DrSc.

Topic: **Predictive Control and Economic Optimization for Energy Management Systems**

Language of thesis: English

Specification of Assignment:

Model predictive control has emerged as the dominant methodology for energy management in microgrids, owing to its ability to incorporate system constraints, forecasts, and economic objectives within a unified receding-horizon framework. Deterministic formulations handle forecast uncertainty implicitly through repeated re-optimisation, offering no formal guarantees under distributional deviations. Stochastic formulations address uncertainty explicitly but incur computational costs that render them intractable at the timescales required by operational control. Beyond the scheduling layer, a complete energy management system must also coordinate storage units in real time and support investment decisions prior to deployment. These adjacent tasks are typically addressed by independent, layer-specific tools with no guarantee of mutual consistency. The result is a gap between theoretically sound MPC formulations and systems that function reliably across all operational layers. The goal of this dissertation is to bridge this gap by developing predictive and optimisation-based control methods that are simultaneously grounded in rigorous optimisation theory and applicable across the full hierarchy of an energy management systemm, from real-time power coordination among storage units, through predictive scheduling under uncertainty, to long-term investment planning, such that the models, assumptions, and objectives at each layer are compatible with one another.

Deadline for submission of Dissertation thesis:	31. 05. 2026
Approval of assignment of Dissertation thesis:	30. 05. 2026
Assignment of Dissertation thesis approved by:	prof. Ing. Miroslav Fikar, DrSc. – Chairperson of Field of Study Board

Acknowledgment

First and foremost, I would like to express my gratitude to my supervisor, Prof. Michal Kvasnica, for his invaluable guidance and continuous support throughout my doctoral journey. I am especially thankful for his motivation that initially led me to pursue this degree and for the encouragement he has offered not only in my studies, but also in my work and life. His expertise, high standards, and thoughtful mentorship have shaped my professional path and have given me the courage and inspiration to follow my goals with confidence.

My heartfelt thanks go to my colleagues and teammates, with whom I had the pleasure of collaborating. Working together made even the most challenging moments enjoyable, and I truly appreciate the shared efforts, ideas, and the supportive environment we created. I sincerely hope our paths will cross again in the future.

I am also grateful for the unique opportunity to be involved in both academic research and industry practice. The privilege to work with real systems and translate theoretical developments into operational solutions has greatly enriched this thesis and provided insights that could only be gained through hands-on experience.

Lastly, and most importantly, I owe special thanks to my family for their unconditional support. Their encouragement, patience, and belief in me have been a constant source of strength throughout this journey—without them, none of this would have been possible.

Abstract

This thesis addresses the design, implementation, and real-world deployment of an energy management system (EMS) for microgrids that integrates model predictive control (MPC), power distribution, and component sizing into a unified, hierarchical architecture. Microgrids, composed of renewable sources, controllable and uncontrollable loads, and battery energy storage systems (BESS), are emerging as key components of a decentralized, resilient, and economically viable energy future. However, their efficient and reliable operation requires advanced control strategies capable of handling uncertainties, diverse configurations, and conflicting objectives. This work proposes a scalable EMS framework structured in four layers—from strategic business planning to real-time execution—and introduces the Energy Management-as-a-Service concept, where EMS is delivered to clients as a service. At the core of the energy management layer lies a two-stage risk-aware MPC approach that balances performance and robustness under uncertainty. In the power layer, a real-time quadratic optimization algorithm ensures distribution of power reference signal sent from the upper layer among aggregated heterogeneous battery units, accounting for their individual limits, state imbalances, and thermal behavior. At the planning level, a long-horizon economic optimization model is developed for optimal sizing of BESS, maximizing the net present value over the project lifetime. All proposed methods are validated in real-world microgrid projects, confirming their practical applicability, computational tractability, and measurable economic benefits. In a commercial deployment, the MPC delivered an annual profit of 159 €/kW of installed battery power, above published benchmarks, while the real-time power-distribution algorithm scales to 100 battery units in under 30 ms. The thesis combines principles from process control, mathematical optimization, and energy systems engineering, while reflecting real business needs through direct collaboration with the industry.

Abstrakt

Táto dizertačná práca sa zaoberá návrhom, implementáciou a reálnym nasadením systému energetického manažmentu pre mikrosieť, ktorý integruje prediktívne riadenie, distribúciu výkonu a dimenzovanie komponentov do jednotnej hierarchickej architektúry. Mikrosiete, zložené z obnoviteľných zdrojov, riaditeľných a neriaditeľných záťaží a batériových úložísk, predstavujú kľúčový prvok decentralizovanej, stabilnej a ekonomicky udržateľnej energetickej budúcnosti. Ich efektívna a spoľahlivá prevádzka si však vyžaduje pokročilé riadiace stratégie schopné reagovať na neurčitosti, rôznorodé konfigurácie a protichodné ciele. Práca navrhuje škálovateľný systém riadiaceho energetického manažmentu rozdelený do štyroch vrstiev – od strategického plánovania po vykonávanie v reálnom čase – a zavádza koncept "Energy Management-as-a-Service", v ktorom je energetický manažment poskytovaný zákazníkom ako služba. Jadro energetického manažmentu tvorí dvojstupňové prediktívne riadenie so zohľadnením rizika, ktoré vyvažuje výkonnosť a robustnosť voči neistotám. V rámci výkonovej vrstvy zabezpečuje kvadratický optimalizačný algoritmus distribúciu výkonovej referencie z vyššej vrstvy medzi skupinu heterogénnych batériových jednotiek, pričom rešpektuje ich individuálne obmedzenia, nevyváženosť stavov nabitia a tepelnú dynamiku. Na úrovni plánovania je vyvinutý optimalizačný model s dlhým horizontom, ktorý slúži na určenie optimálnej veľkosti batériového úložiska s cieľom maximalizovať čistú súčasnú hodnotu počas životnosti projektu. Navrhované metódy boli nasadené v reálnej prevádzke, čo potvrdzuje ich praktickú použiteľnosť, výpočtovú efektivitu a ekonomické prínosy. V komerčnom nasadení prediktívne riadenie dosiahlo ročný zisk 159 €/kW inštalovaného výkonu batérie, prevyšujúc hodnoty uvádzané v literatúre, pričom algoritmus distribúcie výkonu v reálnom čase škáluje až na 100 jednotiek pod 30 ms. Práca kombinuje poznatky z oblasti procesného riadenia, matematickej optimalizácie a energetických systémov a zároveň reflektuje reálne požiadavky trhu vďaka úzkej spolupráci s priemyslom.

Contents

Chapter 1

Introduction

In recent years, the energy sector has been undergoing a profound transformation driven by rising environmental concerns, the rapid expansion of renewable energy sources, and the decentralization of energy generation. This transition has led to the emergence of microgrids—localized, self-managed energy systems. Microgrids integrate components such as renewable energy sources, controllable and non-controllable loads, and energy storage technologies. Their main objectives include improving reliability and resilience, optimizing energy usage, and achieving economically and environmentally sustainable operation.

Among the core components that enable the flexibility of microgrids are battery energy storage systems (BESS). Batteries not only enhance system stability and resilience, but also provide services such as peak shaving, electricity market arbitrage, and ancillary services, thereby improving economic performance and increasing the overall attractiveness of microgrids. Accordingly, significant attention is devoted to battery systems in this thesis. Managing these complex systems—characterized by variable generation, multiple control objectives, economic constraints, and operational limitations—requires intelligent and adaptive coordination mechanisms. This is where energy management systems (EMS) play a central role.

An EMS acts as the brain of the microgrid, integrating data, forecasts, models, and optimization routines to support informed decision-making in real time or over longer planning horizons. The successful deployment of an EMS largely determines whether a microgrid can meet its intended goals in a reliable and cost-effective manner. However, the design and implementation of such systems remain challenging. Key difficulties include the unpredictability of renewable resources, the complex dynamics and constraints of energy storage devices, the coordination of multiple system components, and the alignment of operational decisions with both technical and economic objectives.

This thesis focuses on the development, implementation, and real-world deployment of a comprehensive energy management system tailored for microgrids with battery storage and renewable energy sources. The work combines methods from process control and mathematical optimization with domain-specific knowledge of power and energy systems. While many academic contributions in process control remain at the simulation or laboratory level, this thesis emphasizes real-world applicability. The proposed EMS has not only been designed but also deployed and validated in operational microgrids. As concrete benchmarks of field readiness, the power-distribution algorithm scales to 100 battery units in under 30 ms, well within the latency required for real-time deployment, while the risk-aware MPC achieved an annual profit of 159 €/kW of installed battery power in a commercial deployment, above published benchmarks.

Among the various EMS methodologies, model predictive control (MPC) stands out due to its ability to optimize system performance over a receding horizon, explicitly account for future system behavior, and directly incorporate physical constraints and economic objectives into the decision-making process. Consequently, a substantial portion of this work is devoted to both the theoretical and practical aspects of MPC, with particular emphasis on microgrid applications.

What distinguishes this work from conventional research is its strong application-oriented focus. The primary motivation has been to design solutions that can be directly deployed in practice and deliver measurable value. The EMS described in this thesis underwent a full development lifecycle, starting from a single pilot installation and evolving into a solution managing multiple microgrid sites across several countries. Throughout this process, the EMS framework adapted to changing environmental, technical, and economic conditions.

Another distinguishing aspect of the thesis is its business-aware perspective. Here, the EMS is not viewed solely as a control algorithm, but as a service—Energy Management-as-a-Service (EMaaS)—delivered by a provider (i.e., the researcher, designer, or company behind the EMS) to microgrid owners or operators. This perspective introduces additional requirements, including scalability, cost-efficiency, and configurability of the energy management system.

Through close collaboration with industry partners, the methods developed in this work reflect real operational needs and constraints faced by commercial and industrial actors. Rather than proposing generic solutions, the algorithms and frameworks presented here were shaped by direct feedback from system owners, operators, and customers. Each deployment introduced specific requirements—whether related to functional objectives, economic goals, regulatory context, or technological constraints—which were systematically incorporated into the design and implementation process.

1.1 Problem Statement

The problem addressed in this thesis can be stated as follows: Given a microgrid composed of one or more battery energy storage systems, renewable energy sources—predominantly photovoltaic generation—and controllable and non-controllable loads, operating either in grid-connected or islanded mode and participating in electricity markets under contractual and regulatory obligations, design an energy management system that determines the operation of the controllable assets such that the microgrid is operated reliably, economically, and at scale. This problem can be characterized more precisely through the following four aspects.

Inputs. The EMS receives:

- forecasts of renewable generation and demand over horizons from minutes to days, together with electricity market prices;
- real-time measurements of power flows, state of charge, and component temperatures;
- microgrid parameters such as installed capacities and conversion efficiencies;
- external conditions, including market structure (day-ahead, balancing), contractual obligations toward customers, and regulatory requirements imposed on the system operator.

Outputs. The EMS produces:

- optimal energy schedules over the prediction horizon for groups of assets (battery storage, renewable sources, controllable loads);
- real-time power setpoints for individual devices within each asset group.

Constraints. The decisions are subject to:

- physical limits of the components—inverter capacities, ramp rates, charging and discharging power, state-of-charge bounds, and thermal limits;
- dynamic battery behavior, including round-trip efficiency and degradation;
- market and regulatory constraints, such as contracted positions and imbalance pricing;

- forecast uncertainty arising from the variability of renewable generation and demand;
- real-time computability of the control algorithms within the required sampling intervals.

Success criteria. The proposed EMS is considered successful when it delivers:

- measurable economic benefits over the system's lifetime (cost reduction, revenue from market participation, attractive payback time and internal rate of return);
- robust performance under forecast uncertainty through risk-aware decision-making, with a tunable level of risk aversion;
- equitable utilization of heterogeneous battery units, respecting individual limits and supporting longevity by balancing state of charge and limiting thermal stress;
- real-time feasibility on hardware available in commercial microgrid deployments;
- scalability to a portfolio of microgrid sites under the Energy Management-as-a-Service model.

1.2 Research Gap

Although energy management for microgrids has received substantial attention in the literature, existing approaches fail to address jointly the identified requirements. Detailed reviews are given in Sections 3.3, 3.4, and 3.5; their findings can be summarized as follows:

- **Uncertainty handling vs. real-time deployment.** Deterministic MPC formulations [1, 2, 3] are computationally efficient but cannot guarantee constraint satisfaction under forecast uncertainty; stochastic and scenario-based extensions [4, 5, 6] handle uncertainty but become computationally infeasible for real-time deployment with high-fidelity models. Existing risk-aware MPC approaches [7, 8, 9] are limited to storage-only systems and do not consider full microgrid contexts with renewables and flexible loads.
- **Multi-unit power distribution.** Methods for distributing power among multiple battery units [10, 11, 12, 13] rarely account jointly for heterogeneous capacity, state of charge, power, and thermal limits, do not allow controlled energy exchange between units [14], and lack demonstrations of scalability or real-system validation [15].
- **Sizing-policy mismatch.** Battery sizing studies [16, 17, 18] typically use short evaluation horizons (a single representative day or up to one week), fix the energy-to-power ratio a priori, and do not transfer the resulting sizes to the actual control policy that will operate the storage.
- **Validation in real deployment.** Most contributions are evaluated in simulation or short-term laboratory experiments [6], leaving long-term operational performance and field-deployment feasibility uncertain.
- **Provider-side economics.** The cost structure of the EMS itself—the expense of delivering the control as a service—is rarely analyzed in the literature, with [19] a notable exception.

The research gap addressed by this thesis is the absence of a unified EMS framework that simultaneously handles forecast uncertainty in a risk-aware yet real-time-feasible manner, distributes power across heterogeneous battery units at commercial scale, sizes storage with a long-horizon evaluation reflecting the operating policy, and accounts for the provider-side economics. All are validated jointly on multi-month operational data from commercial microgrid sites.

1.3 Research Motivations and Contributions

The research presented in this thesis grew out of practical questions that recurred across multiple microgrid deployments: how an EMS should act when reality deviates from the forecast; how a single control framework can be reused across microgrids with very different configurations; how several battery units differing in capacity, state of charge, and temperature can be coordinated jointly; how battery storage can be sized economically before a project is built; how an algorithm proven in simulation can be transferred to the field under realistic constraints on computation; and how the value the EMS creates for the microgrid owner can be turned into sustainable revenue for the EMS provider. These concerns resist clean separation, and a useful EMS must address them jointly. They distil into three research questions, each answered by one contribution of this thesis:

1. **Risk-aware predictive control based on stochastic model predictive control.**

   Research question: How can a model predictive control scheme handle forecast uncertainty while remaining computationally tractable for real-time microgrid operation?

   Within the proposed hierarchical EMS architecture, a stochastic MPC is developed to optimize the daily operation of a microgrid using Conditional Value-at-Risk (CVaR), with:

   - A two-stage formulation: a simplified stochastic stage captures uncertainty; a deterministic stage with a high-fidelity model computes the actionable decisions.
   - Parametrizable control design supporting different microgrid components, objectives, constraints, and levels of risk aversion.
   - A provider-side perspective addressing the cost-efficiency of the EMS itself.
   - Deployment and validation in a commercial microgrid, demonstrating feasibility, profitability, and the practical value of risk-aware decisions.

2. **Real-time optimization-based algorithm for power distribution among heterogeneous battery units.**

   Research question: How can power be distributed in real time across heterogeneous battery units to jointly balance state of charge, individual operational limits, and thermal stress at the scale of commercial deployments?

   A coordination scheme for multiple battery energy storage systems is developed, with:

- A quadratic programming (QP) formulation that allocates power across units differing in capacity, state of charge (SoC), power limits, and thermal constraints, improving reliability and longevity.
- A richer feature set than existing approaches, including a tunable amount of mutual recharge.
- Scalability: solutions in under 30 ms for systems with up to 100 battery units.
- Validation in simulation and field deployments, including an industrial microgrid.

3. **Optimization-based methodology for economic component sizing.**

   Research question: How can the optimal size of a microgrid's battery storage be determined under a long-horizon evaluation that reflects its actual operating policy?

   A long-term planning tool for sizing key components based on economic indicators, with:

   - Integration of the predictive MPC core into the sizing loop based on net present cost (NPC) optimization, aligning investment decisions with operational behavior.
   - A real-world case study on an industrial microgrid in Slovakia, yielding 10.3% internal rate of return (IRR) and a 6.7-year payback time, robust to input variations.

1.4 Document Structure

This thesis is structured to guide the reader through the development of the energy management system, beginning in Chapter 2, which provides background on microgrids, their role in modern power systems, and their components, with special emphasis on renewable energy sources and battery energy storage systems. Section 2.3.2.2 is especially devoted to modeling battery storage systems.

Chapter 3 presents the design of a hierarchical control architecture, composed of four layers—business, management, power, and execution—and introduces the EMaaS model. The core of the EMS lies in predictive control, detailed in Section 3.3, which includes a two-stage risk-aware model predictive control algorithm combining deterministic (3.3.4) and stochastic (3.3.5) formulations. Section 3.4 introduces a quadratic programming approach for real-time power distribution among heterogeneous battery units. Section 3.5 develops a long-term optimization framework for optimal component sizing, focusing on battery capacity and inverter power to maximize economic performance over the system's lifetime.

Chapter 4 validates the proposed methods through three real-world case studies: deployment of the MPC-based EMS in a commercial microgrid (4.2), real-time control of aggregated battery units (4.3), and techno-economic sizing of battery storage systems (4.4).

1.5 Relation to Previously Published Work

This thesis is an original work that builds upon and extends the author's previously published peer-reviewed contributions, integrating them into a unified framework. The battery storage model in Section 2.3.2.2 was first introduced in [20]. The optimization-based power-distribution method in Section 3.4 was first proposed in [21]; the QP formulation and the hierarchical integration are developed in this thesis. The risk-aware stochastic MPC formulation of Section 3.3.5 was first presented in the conference paper [22] and extended in the journal paper [23], which also reports the four-layer hierarchical EMS architecture (Chapter 3), the commercial deployment results in Section 4.2, and the cloud-based EMaaS economic analysis. The component-sizing methodology in Section 3.5 and the corresponding case study in Section 4.4 are new contributions of this thesis.

Chapter 2

Microgrids

This chapter establishes the foundations of microgrid systems, upon which the control design developed in this thesis is built. An understanding of the basic principles facilitates reading of the subsequent chapters, as it provides the necessary context for the main drivers of microgrid operation. This background also enables us to identify opportunities and potential improvements in energy management. The chapter introduces the broader environment in which microgrids are set, their principles of operation, and the main components that play a significant role in the control design.

2.1 Overview

Microgrids are localized energy systems composed of distributed energy resources, controllable loads, and energy storage systems, capable of operating either in conjunction with or independently from the main power grid [24]. As a paradigm shift in modern power systems, microgrids enable decentralized control, improved energy resilience, and enhanced integration of renewable energy sources at the distribution level.

At their core, microgrids aim to optimize energy flows within a confined electrical boundary while maintaining reliability and stability. Microgrids have two modes of operation: grid-connected and islanded (standalone) mode [25]. In grid-connected mode, the microgrid interacts with the utility grid to import or export power depending on internal demand and generation conditions. In islanded mode, the microgrid operates autonomously, which requires careful balancing of supply and demand to maintain frequency and voltage within operational limits.

Microgrids incorporate various power generation sources, including renewable power plants, conventional generators, energy storage systems, and controllable loads. A defining feature of microgrids is the ability to manage this diverse set of resources and objectives through advanced control algorithms. Typical objectives include energy cost minimization, carbon emission reduction, or outages and interruption avoidance [26]. The presence of intelligent control systems is therefore essential for coordinating the operation of distributed energy resources, storage, and loads in real time in line with the long-term plan.

Economic drivers play a central role in microgrid operation. As part of the broader power network, microgrids participate in electricity markets and interact with energy retailers, transmission system operators, and balance service providers. Through intelligent control and scheduling, microgrids can unlock multiple value streams. These include time-shifting energy use to exploit price volatility (energy arbitrage), reducing peak demand charges (peak shaving), and maximizing self-consumption of on-site renewable generation [27].

2.2 Power Systems and Energy Markets

Microgrids are not isolated constructs; they are embedded within a broader electrical and economic ecosystem governed by power system architecture, operational stability requirements, and regulatory market frameworks. In liberalized electricity markets, system operators rely on the concept of balance responsibility to ensure that electricity supply and demand are matched in real time. Entities known as balance responsible parties (BRPs) are financially accountable for deviations from their forecasted positions [28]. This structure incentivizes accurate forecasting and the deployment of demand-response strategies.

Microgrids, depending on their configuration and market participation model, may either act as independent BRPs or be aggregated under larger entities. Participation as a BRP requires robust forecasting, scheduling, and real-time control, making advanced energy management systems essential. Furthermore, microgrids must account for intraday adjustments and real-time balancing actions to mitigate penalties arising from imbalances.

The operation and economic optimization of microgrids are strongly influenced by the structure and dynamics of energy markets. By engaging with different market layers, microgrids can not only manage their own consumption and generation but also contribute to system-level flexibility. The most relevant market mechanisms affecting microgrid economics are summarized below:

- **Day-Ahead Energy Market:** Energy prices are determined in a daily auction and reflect the expected balance between supply and demand [29]. Microgrids may participate as BRPs directly in the auction, paying market-clearing prices, or they may be charged dynamically priced energy costs by an energy supplier that procures electricity on the market on their behalf.
- **Imbalance Market:** Despite best forecasting efforts, actual consumption and generation may deviate from scheduled energy positions. These deviations are settled in the imbalance market, where BRPs are financially liable for discrepancies. Imbalance prices are usually higher and more volatile than day-ahead prices and are designed to incentivize accurate scheduling. Market entities may exploit the price gap to generate revenue [30]. For microgrids participating as BRPs, this creates a strong incentive to deploy real-time control strategies and short-term forecast corrections.
- **Capacity and Demand Charges:** In addition to energy prices, many electricity tariffs include capacity or demand charges that penalize high peak power demand, regardless of total energy consumption [31]. These charges are based on the maximum power draw (kW) during a billing period and can constitute a substantial portion of the energy bill, particularly for industrial and commercial users. Microgrids equipped with energy storage or controllable loads can implement peak shaving strategies to reduce or shift peak demand and avoid high charges.
- **Network Fees and Renewable Energy Incentives:** Microgrid operators are subject to network access fees and grid usage tariffs, which are usually regulated by national or regional authorities. Conversely, self-generation of energy from renewable sources can be rewarded with feed-in tariffs or various subsidy schemes and incentives.

2.3 Components

Microgrids can be broadly classified into three configurations—AC microgrids, DC microgrids, and hybrid AC/DC microgrids [25], depending on the nature of the main electrical bus and asset connections. AC microgrids are the most common in practice due to their compatibility with existing utility infrastructure, standardized equipment, and ease of interconnection with the main grid. Conversely, DC microgrids are emerging in specific applications, such as DC-coupled storage systems or electric vehicle charging stations, due to improved conversion efficiency and simplified integration of native DC devices [32].

This thesis focuses on AC microgrids. All assets are assumed to interface with a common AC bus, either directly (e.g., AC loads) or through DC–AC converter interfaces (e.g., photovoltaic systems and batteries). These power electronic converters serve as the control access points through which the energy management system dispatches energy, enabling real-time manipulation of power flows in accordance with given control signals.

The components of a general microgrid can be categorized into four primary groups. The schematic configuration is illustrated in Figure 2.1. The associated power variables are introduced below for use in later control problem formulations:

- **Energy Sources:** These include distributed generation units, primarily renewable energy sources such as photovoltaic (PV) arrays and wind turbines. Their available power output, denoted as P_{RES}, depends on weather and environmental conditions. However, the actual power injected into the microgrid may be curtailed to satisfy power balance or operational constraints. The controllable injected power is therefore expressed as $P_{\text{RES}} - P_{\text{curt}}$, where P_{curt} denotes the curtailment action.

- **Loads:** These represent the demand side of the microgrid. Two types are distinguished: controllable and non-controllable loads. The total load demand is denoted by P_{load}, with the controllable portion adjustable via the input variable P_{adj}, while the non-controllable portion is assumed to be rigid and must be supplied at all times.

- **Storages:** Energy storage units can absorb power when charging (P_{ch}) or supply power when discharging (P_{dch}), which makes them the most power-flexible assets within the microgrid. Unlike renewable energy sources, storage systems are characterized by their high flexibility and availability.

- **Utility Grid:** The point of interconnection with the external grid enables bidirectional power exchange. Power imported from the main grid is denoted by P_{imp}, while exported power is represented by P_{exp}. These flows are constrained by technical limits and contractual agreements.

Each group may consist of multiple units, which are treated either as an aggregated single entity or as separate units, depending on the level within the control hierarchy.

The operation of a microgrid is governed by the fundamental principle of energy conservation, which requires that, at every moment in time t, the total power supply equals the total power demand. This condition is enforced through the power balance

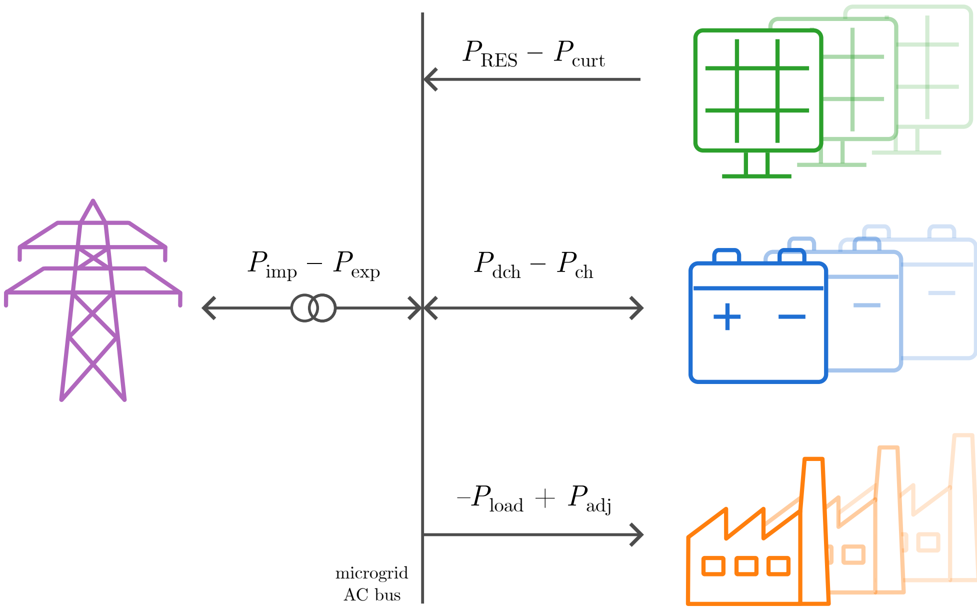

Figure 2.1: Schematic representation of a microgrid with its main components and power flow variables.

equation, which couples all internal power flows and the exchange with the external grid:

$$P_{\mathrm{imp}}(t) + P_{\mathrm{dch}}(t) + P_{\mathrm{RES}}(t) + P_{\mathrm{adj}}(t) = P_{\mathrm{exp}}(t) + P_{\mathrm{ch}}(t) + P_{\mathrm{load}}(t) + P_{\mathrm{curt}}(t) \quad (2.1)$$

Here, the left-hand side represents the total power available to the microgrid: imported power from the grid, battery discharging, renewable generation, and demand-side adjustments that reduce consumption (modeled as negative load). The right-hand side represents the total power consumed within the microgrid or exported: load demand, battery charging, curtailed renewable energy, and power exported to the main grid.

Notably, the actual renewable generation utilized is given by $P_{\mathrm{RES}}(t) - P_{\mathrm{curt}}(t)$, while the effective demand is $P_{\mathrm{load}}(t) - P_{\mathrm{adj}}(t)$. The adjustment term $P_{\mathrm{adj}}(t)$ reflects flexible demand control: a negative value indicates an increase in consumption (e.g., incentivized load shifting), while a positive value indicates demand reduction (e.g., demand response curtailment).

2.3.1 Renewable Energy Sources

Common renewable energy source (RES) technologies include photovoltaic systems, wind turbines, small hydropower plants, and biomass-based generation. These technologies are widely integrated into modern microgrids due to their environmental benefits and potential to reduce operational costs. While various forms of RES can be employed within a microgrid, this work focuses specifically on photovoltaic systems, as they are the most widely adopted and are directly relevant to the case studies considered. Due to their dependence on solar irradiance, PV systems exhibit intermittent and non-dispatchable power output, influenced by weather conditions, time of day, and seasonality. The energy management system must therefore address both real-time variability and solar power forecasting.

PV systems vary significantly in scale, ranging from small rooftop installations for residential use, typically a few kWp, to utility-scale solar farms exceeding hundreds of MWp. Residential and commercial installations are usually designed for self-consumption in order to reduce grid energy usage, with excess generation optionally fed into the distribution network and incentivized through support schemes. In contrast, utility-scale PV plants operate as large power producers contributing directly to the transmission network.

PV panels consist of interconnected semiconductor cells that convert sunlight into direct current through the photovoltaic effect, electrons excited by absorbed photons generate an electric current when the circuit is closed [33]. The DC output is converted to alternating current using DC–AC inverters to ensure grid compatibility. Monocrystalline silicon cells dominate the global market, accounting for approximately 80% of total PV deployment [34]. While conversion efficiencies in laboratory settings have reached 26.7%, with theoretical upper limits of ~33% for single-junction devices [35], typical commercial modules achieve lower efficiencies.

2.3.1.1 Parameters and Model

Basic unit for PV system capacity is specified in kilowatt-peak (kWp), the nominal power is measured under standardized test conditions with irradiance of $1000\,\mathrm{W/m^2}$, air mass of 1.5, and cell temperature of 25°C [33]. Inverters are rated in kilovolt-amperes (kVA). Real-world performance typically falls below nominal capacity due to thermal and atmospheric effects. As a result, the inverter capacity (here denoted with variable $\overline{P}_{\mathrm{PV}}$) is often undersized relative to the size of PV panels (i.e., kWp > kVA), and any excess instantaneous production is clipped (clipping – internal design limit, curtailing –

intentional reduction).

In the control problem, the power output of the PV plant (P_{PV}) represents the available power. In accordance with control objectives a portion of this power can be curtailed, here denoted with P_{curt}, which is a manipulated variable. The actual power used in the microgrid is $P_{\mathrm{PV}}(t) - P_{\mathrm{curt}}(t)$. The following constraint ensures the feasibility of P_{curt}:

$$0 \leq P_{\mathrm{curt}}(t) \leq P_{\mathrm{PV}}(t) \leq \overline{P}_{\mathrm{PV}}, \tag{2.2}$$

where P_{curt} cannot exceed the available power P_{PV}, which is restricted with the parameter of size of inverter electronics $\overline{P}_{\mathrm{PV}}$.

2.3.1.2 Power Output Prediction

Accurate forecasting of PV output is critical for microgrid operation, scheduling, and predictive control. Since solar generation depends on weather, PV power prediction is fundamentally a weather forecasting problem. Once solar irradiance and ambient temperature are forecasted, system-specific parameters are used to compute expected power output [36]:

$$P_{\mathrm{PV}}(t) = P_{\max}\, N_p\, \frac{G(t)}{G_{\mathrm{STC}}}\, \eta_{\mathrm{PV}}(t), \tag{2.3}$$

where $P_{\max}$ and N_p is maximum power output of the specific panel and their number, respectively, $G(t)$ is total solar irradiance, $G_{\mathrm{STC}} = 1000\,\mathrm{W/m^2}$ is solar irradiance at standard test conditions, and $\eta_{\mathrm{PV}}(t)$ accounts for temperature-dependent module efficiency:

$$\eta_{\mathrm{PV}}(t) = \eta_{\mathrm{ref}}\left[1 - \beta_{\mathrm{ref}}\big(T_{\mathrm{C}}(t) - T_{\mathrm{STC}}\big)\right], \tag{2.4}$$

where parameters η_{ref} (module's efficiency at the reference temperature) and β_{ref} (temperature coefficient) are given by the PV manufacturer or could be obtained from the tests. T_{STC} is standard test condition temperature, while the cell temperature T_{C} is modeled as a function of solar irradiance $G(t)$ and measured ambient temperature $T_{\mathrm{amb}}(t)$ [37]:

$$T_{\mathrm{C}}(t) = T_{\mathrm{amb}}(t) + \frac{G(t)}{G_{\mathrm{NOCT}}}\,(T_{\mathrm{NOCT}} - T_{\mathrm{amb,NOCT}}), \tag{2.5}$$

where T_{NOCT} is nominal operating cell temperature, $T_{\mathrm{amb,NOCT}} = 20°\mathrm{C}$ and $G_{\mathrm{NOCT}} = 800\,\mathrm{W/m^2}$ are ambient temperature and solar radiation at which the nominal operating cell temperature is defined. Thus, forecasting PV output requires prediction of $T_{\mathrm{amb}}(t)$ and $G(t)$.

Prediction methods fall into three main categories: statistical (data-driven), physical (model-based), and hybrid. Statistical approaches include autoregressive models (ARMA, ARIMA), Markov chains, and machine learning techniques such as support vector machines, k-nearest neighbors, and artificial neural networks [38]. These are especially effective for short-term forecasting and nowcasting. Physical models simulate the dynamic behavior of the atmosphere using meteorological data, numerical weather prediction, satellite imaging, or sky cameras. Although computationally intensive, these methods offer improved accuracy under stable weather conditions. Hybrid models combine statistical learning with physical forecasts, such as neural network enhanced numerical weather predictions, and provide robust performance at the cost of complexity [39].

In relation to this work, the prediction models are essential part of the developed energy management system, but their construction is not in the scope of the thesis. However, it is assumed the outputs from the models are available for the control problem.

2.3.2 Energy Storage Systems

In power systems, the management of supply and demand is inherently constrained by the fact that electrical energy cannot be stored directly or efficiently at large scales. Unlike other commodities, electricity must be consumed as it is generated. To address this limitation, it is common to convert electrical energy into other storable forms, the main classification of energy storage technologies include [40, 41]:

- **Electrochemical storage**, primarily represented by batteries, where electrical energy is stored through reversible electrochemical reactions.
- **Chemical energy storage**, such as synthetic natural gas or hydrogen production through electrolysis, which enables long-term storage and use in fuel cells.
- **Mechanical energy storage**, including pumped hydroelectric storage and flywheels, which store energy in the form of gravitational potential or rotational kinetic energy.
- **Thermal energy storage**, where energy is stored as heat or cold, for example in molten salts or ice, and used in heating/cooling applications or power generation.

Among these, electrochemical storage in the form of batteries has become the most prevalent solution in microgrid applications. Their expansion stems from several favorable properties, including high energy and power density, fast response times, high round-trip efficiency, and the potential for long operational lifetimes. Given their widespread adoption and practical importance, the remainder of this work will focus exclusively on battery energy storage systems (BESS).

Battery energy storages operate on the principle of reversible electrochemical reactions within individual cells. Each cell comprises a positive and a negative electrode separated by an electrolyte that enables ion transport. During discharge, chemical energy is converted into electrical energy as electrons flow through an external circuit. This process is reversed during charging by applying an external voltage [42].

Various chemistries have been developed, each offering different trade-offs in terms of efficiency, cost, cycle life, and energy density. Traditional lead-acid batteries remain in use due to their low cost and reliability, though they suffer from limited cycle life and low energy density. Nickel-based batteries, such as nickel-cadmium and nickel-metal hydride, offer good power density but at higher cost. Lithium-ion batteries are currently the dominant technology in portable electronics, electric vehicles and large-scale applications including microgrid systems due to their high energy and power density (>200 Wh/kg, >300 W/kg), long cycle life (up to 10 000), and improving affordability. Common variants include lithium iron phosphate (LFP) and lithium nickel manganese cobalt oxide (NMC) [42].

2.3.2.1 Parameters

To integrate battery energy storage systems into microgrid operation and control frameworks, it is necessary to characterize their key parameters and their relation to the energy management.

Nominal and Usable Capacity

Nominal capacity given in amp-hours (Ah) or watt-hours (Wh) refers to the manufacturer-specified energy content. Usable capacity may be lower due to operational constraints. The capacity is defined as amount of charge the storage can provide from its full state to cut off voltage state [43]. In microgrid applications, battery systems range from small-scale residential units (5–50 kWh), through commercial and industrial systems (50–1000 kWh), to large-scale installations (>1000 kWh) depending on their use case.

Power Rating

Specifies the maximum charge/discharge power (in kW). C-rate describes the rate at which the battery is charged or discharged relative to its capacity. A 1C rate means full charge/discharge in one hour, higher C-rates imply faster operation but may affect lifespan.

State of Charge

The state of charge (SoC) is a dimensionless variable representing the current charge level $Q(t)$ relative to its nominal capacity Q_{nom}, typically expressed as a percentage:

$$S_{\mathrm{oC}}(t) = \frac{Q(t)}{Q_{\mathrm{nom}}} \times 100\% \,. \tag{2.6}$$

The SoC is a critical parameter for managing battery operation, as it directly influences how much energy can be dispatched or stored at any given moment. Operating the battery within a recommended SoC range helps extend its lifespan by avoiding deep discharges and overcharging.

SoC cannot be directly measured and must be estimated, these estimation methods are classified into conventional, model-based, and data-driven approaches [44]. Conventional methods such as open-circuit voltage measurement and Coulomb counting are simple to implement but sensitive to disturbances like temperature variations, aging, and measurement errors, which may degrade accuracy over time. Coulomb counting measures integrated current, I, over time to estimate SoC [43]:

$$S_{\mathrm{oC}}(t) = S_{\mathrm{oC}}(t_0) - \frac{1}{Q_{\mathrm{nom}}} \int_{t_0}^{t} I(\tau)\,\mathrm{d}\tau \,. \tag{2.7}$$

Model-based methods utilize battery models—typically electrical equivalent circuit or empirical models—and apply state estimators such as Kalman filters, particle filters, or observer-based techniques to improve estimation precision. These methods offer better accuracy than conventional ones but are computationally more intensive and may lack robustness under varying conditions. Data-driven approaches, including neural networks and machine learning algorithms, rely on historical and real-time data rather than physical modeling. While they provide flexibility and adaptability, they require extensive training data and careful validation to ensure reliability [45].

State of Health

The state of health (SoH) is a dimensionless variable that quantifies the maximum available battery capacity $Q_{\max}(t)$ relative to the nominal capacity of the new battery

$$S_{\mathrm{oH}}(t) = \frac{Q_{\max}(t)}{Q_{\mathrm{nom}}} \times 100\% \,. \tag{2.8}$$

It is typically expressed as a percentage and reflects the battery overall condition, including its ability to hold charge and deliver power. A SoH of 100% indicates a new battery, while lower values indicate degradation. Reaching 70% or 80% of SoH is by the manufacturer defined as end of life (EoL)—beyond this point the battery properties are not guaranteed and is recommended to replace the battery packs. Typical number of cycles for lithium-ion batteries is ranging 1000–3000 cycles, depending on the chemistry and operating conditions [46]. SoH is influenced by factors such as temperature, usage, C-rate, and aging effects. For lithium-ion batteries, processes leading to the capacity loss are structural changes, active material decomposition, growth of solid electrolyte interphase and transition metal dissolution [47].

SoH estimation methods are generally categorized into experimental and model-based approaches. Experimental methods can be direct—such as cycle number counting or Coulomb counting—or indirect, relying on empirical relationships between measurable parameters and aging indicators like capacity fade or internal resistance. While these techniques offer high accuracy in controlled settings, they are often impractical for real-time applications. For this reason, model-based approaches are more suitable for integration in battery management systems and can be further divided into adaptive filtering and data-driven methods. Adaptive filtering techniques employ closed-loop control, utilizing electrochemical or equivalent circuit models to track battery degradation in real time. In contrast, data-driven methods rely on black-box modeling, machine learning algorithms, and pattern recognition to estimate SoH from historical and operational data [47, 48].

Depth of Discharge

Depth of discharge (DoD) is a critical parameter that significantly affects battery lifetime and durability. It represents the percentage of the battery's total capacity discharged during a given cycle and is defined as the difference between the maximum and minimum state of charge reached within that cycle [49]:

$$\mathrm{DoD} = \max(\mathrm{SoC}) - \min(\mathrm{SoC}). \tag{2.9}$$

Excessive or deep discharges (i.e., high DoD) accelerate battery degradation, reducing both the number of achievable charge–discharge cycles and the overall battery lifespan. Conversely, shallow cycling—where the battery operates within a narrower SoC range—can substantially extend cycle life. For this reason, battery manufacturers typically recommend operation within a moderate SoC window, avoiding both deep discharge and prolonged exposure to high SoC levels. In practical applications, these constraints are embedded directly into the control strategy of the BESS. Within an energy management system, DoD limits are enforced to ensure safe and optimal battery utilization. DoD-aware SoC limits are used within the EMS to schedule battery operation and regulate charge and discharge commands, balancing energy delivery and battery health.

Round-Trip Efficiency

Round-trip efficiency (RTE) quantifies the energy losses incurred during the charging and discharging processes of a battery. It is defined as the ratio of the energy delivered during discharge to the energy consumed during charging, thereby capturing the cumulative losses over a complete charge–discharge cycle. These losses arise primarily from internal resistances within the battery electrodes and electrolyte and are dissipated as heat. Round-trip efficiency is not constant; it varies with charging and discharging rates, temperature, state of charge, the battery's age, and state of health. Different lithium-ion chemistries exhibit distinct efficiency characteristics, with LFP and NMC batteries typically achieving RTE values in the range of 92–96% [50]. In energy management and control applications, explicitly accounting for these inefficiencies is necessary for realistic power flow calculations and system optimization.

In addition to round-trip efficiency losses, batteries experience self-discharge, which refers to the gradual loss of stored charge even when the battery is not connected to a load or actively used. The self-discharge rate depends on factors such as temperature, battery chemistry, and age. For lithium-ion batteries, typical self-discharge rates are relatively low, on the order of 2% to 3% per month [51]. While this effect may be included in detailed battery models, it is often neglected in control applications due to the short time horizons considered.

2.3.2.2 Mathematical Model

Mathematical modeling of battery behavior is essential for the design and implementation of advanced control strategies. A battery model enables the controller to predict the system's future states, optimize energy flow, and respect operational constraints such as state of charge, depth of discharge, and account for energy losses. Model should capture the relationship between the actions or input variables (charging/discharging power) and state or output variables (state of charge). The model should also be computationally efficient to allow for real-time control applications, ideally formulated as linear program (LP). Therefore, this section is dedicated to describe inherently nonlinear BESS model and overview of the model variants used in the control design. In our approach, we will use the combination of the models to suit the needs according to trade-off between accuracy and complexity.

Nonlinear Model

For modeling purposes, the battery energy storage is defined as a storage device capable of transforming the electrical energy to store it, and reverting the process to deliver the stored energy back to the system [52]. In the model, there are fundamentally two types of variables: parameters which are known at each time instance, and decision or optimized variables to be determined by solving the optimization problem. The state variable—in the battery model it is the energy level denoted with $E(t)$ given in kWh—is also optimized variable. The change in the energy level is described with differential state equation

$$\frac{\mathrm{d}E(t)}{\mathrm{d}t} = -\sigma\big(E(t)\big) + \eta_{\mathrm{ch}}\big(P_{\mathrm{ch}}(t)\big)\, P_{\mathrm{ch}}(t) - \frac{1}{\eta_{\mathrm{dch}}\big(P_{\mathrm{dch}}(t)\big)}\, P_{\mathrm{dch}}(t)\,, \tag{2.10}$$

with initial state $E(0) = E_0$, where $P_{\mathrm{ch}}(t)$ and $P_{\mathrm{dch}}(t)$ are applied charging and discharging power rates, which are the main decision variables or control actions. Variable $\sigma\big(E_{\mathrm{bat}}(t)\big)$ stands for self-discharge rate that is dependent on the battery state, $\eta_{\mathrm{ch}}\big(P_{\mathrm{ch}}(t)\big)$ and $\eta_{\mathrm{dch}}\big(P_{\mathrm{dch}}(t)\big)$ are charging and discharging efficiencies that are dependent on charging and discharging power [53]. The charging and discharging efficiencies could be modeled as piecewise linear functions [54], but because of the small effect they are often assumed to be constant. To reduce the model complexity, similarly the self-discharge is neglected when considering short horizons, and the model is simplified to

$$\frac{\mathrm{d}E(t)}{\mathrm{d}t} = \eta_{\mathrm{ch}}\, P_{\mathrm{ch}}(t) - \frac{1}{\eta_{\mathrm{dch}}}\, P_{\mathrm{dch}}(t)\,. \tag{2.11}$$

As a remainder, variables indexed with (t) may vary over time, while variables without index are constant during the time horizon.

The state variable $E(t)$ is bounded by the maximum and minimum energy levels, which are defined by the nominal capacity of the battery, lowered by the actual state of health and SoC limits reflecting the depth of discharge. The energy level is then bound by the following constraints:

$$\underline{S}_{\mathrm{oC}}(t)\, S_{\mathrm{oH}}(t)\, E_{\mathrm{nom}} \leq E(t) \leq \overline{S}_{\mathrm{oC}}(t)\, S_{\mathrm{oH}}(t)\, E_{\mathrm{nom}}\,, \tag{2.12}$$

where $\underline{S}_{\rm oC}(t), \overline{S}_{\rm oC}(t) \in [0,1]$ are the minimum and maximum state of charge levels. Non-negative charging and discharging powers are also bounded by the maximum power rating of the battery, which is defined by the maximum charging and discharging power, $\overline{P}_{\rm ch}$ and $\overline{P}_{\rm dch}$. The power limits are defined as

$$0 \leq P_{\rm ch}(t) \leq \overline{P}_{\rm ch}\,, \tag{2.13}$$

$$0 \leq P_{\rm dch}(t) \leq \overline{P}_{\rm dch}\,. \tag{2.14}$$

Nonlinearity of the battery storage model that cannot be overlooked arises with presence of mutually exclusive operational states—charging, discharging, and idle. The charging and discharging power cannot be applied at the same time, which is prevented with the complementarity constraint

$$P_{\rm ch}(t) \cdot P_{\rm dch}(t) = 0\,. \tag{2.15}$$

Including the complementarity constraint creates nonlinear programming (NLP) problem. Existing NLP solvers, when dealing with large-scale problems, face convergence issues which are possibly reduced by replacing the equality constraint (2.15) with relaxed inequalities $-\epsilon \leq P_{\rm ch}(t) \cdot P_{\rm dch}(t) \leq 0$ for small ϵ, or with reformulation as mixed-integer linear programming (MILP) problem [55].

Mixed-Integer Linear Model

The nonlinear model can be reformulated as a mixed-integer linear programming problem by introducing binary variables to represent the operational states of the battery. Following the big-M method introduced in [56], separate binary variables are used for charging and discharging to explicitly prevent both processes from occurring at the same time, and constraints (2.13), (2.14) and (2.15) are replaced with:

$$P_{\rm ch}(t) \leq \delta_{\rm ch}(t)\overline{P}_{\rm ch} \tag{2.16a}$$

$$P_{\rm dch}(t) \leq \delta_{\rm dch}(t)\overline{P}_{\rm dch} \tag{2.16b}$$

$$\delta_{\rm ch}(t) + \delta_{\rm dch}(t) \leq 1 \tag{2.16c}$$

where $\delta_{\rm ch}(t)$ and $\delta_{\rm dch}(t)$ are binary variables indicating whether charging or discharging is active.

Relaxed Linear Model

By simply removing the complementarity constraint (2.15) from the exact formulation, we get an LP problem. Resulting mathematical description is the most common approach for modeling storage devices found in literature because of its convenience [57].

In some applications it is assumed that simultaneous charging and discharging will not occur when the solution converges to the optimum, as it incurs additional costs. However, this assumption is not always valid as it depends on the choice of the objective function and the problem formulation.

Simplified Linear Model

There is an alternative LP formulation of the battery model, which does prevent simultaneous charging and discharging, but does not account for the energy losses. Battery power is represented with a single variable $P_{\mathrm{bat}}(t)$, which can be positive when charging or negative when discharging, $P_{\mathrm{bat}}(t) = P_{\mathrm{ch}}(t) - P_{\mathrm{dch}}(t)$. The state equation (2.11) is then replaced with

$$\frac{\mathrm{d}E(t)}{\mathrm{d}t} = P_{\mathrm{bat}}(t) \tag{2.17}$$

and the power limits (2.13), (2.14) are replaced with

$$-\overline{P}_{\mathrm{dch}} \leq P_{\mathrm{bat}}(t) \leq \overline{P}_{\mathrm{ch}}\,. \tag{2.18}$$

Even though this model does not include charging and discharging efficiencies, it is still a good approximation and suitable for some applications.

Combined Relaxed and Simplified Linear Model

An alternative model was proposed in [58], which combines the relaxed linear model with the simplified linear model to get rid of the complementarity constraint and binary variables while still accounting for the energy losses. The drawback of this model is that it leads to a more conservative battery scheduling as it tightens the allowable range of state of charge in the open-loop trajectory. The model has two state equations for both, the relaxed and simplified representation of the energy level, $E_{\mathrm{r}}(t)$ and $E_{\mathrm{s}}(t)$, respectively:

$$\frac{\mathrm{d}E_{\mathrm{r}}(t)}{\mathrm{d}t} = \eta_{\mathrm{ch}} P_{\mathrm{ch}}(t) - \frac{1}{\eta_{\mathrm{dch}}} P_{\mathrm{dch}}(t)\,, \tag{2.19a}$$

$$\frac{\mathrm{d}E_{\mathrm{s}}(t)}{\mathrm{d}t} = \eta\big(P_{\mathrm{ch}}(t) - P_{\mathrm{dch}}(t)\big)\,, \tag{2.19b}$$

where newly added η is a single net-charge efficiency selected from the range $[\eta_{\mathrm{ch}}, \frac{1}{\eta_{\mathrm{dch}}}]$. As correctly pointed out in [57], appropriate selection $\eta = \frac{1}{2}\big(\eta_{\mathrm{ch}} + \frac{1}{\eta_{\mathrm{dch}}}\big)$ could lead to $\eta > 1$. Authors of the model proved that the open-loop trajectory of the actual state $E(t)$ is always $E_{\mathrm{r}}(t) \leq E(t) \leq E_{\mathrm{s}}(t)$ for $\eta_{\mathrm{ch}}, \eta_{\mathrm{dch}} \in (0, 1]$ and that the model mismatch is below $\frac{\overline{P}_{\mathrm{bat}}}{10}$ for regular round-trip efficiencies.

Extended Linear Model

In [57] the authors proposed an extension to the relaxed linear model with additional constraints on charging and discharging powers to tighten the feasible region. In addition to (2.11)–(2.14), the model includes following constraints:

$$
\begin{aligned}
P_{\mathrm{ch}}(t) &\leq (\overline{S}_{\mathrm{oC}}(t)\, E_{\mathrm{nom}} - E_0)/\eta_{\mathrm{ch}}\,, && (2.20\mathrm{a})\\
P_{\mathrm{dch}}(t) &\leq (E_0 - \underline{S}_{\mathrm{oC}}(t)\, E_{\mathrm{nom}})\, \eta_{\mathrm{dch}}\,, && (2.20\mathrm{b})\\
P_{\mathrm{dch}}(t) &\leq \overline{P}_{\mathrm{dch}} - (\overline{P}_{\mathrm{dch}}/\overline{P}_{\mathrm{ch}})\, P_{\mathrm{ch}}(t)\,. && (2.20\mathrm{c})
\end{aligned}
$$

The model remains in LP domain, and while the tighter bounds help, they do not completely prevent the simultaneous charging/discharging. In the end, the model selection will depend on the application use case and overall problem computability.

Chapter 3

Energy Management System

After a brief overview, this chapter is predominantly devoted to building the energy management system (EMS) for microgrid operation according to our design. The comprehensive EMS is based on a hierarchical control architecture, where each layer represents its own contribution and is discussed in detail. The layers act independently with different objectives, but are built on the same foundations of mathematical optimization. Together, they allow microgrid deployment from the design phase to real-time operation. Only the theory and methodology are presented further.

3.1 Overview

The problem solved by the EMS in this thesis is formulated as follows. Given a microgrid consisting of batteries, photovoltaic systems, controllable loads, and a grid connection, together with forecasts of generation and demand, electricity prices, real-time measurements, and the contractual and regulatory obligations imposed on its operation, the EMS must decide, at every control instant, the power setpoints for the controllable assets so that energy flows are distributed optimally across the entire control hierarchy and the efficiency, reliability, and economic performance of the microgrid are preserved under all operational constraints [59]. A precise account of inputs, outputs, constraints, and success criteria is given in Section 1.1.

Considering the variability of renewable generation and load demand within the microgrid, which operates in a complex environment of energy markets and regulations, advanced control strategies such as model predictive control (MPC) are commonly used within the EMS framework. MPC enables forward-looking decision-making by incorporating uncertain forecasts, constraints, and dynamic models, particularly of the battery storage system, into an optimization problem. While the MPC is the core of the EMS, it must cooperate with the other control layers, which are equally essential.

3.1.1 Control Architectures

This section classifies and reviews the main EMS control architectures, identifies their advantages and limitations, and presents representative examples from recent literature. Control architectures for EMS are commonly categorized as centralized, decentralized, distributed, and hierarchical [60]. These architectures differ in terms of communication structure, computational requirements, scalability, and fault tolerance. Across all architectures, a wide range of control and optimization strategies has been employed. Conventional approaches frequently include model predictive control, mixed-integer linear programming, dynamic programming, as well as stochastic and robust optimization. In addition, AI-based EMS approaches have been proposed, employing techniques such as neural networks, Markov decision processes, reinforcement learning, multi-agent systems, particle swarm optimization, fuzzy logic, and other less commonly used methods [61]. The optimization objectives vary and may be single- or multi-criteria, most often focusing on cost minimization, carbon footprint reduction, or reliability enhancement. Typical microgrid configurations include energy storage systems combined with renewable energy sources, predominantly photovoltaic panels, occasionally supplemented with wind turbines. Some microgrids further incorporate combined heat and power units, diesel generators, microturbines, electric vehicles, heat pumps, or other controllable appliances [62].

- **Centralized** EMS architectures rely on a single controller that gathers all system data and sends control signals to each energy resource. This configuration benefits from full system observability and can provide globally optimal solutions. However, it suffers from drawbacks such as high computational burden, limited scalability, and the presence of a single point of failure. Representative centralized EMS implementations include systems that maximize the utilization of solar, wind, and battery resources while maintaining stable voltage and frequency, such as the real-time monitoring solution presented in [63], MILP-based optimization for minimizing the net present cost of shiftable and non-shiftable appliances [64], and MPC-based scheduling approaches aimed at minimizing energy drawn from the grid [65].

- **Decentralized** EMS architectures are characterized by autonomous operation of individual units, each equipped with its own controller. These controllers may exchange limited information, enabling faster decision-making and reduced computational demand, albeit at the expense of global optimality [66]. Decentralized approaches have been applied to electric vehicle charging using particle swarm optimization with dual objectives [67], demand-side load shifting [68], and agent-based reinforcement learning for autonomous energy units, including photovoltaic panels, wind turbine generators, diesel generators, battery energy storage systems, and local loads [69].

- **Distributed** EMS architectures combine features of centralized and decentralized control. Local controllers make decisions based on their own states and partial information exchanged with neighboring units. These systems are generally more scalable and robust, resilient to failures, and capable of faster responses, but they are also more complex to monitor and maintain [70]. Distributed approaches are particularly prevalent in multi-microgrid settings, such as the cooperative microgrid framework addressing distribution network constraints presented in [71], or the application of distributed MPC for coordinating energy exchanges among multiple microgrids in [72].

- **Hierarchical** EMS structures employ multiple control layers—typically two, three, or even four—each targeting different timescales and control objectives. At the lowest layer, local controllers perform fast regulation of voltage, frequency, and current. Intermediate layers handle coordination and power sharing, while the top layer focuses on long-term planning, scheduling, and economic optimization. Communication occurs primarily between adjacent layers, while units within a layer may operate independently. A representative three-layer architecture is outlined in [73], where the primary layer controls the output voltage and current of power electronic converters in real time, the secondary layer distributes power among energy resources and balances the state of charge of storage units, and the tertiary layer performs economic scheduling of loads and distributed energy resources.

3.1.2 Control Hierarchy

This section is devoted to the design of the energy management system proposed in this work, which is based on a hierarchical control architecture. The need for separating the control layers emerged from the complexity of the microgrids encountered and from the natural separation of relevant time scales. The proposed control architecture employs four distinct layers, which was firstly elaborated in our earlier work [23]. Each layer operates at a different level of abstraction, with its own objectives and time scales, as summarized in Table 3.1 and illustrated in Figure 3.1. Information flows between adjacent layers, with upper layers providing control signals or reference information to lower layers, while lower layers report state and operational information back to higher layers.

Table 3.1: Control hierarchy of the EMS with four layers. Interactions occur only between adjacent layers.

	Business layer	**Energy management layer**	**Power management layer**	**Device control layer**
Role	Design microgrid, define goals	Optimize energy flows	Distribute power setpoints, SoC balancing	Execute power commands
Inputs	Microgrid parameters, external conditions	Forecasts, objectives, real-time measurements	Energy schedule, real-time measurements	Individual power setpoints
Outputs	Objectives for energy management	Optimal energy schedule for each asset group	Power setpoints for individual devices	Voltage and current regulation
Controller	Informed expert decision	Model predictive controller	Rule-based controller	PID controller
Horizon	Years	Hours	Seconds	Milliseconds

Business Layer

The business layer represents the highest level of the control hierarchy and is responsible for strategic decision-making on timescales ranging from months to years. Its primary function is to define the long-term goals and operational priorities of the microgrid, such as whether the focus should be on cost minimization or carbon emission reduction, as well as the means to achieve these objectives, for example by maximizing renewable energy utilization or participating in the imbalance market. These objectives arise from the structural composition of the microgrid, external market conditions, contractual obligations, and regulatory requirements imposed on its operation.

Decisions at this level are typically made by informed experts—such as business stakeholders, managers, microgrid owners, or operators—while the role of the EMS is to provide an interface and the necessary information, potentially supported by analyses of the expected impact of different decisions. The output of the business layer consists of abstract objectives and operational preferences, which are passed to the energy management layer in the form of optimization targets and constraints. At this level of abstraction, the microgrid is considered as a single aggregated system.

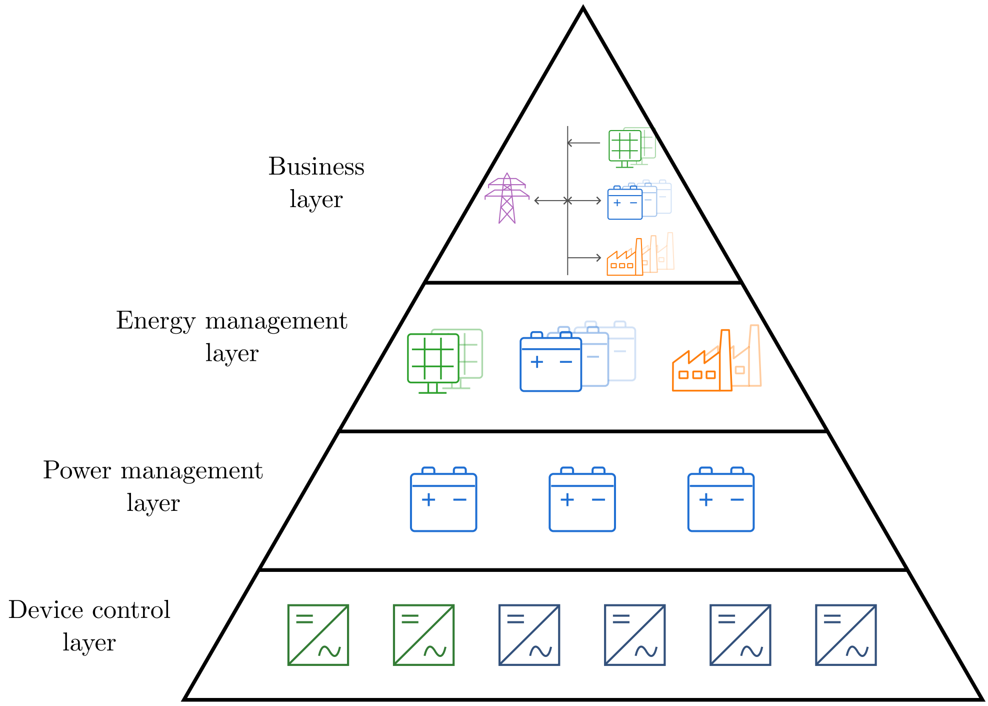

Figure 3.1: Control hierarchy of the EMS with four layers. Each has own level of abstraction: business layer considers the microgrid as a whole, energy management layer operates with groups of assets, power management layer distributes power to individual units, and device control layer executes commands at the level of individual power electronic devices.

Energy Management Layer

The energy management layer is responsible for operational planning and scheduling, bridging long-term strategies and real-time control. It operates with a predictive horizon ranging from several hours to days and a sampling interval aligned with typical market time resolutions (e.g., 15 minutes). At this level, the system processes forecasts of renewable generation, demand profiles, and electricity market prices, which are commonly available at the same temporal resolution. The layer distinguishes between functional groups of assets, such as battery energy storage systems, renewable energy sources, and controllable loads, and determines the energy quantities allocated to each group.

The core of this layer is model predictive control, which is particularly well suited due to its ability to handle multi-objective, multivariable constrained optimization over a receding horizon. MPC allows the integration of physical models of microgrid components, multiple objectives, forecast uncertainties, and operational constraints within a unified optimization framework. Its role is to compute an optimal energy schedule over the predictive horizon, which is repeatedly updated as new information becomes available. The proposed MPC formulation is further detailed in Section 3.3.

The controller computes optimal energy allocation schedules that reflect the objectives defined at the business layer. These schedules are passed to the power management layer for further processing. At this level of abstraction, the microgrid is not managed at the level of individual devices; instead, energy targets are allocated to asset groups in accordance with higher-level objectives.

Power Management Layer

The power management layer acts as an intermediary between high-level energy schedules and low-level control execution. It operates on a faster timescale, typically on the order of seconds, and is responsible for translating aggregate energy commands into individual power references for specific devices. This layer ensures that real-time dynamics and operational limits—such as inverter capacities, ramp rates, and SoC bounds—are respected. Multiple local controllers may be employed within this layer, each responsible for a particular asset group. These controllers are typically rule-based or threshold-based due to their speed and simplicity, but may also employ optimization techniques when required.

This layer is responsible for power disaggregation within asset groups. It performs tasks such as SoC balancing across multiple storage units or curtailment of selected renewable sources. For example, it distributes aggregate battery charging power among distributed battery units to balance their SoC and utilization. This approach improves system scalability without increasing the computational burden at the energy management layer. The algorithms developed for this layer, addressing optimal power allocation, are detailed further in Section 3.4.

Device Control Layer

The device control layer, also referred to as the execution layer, is the lowest level in the control hierarchy and operates at the millisecond timescale. It is responsible for the real-time execution of power commands at the level of individual power electronic devices. Each unit—such as an inverter or a DC–DC converter—is equipped with an embedded controller that regulates voltage, current, and power output to track the reference setpoints provided by the upper layer.

In systems where a single asset, such as a battery energy storage system, comprises multiple inverters, the device control layer ensures that each inverter is loaded in accordance with the commands received from the power management layer. Controllers at this level are typically implemented using conventional control strategies, such as proportional–integral–derivative (PID) control, and are embedded in hardware to ensure real-time responsiveness. This layer operates at the lowest level of abstraction, dealing directly with electrical quantities and physical device characteristics. As this layer complements the EMS, it is not the focus of this thesis and is therefore not discussed further.

3.1.3 Energy Management-as-a-Service

While the primary focus of most energy management systems lies in their technical design and in optimizing microgrid operation—such as minimizing costs and maximizing revenue for the microgrid itself—much less attention is paid to the economic model behind delivering such a service. In our case, the EMS is not a one-time software product but a continuously operated service offered to customers such as microgrid or asset owners. These end users benefit from reduced operating costs or new revenue streams, while the EMS provider bears the responsibility for maintaining and operating the solution in a sustainable manner.

The EMaaS concept has been explored in [19], where a cloud-based linear-programming framework coordinates distributed energy resources within virtual retail electricity providers, optimizing the day-ahead multiperiod cost across a green community. This thesis extends the EMaaS concept along two dimensions: the underlying control is an MPC operating in real time on individual commercial microgrids, rather than a day-ahead LP on a virtual aggregator; and the provider-side economics—cloud computing costs, scalability across a portfolio, and a revenue-sharing model with the microgrid owner—are modeled explicitly and used to characterize break-even conditions.

Delivering an EMS as a service involves more than running control algorithms. A complete EMaaS offering must include real-time monitoring, historical data management, user interfaces (e.g., dashboards, web portals, HMIs), alerting mechanisms, and ongoing support. These features require a supporting infrastructure, including database systems, communication networks, cloud hosting, real-time data processing, and user management systems. All of these introduce both fixed and variable costs for the provider. Control algorithms—particularly model predictive control—may require considerable computational resources, whether deployed on local hardware or in cloud environments. If the EMS is scaled across multiple clients, computational demands directly affect operating expenses. Therefore, optimizing control strategies not only improves microgrid operation but also enhances the economic viability of the EMaaS model by reducing overhead costs.

Scalability plays a central role in making EMaaS economically sustainable. To reach the break-even point and operate profitably, it is crucial to manage a portfolio of microgrid clients. This, in turn, requires a modular and flexible framework that can be adapted to different system configurations without excessive customization. Case-specific implementations are not sustainable at scale. The proposed EMS framework is designed from the outset to support multi-client operation and to be sufficiently configurable and robust to handle diverse energy assets, market structures, and user preferences.

The proposed economic model is based on revenue sharing, where the EMS provider receives a percentage of the financial gains delivered to the microgrid owner. This approach aligns incentives between both parties and ensures that value creation for the microgrid operator translates into viable income for the service provider. The model is illustrated in Figure 3.2.

The intention of the service provider is to maximize net profit, which is achieved by increasing the benefits generated at the microgrid level while minimizing operational expenses. As these expenses are closely related to computational requirements, the efficiency of the control algorithms must be considered as an integral part of the EMS design.

3.2 Assumptions

The methods developed in this chapter assume a specific microgrid configuration, market structure, forecasting setup, and component dynamics, summarized below.

Microgrid configuration.

- All assets interface with a common AC bus, either directly (AC loads) or through DC–AC converters (photovoltaic systems, battery storage).
- Non-controllable loads must be supplied at all times; only the controllable portion of the load is adjustable.

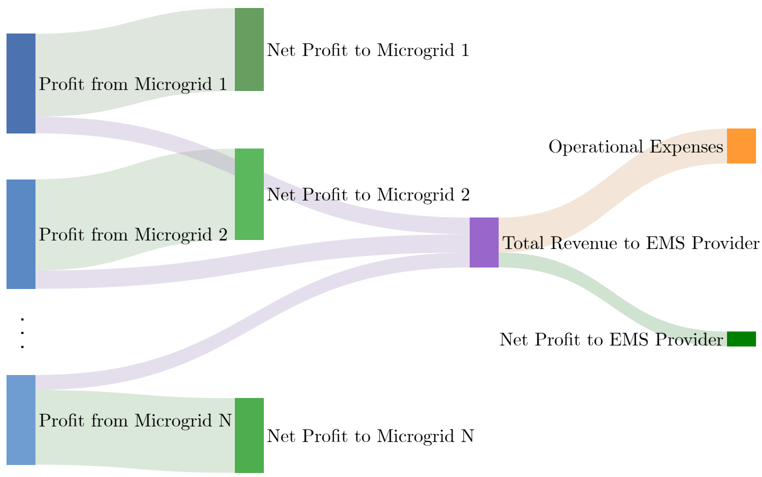

Figure 3.2: Revenue-sharing mechanism between microgrids and the EMS provider. The microgrid is charged for its energy costs, savings are evaluated over a settlement period, and a share of these savings constitutes revenue for the EMS provider. The EMS net profit depends on the size of the microgrid portfolio, control performance, and operational expenditures.

- For renewable sources, curtailment is the manipulated variable; the utilized output equals the available power minus the curtailed portion.

Electricity market.

- The microgrid operates under a liberalized electricity market with day-ahead and balancing segments, and is financially exposed to imbalance settlement as a balance responsible party, either directly or aggregated under a larger entity.

Forecasts.

- Forecasts of renewable generation and demand, together with their confidence intervals, are available as inputs to the EMS; the forecasting models themselves are outside the scope of this thesis.

- Day-ahead electricity prices are known in advance; imbalance prices are estimated from historical patterns.
- In the stochastic formulation, scenarios are sampled from Gaussian distributions defined by the forecast confidence intervals, and each scenario is assigned equal probability.

Battery model.

- Charging and discharging efficiencies are treated as constants over the horizons considered.
- Self-discharge is neglected for the short prediction horizons used at the energy management layer.

Long-term planning.

- In the sizing problem, long-term variability of generation and demand is treated as averaging out over the evaluation horizon.
- The battery is taken to reach its end of life when its state of health drops to a defined threshold after a specified number of operating years.

3.3 Model Predictive Control

The aim is to develop a model predictive control strategy suitable for the EMS that operates the microgrid system. Its role is to optimize the energy flows between energy resources, such as battery energy storage systems, renewable sources, and loads. The requirements for the MPC are the ability to handle multiple objectives, multiple constraints, and uncertainties, while remaining computationally efficient enough to operate in real time. The MPC is designed to operate at the energy management layer of the hierarchical control architecture, which was described in the previous section.

Model predictive control is defined as a control strategy in which control actions are computed by repeatedly solving an open-loop constrained optimization problem with a finite horizon in a receding manner [74]. Each computation is initialized with the current state and yields an optimal control sequence, from which the first control action is applied to the system. Unlike conventional feedback control with an explicit control law, MPC must be solved online, which requires the optimization problem to be formulated in a computationally efficient manner. Standard MPC is designed for reference-tracking problems, where a setpoint is given; however, the MPC framework can also be used with an objective function representing real costs rather than deviation from a reference. In this case, the reference is not predefined but results from the optimal solution. This formulation is commonly referred to as economic model predictive control [75].

There are several approaches to dealing with uncertainties. Conventional MPC, or deterministic MPC (dMPC), handles uncertainties to some extent by repeatedly solving the optimization problem in a receding-horizon fashion. A more systematic approach is robust MPC (rMPC), which explicitly considers uncertainties within a bounded set, typically represented as a polytope [76]. Robust MPC is traditionally formulated either as a min–max optimization problem, in which the worst-case scenario is considered, or using the more recently developed tube-based MPC, which employs invariant tubes around a nominal trajectory to represent uncertainty [77]. Robust MPC is suitable for systems with bounded and deterministic uncertainties; however, in practice, uncertainties often exhibit a probabilistic nature.

When uncertainties are described probabilistically, stochastic MPC (stMPC) formulates the optimization problem using chance constraints, ensuring that state and output constraints are satisfied with a predefined probability level. This approach enables a systematic trade-off between control performance and the risk of constraint violation, as the solution is robust against the majority of possible realizations rather than against all worst-case scenarios [78]. Scenario-based MPC (sMPC) is derived from stochastic MPC and represents uncertainties using a finite number of sampled scenarios [79]. This improves solvability by converting probabilistic constraints into a finite number of deterministic constraints, resulting in an optimization problem with N_{S} scenarios [80].

The aforementioned approaches are based on risk-neutral formulations that rely on expected values of uncertainties, which may be insufficient in applications where large deviations from the nominal trajectory can lead to unsafe or undesirable outcomes. Risk-aware MPC extends these formulations by incorporating risk measures—such as Conditional Value-at-Risk (CVaR) or other coherent risk metrics—into the optimization problem, thereby penalizing unfavorable scenarios more strongly [81]. This control approach enables a systematic balance between performance and robustness against rare but critical events. Considering these characteristics and the application requirements—such as real-time computability, uncertainty handling, and risk avoidance—risk-aware scenario-based MPC is selected as the most suitable approach for the proposed EMS.

3.3.1 Related Work

In recent years, many studies have focused on the use of MPC for managing energy flows in microgrids that include battery energy storage systems and renewable energy sources. These works differ in their treatment of uncertainties and in the considered objectives, which are reviewed in this section. A common weakness lies in addressing real-world operational demands, computational complexity, and practical applicability, where this work aims to contribute.

Strategies based on deterministic MPC, which do not explicitly incorporate uncertainty, are among the most common. For example, an economic MPC strategy is proposed in [1] for a residential microgrid to minimize electricity costs and battery usage. However, uncertainty in generation and load is addressed only implicitly through the receding horizon, and the method is evaluated using a 1-hour control interval, which limits its applicability in systems with faster dynamics. Similarly, the framework in [2] combines energy cost arbitrage with schedule deviation penalties and integrates a battery degradation model, but remains deterministic in nature. A hardware-validated deterministic MPC is reported in [3], where a 240 kW/180 kWh battery, photovoltaic generation, and buildings with thermal flexibility are jointly optimized for energy cost and CO_2 emissions on a real microgrid testbed; while real-time experimental validation strengthens the result, the framework relies on point forecasts and does not explicitly handle forecast uncertainty. Although these methods are computationally efficient, they lack the robustness required to ensure constraint satisfaction under uncertainty. Robust MPC approaches, on the other hand, provide conservative handling of uncertainty by explicitly considering bounded disturbances. In [82], a robust optimization strategy is proposed for managing shared energy storage across multiple microgrids, ensuring operational reliability while minimizing costs. However, such robust approaches assume worst-case scenarios, which can limit economic performance.

Stochastic MPC methods address probabilistic uncertainties, as in [4], where a stochastic MPC is proposed for grid-connected microgrids. Uncertainties in production, consumption, and prices are modeled as scenarios in a mixed-integer quadratic program. However, the authors report computational times that are an order of magnitude higher than those of deterministic MPC and that grow exponentially with the number of scenarios. A two-timescale stochastic approach is developed in [5], where a day-ahead plan is optimized using stochastic programming, while intraday deviations are managed through rolling-horizon control. Nevertheless, a 1-hour update interval limits responsiveness to rapid fluctuations. Another study focuses on uncertainties related to battery states and electric vehicle (EV) availability [83], proposing a two-layer MPC in which the upper layer handles economic optimization and the lower layer manages

EV allocation. While effective in simulations, real-time applicability is not explored. Similarly, [84] proposes a two-layer stochastic MPC, where the upper layer relies on nominal forecasts and the lower layer adjusts decisions based on real-time disturbances. In [85], a multi-objective stochastic MPC formulation is introduced for microgrids with diesel generation and storage and is converted into a single-objective problem via weighted sums. However, both approaches operate on 1-hour average power values, limiting control granularity. The study in [6] proposes a scenario-based MPC with a two-layer hierarchy, where computational burden is reduced using ADMM (alternating direction method of multipliers). The method is validated in a laboratory-scale nanogrid, where it outperforms chance-constrained and rule-based EMSs, but it relies on a simplified battery model that allows the problem to be formulated as a quadratic program (QP).

Risk-aware MPC approaches extend stochastic formulations by penalizing unfavorable outcomes using coherent risk metrics, such as Conditional Value-at-Risk. These methods aim to address rare but high-impact events. In [7], CVaR is employed within a risk-averse MPC to reduce exposure to extreme financial losses. Unlike worst-case robust methods, this formulation offers an adjustable trade-off between risk and profitability, although decisions are updated only every 30 minutes. Similarly, [8] applies CVaR-based MPC to optimize battery operation in electricity markets while considering degradation costs and financial risks. A more market-focused implementation is presented in [9, 86], where a risk-averse aggregator uses CVaR and MILP formulations for reserve market participation and imbalance management. While these approaches improve economic resilience, they are limited to storage-only systems and do not consider renewable generation or highly dynamic operating conditions. In [87], robust and chance-constrained decision-making is applied to price arbitrage with storage; however, the model lacks a full microgrid context, limiting its practical applicability.

Most of the reviewed approaches formulate the control objective primarily as cost minimization, focusing on electricity procurement and battery degradation [1, 5, 82, 87]. Other objectives include peak shaving and load profile flattening [7, 88, 89], grid exchange minimization [90], or imbalance reduction. However, the economic structure of real imbalance markets is often overlooked, and only a few studies explicitly exploit imbalance pricing mechanisms [91, 8, 9]. Environmental aspects have also been considered in some works through pollutant treatment cost models [85, 92].

Despite these advances, existing MPC frameworks still face challenges related to modularity, scalability, and real-world deployment. Many solutions are tailored to specific configurations with limited flexibility, and most validations are conducted in simulations or short-term experiments [6], leaving long-term operational performance uncertain. The integration of a business-layer perspective is rare, and the computational demands of advanced MPC formulations continue to hinder real-time deployment.

3.3.2 Method Outline

To overcome the computational limitations of conventional scenario-based stochastic MPC in real-time microgrid energy management, while retaining the benefits of uncertainty awareness, a two-stage MPC framework is proposed that balances computational tractability and robustness. In conventional scenario-based MPC, a single optimization problem incorporating multiple uncertainty realizations is solved directly. This approach becomes computationally infeasible for complex or nonlinear models when limited computational resources are available in real operation. The proposed method mitigates this issue through a two-stage process:

1. **Stage One – Scenario-Based MPC with Relaxed Model:** A simplified linear model is used to solve a stochastic MPC problem across multiple scenarios. This formulation captures the essential variability of uncertainties while significantly reducing computational time.

2. **Stage Two – Deterministic MPC with Full Model:** A single scenario is identified from the first-stage solution based on a specified risk metric (e.g., CVaR). This scenario is then used as input to a deterministic MPC that employs the full nonlinear model, enabling accurate control actions to be computed efficiently.

This two-stage structure allows the second stage to approximate stochastic behavior with substantially lower computational overhead, making the method suitable for real-time applications such as microgrids that require sub-minute control intervals. Furthermore, to eliminate delays introduced by sequential execution, the proposed method implements parallel execution of both stages. This parallel structure enables timely control decisions while preserving the benefits of risk-aware scenario evaluation and full-model accuracy.

The following sections are dedicated to the detailed formulation of the two-stage MPC. First, the microgrid model is described, consisting of constraints and objectives. Next, the deterministic MPC formulation is presented, from which the stochastic MPC is derived. Finally, the complete procedure is summarized.

3.3.3 Optimization Model

The microgrid system can be characterized by a set of decision variables, parameters, constraints, and associated costs and revenues forming the objective function.

3.3.3.1 Constraints

Central to microgrid operation is the power balance equation previously defined in (2.1), which must be satisfied at every time step. In discrete time step k, it is written as

$$\begin{aligned}P_{\mathrm{imp}}(k) + P_{\mathrm{dch}}(k) + P_{\mathrm{RES}}(k) + P_{\mathrm{adj}}(k) = \\ P_{\mathrm{exp}}(k) + P_{\mathrm{ch}}(k) + P_{\mathrm{load}}(k) + P_{\mathrm{curt}}(k)\,.\end{aligned} \tag{3.1}$$

In this formulation, variables $P_{\mathrm{RES}}(k)$ and $P_{\mathrm{load}}(k)$ act as parameters in the optimization problem, while the remaining variables are decision variables. Each decision variable is subject to individual bounds arising from the microgrid environment, which are defined in this section.

The power balance equation is complemented by the energy balance equation of the battery storage system. Here, the state model (2.11) discretized in time is employed and is given by

$$E(k+1) = E(k) + \Delta t \left(\eta_{\mathrm{ch}} P_{\mathrm{ch}}(k) - \frac{1}{\eta_{\mathrm{dch}}} P_{\mathrm{dch}}(k) \right)\,. \tag{3.2}$$

This equation is complemented by inequality constraints, where the nonlinearity is reformulated as MILP:

$$\underline{S}(k)\, E_{\mathrm{nom}} - \underline{\epsilon}_{\mathrm{E}}(k) \leq E(k) \leq \overline{S}(k)\, E_{\mathrm{nom}} + \overline{\epsilon}_{\mathrm{E}}(k)\,, \tag{3.3a}$$

$$P_{\mathrm{ch}}(k) \leq \delta_{\mathrm{ch}}(k)\, \overline{P}_{\mathrm{ch}}\,, \tag{3.3b}$$

$$P_{\mathrm{dch}}(k) \leq \delta_{\mathrm{dch}}(k)\, \overline{P}_{\mathrm{dch}}\,, \tag{3.3c}$$

$$\delta_{\mathrm{ch}}(k) + \delta_{\mathrm{dch}}(k) \leq 1\,, \tag{3.3d}$$

where $\underline{S}(k) = \underline{S}_{\mathrm{oC}}(k)\, S_{\mathrm{oH}}(k)$ and $\overline{S}(k) = \overline{S}_{\mathrm{oC}}(k)\, S_{\mathrm{oH}}(k)$ represent the lower and upper bounds on the energy level, already accounting for battery health. The state constraint (3.3a) is softened using slack variables $\underline{\epsilon}_{\mathrm{E}}(k)$ and $\overline{\epsilon}_{\mathrm{E}}(k)$ to ensure feasibility of the optimization problem. The binary constraint (3.3d), combined with the power-limit inequalities above, is the MILP equivalent of the bilinear complementarity (2.15): it prevents simultaneous charging and discharging via integer logic rather than a nonlinear product. From this point onward, this set of constraints is referred to as the *full model*, while the set of constraints with the complementarity constraint (3.3d) removed is referred to as the *relaxed model*.

Another group of constraints addresses the controllable components of the microgrid system that do not hold an energy state. These assets allow partial flexibility, either in consumption or generation. They include curtailable renewable sources and controllable loads, which are modeled through adjustment variables.

The maximum available power from renewable sources $P_{\mathrm{RES}}(k)$ can be curtailed, with $P_{\mathrm{curt}}(k)$ representing the curtailed portion. The actual utilized power is then given by $P_{\mathrm{RES}}(k) - P_{\mathrm{curt}}(k)$. To ensure feasibility, the following constraint is imposed:

$$0 \leq P_{\mathrm{curt}}(k) \leq P_{\mathrm{RES}}(k)\,. \tag{3.4}$$

Similarly, for controllable loads, the adjustment variable $P_{\mathrm{adj}}(k)$ is introduced to modify the actual consumption, resulting in the realized load $P_{\mathrm{load}}(k) - P_{\mathrm{adj}}(k)$. The adjustment is bounded by:

$$\underline{P}_{\mathrm{adj}}(k) \leq P_{\mathrm{adj}}(k) \leq \overline{P}_{\mathrm{adj}}(k)\,, \tag{3.5a}$$

$$P_{\mathrm{adj}}(k) \leq P_{\mathrm{load}}(k)\,. \tag{3.5b}$$

These bounds prevent over-adjustment beyond the actual load and restrict adjustments to the specified lower and upper limits $\underline{P}_{\mathrm{adj}}(k)$ and $\overline{P}_{\mathrm{adj}}(k)$, respectively.

The connection to the utility grid enables bidirectional power exchange through import $P_{\mathrm{imp}}(k)$ and export $P_{\mathrm{exp}}(k)$. These variables are to be decided upon and are constrained to reflect technical or contractual limits:

$$0 \leq P_{\mathrm{imp}}(k) \leq \overline{P}_{\mathrm{imp}} + \epsilon_{\mathrm{imp}}(k)\,, \tag{3.6a}$$

$$0 \leq P_{\mathrm{exp}}(k) \leq \overline{P}_{\mathrm{exp}} + \epsilon_{\mathrm{exp}}(k)\,, \tag{3.6b}$$

where $\overline{P}_{\mathrm{imp}}$ and $\overline{P}_{\mathrm{exp}}$ are the maximum import and export limits, respectively, and $\epsilon_{\mathrm{imp}}(k)$ and $\epsilon_{\mathrm{exp}}(k)$ are slack variables for feasibility. Occasional violations of these limits are allowed, but penalized with an appropriate weight coefficient in the cost function.

In many regulatory frameworks, microgrids are required to submit a day-ahead schedule $P_{\mathrm{DA}}(k)$ and are held responsible for deviations. However, this obligation also opens possibilities for profit through imbalance pricing, where penalties or rewards depend on the system's state. The difference between the actual net exchange, given by

$P_{\text{imp}}(k) - P_{\text{exp}}(k)$, and the scheduled value $P_{\text{DA}}(k)$, constitutes the imbalance at time step k. This deviation is decomposed into two non-negative components:

$$P_{\text{short}}(k) = \max\left(0, P_{\text{imp}}(k) - P_{\text{exp}}(k) - P_{\text{DA}}(k)\right), \tag{3.7a}$$
$$P_{\text{long}}(k) = \max\left(0, P_{\text{DA}}(k) - P_{\text{imp}}(k) + P_{\text{exp}}(k)\right). \tag{3.7b}$$

The variable $P_{\text{short}}(k)$ quantifies the case when the microgrid withdraws more energy than scheduled (i.e., a shortage), while $P_{\text{long}}(k)$ represents the opposite case—a surplus—when the microgrid injects more energy than anticipated or consumes less. Both quantities are non-negative by construction and reflect the operational deviation relative to the scheduled trajectory.

These imbalance terms are incorporated into the optimization problem using the following linear equality:

$$P_{\text{short}}(k) - P_{\text{long}}(k) = P_{\text{imp}}(k) - P_{\text{exp}}(k) - P_{\text{DA}}(k). \tag{3.8}$$

This formulation ensures that only one of the two variables ($P_{\text{short}}(k)$ or $P_{\text{long}}(k)$) is active at any given time. While mutual exclusivity is typically enforced implicitly by the cost structure, a stricter formulation with binary variables can be adopted if necessary in a MILP setting.

The economic implications of imbalance depend on imbalance pricing, which reflects the condition of the larger balancing area (e.g., regional or national grid). For instance, if the balancing area is in surplus, actors contributing further to the surplus (i.e., with $P_{\text{long}}(k) > 0$) may receive reduced remuneration or even pay penalties, while those in shortage are seen as helping restore balance and might be compensated. Conversely, when the balancing area is in shortage, exporting or consuming less than scheduled (i.e., having a positive $P_{\text{long}}(k)$) is beneficial and rewarded, while drawing more than planned results in penalties.

Thus, rather than avoiding imbalance, an optimal control strategy can exploit these pricing signals to minimize operational costs or generate additional revenue. This is particularly relevant for flexible microgrids, where storage, curtailable resources, and adjustable loads allow intentional deviations from the baseline schedule when economically justified. While imbalance power quantities result from the constraints, decisions on when it is economically beneficial are determined by the objective function.

3.3.3.2 Objectives

The objective of the energy management system is to maximize the total economic benefit of the microgrid over the control horizon, which is achieved by combining multiple sub-objectives. This benefit is defined as the difference between revenues and costs associated with both internal operations and external energy market interactions. Each action and power flow in the microgrid is associated with a cost coefficient that reflects generated revenue or incurred cost. The energy management strategy incorporates several key functionalities:

- **Price arbitrage:** Variable market prices for importing (c_{imp}) and exporting (c_{exp}) energy enable the controller to schedule energy imports during low-price periods and exports during high-price periods, thereby maximizing arbitrage profit.
- **Peak shaving:** To avoid exceeding contractual or physical limits on grid exchange, violations of import and export limits are penalized using coefficients q_{imp} and q_{exp}. This supports peak shaving and ensures the microgrid remains within operational boundaries.
- **Asset degradation:** Storage operations are evaluated using cost coefficients c_{ch} and c_{dch}, which reflect battery degradation due to cycling. These costs discourage unnecessary wear and prolong battery life.
- **Renewable self-consumption and curtailment:** Renewable curtailment (c_{curt}) is penalized to discourage wasting locally generated energy. Additionally, a subsidy coefficient (c_{sub}) is used to further incentivize self-consumption of renewable energy, rewarding the microgrid for utilizing locally generated power.
- **Flexible demand management:** Load adjustments are modeled with c_{adj}, which quantifies the disutility or cost associated with altering controllable demand, enabling demand response when economically favorable.
- **Imbalance exploitation:** Deviations from the scheduled energy profile—either shortages (c_{short}) or surpluses (c_{long})—are settled according to imbalance pricing. These deviations are not always penalized; rather, they present opportunities to generate revenue or reduce cost depending on the wider system's condition.

The total cost (or negative profit) to be minimized is formulated as a linear combination of decision variables, written generally as:

$$\min_{\mathbf{x}} \; J = \mathbf{c}^{\top}\mathbf{x}\,, \tag{3.9}$$

where $\mathbf{x}$ is the vector of control actions and $\mathbf{c}$ contains the corresponding cost coefficients. This linear formulation allows for flexible prioritization of multiple functionalities through appropriate tuning of $\mathbf{c}$. This makes revenue stacking across various services possible and enables response to dynamic conditions.

3.3.4 Deterministic MPC Formulation

Let the prediction horizon be defined over the interval $[t_0, t_f]$, divided into N control steps. The discrete time index is $k \in \{0, \ldots, N-1\}$, and the corresponding sampling intervals are $\Delta T(k) = t(k+1) - t(k)$. Non-uniform time steps are permitted to allow flexible temporal resolution.

At each time step k, the system is described by the following arrays:

- $\mathbf{x}(k)$ – battery energy level, representing the state variable.
- $\mathbf{u}(k)$ – control actions, including setpoints for controllable energy assets and power exchange with the grid.
- $\mathbf{c}(k)$ – cost coefficients, representing the revenue or costs associated with actions.
- $\mathbf{e}(k)$ – slack variables, representing violations of soft constraints.
- $\mathbf{q}(k)$ – penalty weights, representing penalties applied to slack variables.
- $\mathbf{w}(k)$ – uncertainties, for which only estimations are known, include forecasts of renewable generation and load demand.
- $\mathbf{p}(k)$ – parameters, known precisely, such as conversion efficiencies, inverter limits, contractual diagrams, and operating bounds.
- $\mathbf{b}(k)$ – binary variables, used to model complementarity constraints, when two actions are mutually exclusive.

Variables may vary across multiple microgrid entities, as they differ in composition and functionalities, but the general form is provided here, which might be adapted to specific microgrid setups. The array variables are given as follows:

$$\mathbf{x}(k) = [E(k)]\,, \tag{3.10a}$$
$$\mathbf{u}(k) = [P_{\text{ch}}(k), P_{\text{dch}}(k), P_{\text{imp}}(k), P_{\text{exp}}(k), P_{\text{short}}(k), P_{\text{long}}(k), P_{\text{curt}}(k), P_{\text{adj}}(k)]^\top\,, \tag{3.10b}$$
$$\mathbf{c}(k) = [c_{\text{ch}}(k), c_{\text{dch}}(k), c_{\text{imp}}(k), c_{\text{exp}}(k), c_{\text{short}}(k), c_{\text{long}}(k), c_{\text{curt}}(k), c_{\text{adj}}(k)]^\top\,, \tag{3.10c}$$
$$\mathbf{e}(k) = [\underline{\epsilon}_{\text{E}}(k), \overline{\epsilon}_{\text{E}}(k), \epsilon_{\text{imp}}(k), \epsilon_{\text{exp}}(k)]^\top\,, \tag{3.10d}$$
$$\mathbf{q}(k) = [\underline{q}_{\text{E}}(k), \overline{q}_{\text{E}}(k), q_{\text{imp}}(k), q_{\text{exp}}(k)]^\top\,, \tag{3.10e}$$
$$\mathbf{w}(k) = [P_{\text{RES}}(k), P_{\text{load}}(k)]^\top\,, \tag{3.10f}$$
$$\mathbf{p}(k) = [E_{\text{nom}}, \underline{S}(k), \overline{S}(k), \eta_{\text{ch}}, \eta_{\text{dch}}, P_{\text{DA}}(k), \overline{P}_{\text{ch}}, \overline{P}_{\text{dch}}, \overline{P}_{\text{imp}}, \overline{P}_{\text{exp}}]^\top\,, \tag{3.10g}$$
$$\mathbf{b}(k) = [\delta_{\text{ch}}(k), \delta_{\text{dch}}(k), \delta_{\text{short}}(k), \delta_{\text{long}}(k)]^\top\,. \tag{3.10h}$$

The full sequence of variables over the prediction horizon is represented by the following matrices (superscript d denotes deterministic formulation to distinguish from stochastic):

$$\mathbf{X}^{\text{d}} = [\mathbf{x}(1),\ \mathbf{x}(2),\ \ldots,\ \mathbf{x}(N)]^\top\,, \tag{3.11a}$$
$$\mathbf{U}^{\text{d}} = [\mathbf{u}(0),\ \mathbf{u}(1),\ \ldots,\ \mathbf{u}(N-1)]^\top\,, \tag{3.11b}$$
$$\mathbf{C}^{\text{d}} = [\mathbf{c}(0),\ \mathbf{c}(1),\ \ldots,\ \mathbf{c}(N-1)]^\top\,, \tag{3.11c}$$
$$\mathbf{E}^{\text{d}} = [\mathbf{e}(0),\ \mathbf{e}(1),\ \ldots,\ \mathbf{e}(N-1)]^\top\,, \tag{3.11d}$$
$$\mathbf{Q}^{\text{d}} = [\mathbf{q}(0),\ \mathbf{q}(1),\ \ldots,\ \mathbf{q}(N-1)]^\top\,, \tag{3.11e}$$
$$\mathbf{W}^{\text{d}} = [\mathbf{w}(0),\ \mathbf{w}(1),\ \ldots,\ \mathbf{w}(N-1)]^\top\,, \tag{3.11f}$$
$$\mathbf{P}^{\text{d}} = [\mathbf{p}(0),\ \mathbf{p}(1),\ \ldots,\ \mathbf{p}(N-1)]^\top\,, \tag{3.11g}$$
$$\mathbf{B}^{\text{d}} = [\mathbf{b}(0),\ \mathbf{b}(1),\ \ldots,\ \mathbf{b}(N-1)]^\top\,. \tag{3.11h}$$

The controller aims to minimize the total operating cost J of microgrid operation over the prediction horizon of N discrete steps. The objective function captures all operational revenues, costs, and penalties for soft constraint violations – resulting in a linear cost formulation over the horizon:

$$J = \sum_{k=0}^{N-1} \big(\Delta T(k)\,\mathbf{c}(k)^\top \mathbf{u}(k) + \mathbf{q}(k)^\top \mathbf{e}(k)\big) = \big\langle \boldsymbol{\Delta T} \odot \mathbf{C}^{\text{d}},\, \mathbf{U}^{\text{d}} \big\rangle + \big\langle \mathbf{Q}^{\text{d}},\, \mathbf{E}^{\text{d}} \big\rangle\,. \tag{3.12}$$

The compact form assumes $\boldsymbol{\Delta T} \in \mathbb{R}^{N}$, $\mathbf{C}^{\text{d}}, \mathbf{U}^{\text{d}} \in \mathbb{R}^{N\times u}$, and $\mathbf{Q}^{\text{d}}, \mathbf{E}^{\text{d}} \in \mathbb{R}^{N\times e}$, where u and e are the number of control and slack variables, respectively. The operation $\langle \cdot, \cdot \rangle$ is a component-wise inner product of two matrices, and $\odot$ is the Hadamard product. The objective function is linear in decision variables. The model predictive control problem is then formulated as:

$$
\begin{aligned}
\min_{\mathbf{X}^{\mathrm{d}},\mathbf{U}^{\mathrm{d}},\mathbf{E}^{\mathrm{d}},\mathbf{B}^{\mathrm{d}}} \quad & \left\langle \boldsymbol{\Delta T} \odot \mathbf{C}^{\mathrm{d}},\, \mathbf{U}^{\mathrm{d}} \right\rangle + \left\langle \mathbf{Q}^{\mathrm{d}},\, \mathbf{E}^{\mathrm{d}} \right\rangle && \text{(3.13a)}\\
\text{s.t.} \quad & \mathbf{x}(k+1) = f\big(\mathbf{x}(k), \mathbf{u}(k), \mathbf{p}(k)\big)\,, \quad \forall k\,, && \text{(3.13b)}\\
& \mathbf{x}(0) = x_t\,, && \text{(3.13c)}\\
& \mathbf{w}(0) = w_t\,, && \text{(3.13d)}\\
& \mathbf{X}^{\mathrm{d}} \in \mathcal{X}\big(\mathbf{E}^{\mathrm{d}}, \mathbf{P}^{\mathrm{d}}\big)\,, && \text{(3.13e)}\\
& \mathbf{U}^{\mathrm{d}} \in \mathcal{U}\big(\mathbf{E}^{\mathrm{d}}, \mathbf{W}^{\mathrm{d}}, \mathbf{P}^{\mathrm{d}}, \mathbf{B}^{\mathrm{d}}\big)\,, && \text{(3.13f)}\\
& \mathbf{E}^{\mathrm{d}} \in \mathbb{R}_{\geq 0}\,, && \text{(3.13g)}\\
& \mathbf{B}^{\mathrm{d}} \in \{0,1\}^{N\times 4}\,. && \text{(3.13h)}
\end{aligned}
$$

The MPC minimizes the operating cost (3.13a) while respecting battery dynamics (3.13b), state constraints (3.13e), and initial conditions (3.13c) and (3.13d). The mutual exclusivity is enforced using the binaries (3.13h). The constraint set $\mathcal{U}$ includes all additional operational limits, such as inverter capacities, grid exchange limits, and the power balance equation.

This optimization is solved in a receding-horizon manner – at each time step, the controller solves (3.13) using the latest available state x_t and measurement w_t. Only the first control action $\mathbf{u}^{\star}(0)$ is applied, after which the horizon shifts forward and the optimization is repeated with updated measurements and forecasts.

3.3.5 Stochastic MPC Formulation

To address uncertainty in power production or consumption, we extend the deterministic MPC formulation into a stochastic MPC. It is needed to introduce multiple scenarios, indexed by $s \in \mathcal{S}$, where $\mathcal{S} = \{1, \ldots, N_S\}$ and N_S denotes the number of considered scenarios. Each scenario represents a potential trajectory of the uncertain variables over the prediction horizon. Accordingly, arrays of variables are extended with an additional scenario index:

$$
\begin{aligned}
\mathbf{X}^{\mathrm{s}}(s) &= [\mathbf{x}(s,1),\ \mathbf{x}(s,2),\, \ldots,\, \mathbf{x}(s,N)]^{\top}\,, && \text{(3.14a)}\\
\mathbf{U}^{\mathrm{s}}(s) &= [\mathbf{u}(s,0),\ \mathbf{u}(s,1),\, \ldots,\, \mathbf{u}(s,N{-}1)]^{\top}\,, && \text{(3.14b)}\\
\mathbf{C}^{\mathrm{s}}(s) &= [\mathbf{c}(s,0),\ \mathbf{c}(s,1),\, \ldots,\, \mathbf{c}(s,N{-}1)]^{\top}\,, && \text{(3.14c)}\\
\mathbf{E}^{\mathrm{s}}(s) &= [\mathbf{e}(s,0),\ \mathbf{e}(s,1),\, \ldots,\, \mathbf{e}(s,N{-}1)]^{\top}\,, && \text{(3.14d)}\\
\mathbf{Q}^{\mathrm{s}}(s) &= [\mathbf{q}(s,0),\ \mathbf{q}(s,1),\, \ldots,\, \mathbf{q}(s,N{-}1)]^{\top}\,, && \text{(3.14e)}\\
\mathbf{W}^{\mathrm{s}}(s) &= [\mathbf{w}(s,0), \mathbf{w}(s,1),\, \ldots,\, \mathbf{w}(s,N{-}1)]^{\top}\,, && \text{(3.14f)}\\
\mathbf{P}^{\mathrm{s}}(s) &= [\mathbf{p}(s,0),\ \mathbf{p}(s,1),\, \ldots,\, \mathbf{p}(s,N{-}1)]^{\top}\,. && \text{(3.14g)}
\end{aligned}
$$

Optimized variables $\mathbf{X}^{\mathrm{s}}(s)$, $\mathbf{U}^{\mathrm{s}}(s)$, and $\mathbf{E}^{\mathrm{s}}(s)$ are calculated for every scenario, while the cost coefficients in $\mathbf{C}^{\mathrm{s}}(s)$, penalty weights $\mathbf{Q}^{\mathrm{s}}(s)$, and known parameters $\mathbf{P}^{\mathrm{s}}(s)$ are considered identical across all scenario realizations. There are no binary variables in the stochastic formulation by design.

Every scenario trajectory in the uncertainty vector $\mathbf{W}^{\mathrm{s}}(s)$ is created according to the scenario generation strategy before solving the optimization problem. The scenario generation strategy is a key prerequisite for this formulation, but is not restricted to any specific method. In this work, uncertain parameters are sampled from Gaussian distributions constructed within forecast confidence intervals. These intervals are derived using a time-series forecasting model adopted from [93, 94], which provides upper and lower bounds from which samples are drawn. Further details on the forecasting model are outside the scope of this work, but it is assumed that the outputs from the model are available.

At the initial time step $k = 0$, all scenarios share the same known information, namely the initial state $\mathbf{x}(s, 0) = x_0$ and forecast $\mathbf{w}(s, 0) = w_0$ for all $s \in \mathcal{S}$. Consequently, it is appropriate to enforce non-anticipativity constraints [95], ensuring that the control action applied at time zero is identical across all scenarios. The constraint takes the form:

$$\mathbf{u}(i, 0) = \mathbf{u}(j, 0) \quad \forall i, j \in \mathcal{S},\ i \neq j. \tag{3.15}$$

In conventional stochastic model predictive control, the control problem is solved by minimizing the expected cost over a set of generated scenarios. This approach inherently assumes a risk-neutral perspective, treating all realizations of uncertainty proportionally and placing equal emphasis on typical and extreme outcomes. While such an approach yields decisions that perform well on average, it may expose the system to significant risk under low-probability, high-impact scenarios. To address this, a risk-aware extension of sMPC is adopted by incorporating a risk measure—specifically, the Conditional Value-at-Risk. Unlike standard sMPC, risk-aware sMPC explicitly accounts for the tail of the cost distribution, allowing the decision-maker to control the degree of conservativeness through a risk-aversion parameter α. By minimizing CVaR instead of expected cost, the controller focuses on the expected cost in the worst α fraction of scenarios. For instance, setting $\alpha = 0.3$ directs the controller to optimize the expected cost over the worst 30 % of forecast scenarios—hedging against adverse realizations of generation and demand. This matters in microgrid operation because end users are sensitive to losses from rare but high-impact events, which an expected-value formulation would underweight.

Let $J(s)$ denote the total cost associated with scenario $s \in \mathcal{S}$. The Value-at-Risk (VaR) at tail probability $\alpha \in (0, 1)$ is defined as the smallest cost threshold $y \in \mathbb{R}$ such that the probability of the scenario cost exceeding y is at most α:

$$\mathrm{VaR}_\alpha \triangleq \min\left\{y \in \mathbb{R} : \mathcal{P}(J(s) > y) \leq \alpha\right\} . \tag{3.16}$$

While VaR captures the threshold above which the loss occurs with probability at most α, it is a non-coherent risk measure and therefore non-convex. This can be overcome using CVaR, which reflects the expected cost in the worst α-tail of the cost distribution:

$$\mathrm{CVaR}_\alpha \triangleq \mathbb{E}\left[J(s) \mid J(s) \geq \mathrm{VaR}_\alpha\right] . \tag{3.17}$$

A tractable, convex approximation of CVaR is available through the linear programming formulation proposed by [96]. Assuming scenario probabilities $\pi(s)$ with $\sum_s \pi(s) = 1$, CVaR can be written as:

$$\mathrm{CVaR}_\alpha = y + \frac{1}{\alpha}\sum_{s\in\mathcal{S}} \pi(s)\big[J(s) - y\big]^+ , \tag{3.18}$$

where $y \in \mathbb{R}$ serves as the VaR estimate, and $[\cdot]^+ = \max(0, \cdot)$. Introducing auxiliary variables $z(s) \triangleq \max\big(0, J(s) - y\big)$, the optimization problem for minimizing CVaR becomes:

$$\min_{y,z} \quad y + \frac{1}{\alpha}\sum_{s\in\mathcal{S}} \pi(s) z(s) \tag{3.19a}$$

$$\text{s.t.} \quad z(s) \geq J(s) - y\,, \quad \forall s \in \mathcal{S}\,, \tag{3.19b}$$

$$z(s) \geq 0\,, \qquad \forall s \in \mathcal{S}\,. \tag{3.19c}$$

We assume that each scenario has the same occurrence probability, $\pi(s) = \frac{1}{N_S}$ for all $s \in \mathcal{S}$, but they are already sampled from a Gaussian distribution, so central scenarios are more represented.

This risk-aware formulation ensures that the controller does not overreact to extreme events, but also takes into account potential high-cost scenarios. The parameters N_S (number of scenarios) and α (risk-aversion level) provide flexibility in tuning the controller's behavior. A larger N_S leads to a finer representation of uncertainty, at the cost of increased computational burden. The parameter α adjusts the degree of risk aversion: smaller values of α place more weight on extreme outcomes, encouraging more conservative actions. This flexibility allows tailoring the control strategy to specific application needs or operator preferences.

The resulting sMPC formulation minimizes the risk-adjusted cost represented by CVaR. The objective is defined in Eq. (3.19a). The optimization seeks decisions that account for uncertainty while satisfying the system dynamics and operational constraints in a scenario-wise manner:

$$\begin{aligned}
\min_{\mathbf{X}^{\mathrm{s}},\, \mathbf{U}^{\mathrm{s}},\, \mathbf{E}^{\mathrm{s}}, y, z} \quad & \mathrm{CVaR}_\alpha && && (3.20a)\\
\text{s.t.} \quad & \mathbf{x}(s,k+1) = f\big(\mathbf{x}(s,k),\, \mathbf{u}(s,k),\, \mathbf{p}(s,k)\big), && \forall s \in \mathcal{S},\, \forall k\,, && (3.20b)\\
& \mathbf{x}(s,0) = x_t\,, && \forall s \in \mathcal{S}\,, && (3.20c)\\
& \mathbf{w}(s,0) = w_t\,, && \forall s \in \mathcal{S}\,, && (3.20d)\\
& \mathbf{X}^{\mathrm{s}}(s) \in \mathcal{X}\big(\mathbf{E}^{\mathrm{s}}(s), \mathbf{P}^{\mathrm{s}}(s)\big), && \forall s \in \mathcal{S}\,, && (3.20e)\\
& \mathbf{U}^{\mathrm{s}}(s) \in \mathcal{U}\big(\mathbf{E}^{\mathrm{s}}(s), \mathbf{W}^{\mathrm{s}}(s), \mathbf{P}^{\mathrm{s}}(s)\big), && \forall s \in \mathcal{S}\,, && (3.20f)\\
& \mathbf{E}^{\mathrm{s}}(s) \in \mathbb{R}^N_{\geq 0}\,, && \forall s \in \mathcal{S}\,, && (3.20g)\\
& \mathbf{u}(i,0) = \mathbf{u}(j,0)\,, && \forall i \neq j \in \mathcal{S}\,, && (3.20h)\\
& z(s) \geq J(s) - y\,, && \forall s \in \mathcal{S}\,, && (3.20i)\\
& z(s) \geq 0\,, && \forall s \in \mathcal{S}\,. && (3.20j)
\end{aligned}$$

Note that in the proposed formulation the complementarity condition is relaxed to increase computational efficiency. As a result, the obtained solution may not strictly satisfy the original complementarity conditions, but the complementarity is enforced when properly combined with dMPC.

3.3.6 MPC Procedure

Following the formulation of both deterministic and stochastic MPC, this section presents the integrated control procedure. The approach relies on two stages that run in parallel with different resolutions. The first stage uses a relaxed stochastic MPC to evaluate expected cost distributions across multiple uncertainty scenarios, while the second stage applies a fast deterministic MPC using a representative scenario that reflects a desired level of risk. The key idea is to identify a single α-scenario whose cost corresponds to the CVaR at a given risk level α, and then use this scenario as the input for the deterministic MPC. The two stages operate independently, with the stochastic MPC updating the α-scenario, while the deterministic MPC continuously runs to provide updated control actions. The procedure consists of the following steps:

1. **Scenario generation:** At a lower frequency (e.g., every 15 minutes), generate N_S future scenarios of uncertain parameters based on probabilistic forecasts. These are constructed using confidence intervals derived from a time-series prediction model.
2. **Stochastic MPC (low frequency):** Solve the stochastic MPC problem, formulated in Eq. (3.20), using a relaxed model across all N_S scenarios. This

provides a distribution of total system costs $J(s)$ across all possible realizations $s \in \mathcal{S}$. To reduce computational complexity, binary variables are excluded in this step. The stochastic MPC runs independently from the deterministic MPC and sends updated α-scenario information to the deterministic stage.

3. **Identification of the α-scenario:** From the cost distribution $J(s)$, identify the scenario s_α corresponding to the CVaR_α. For each uncertain variable in $\mathbf{W}^{\mathrm{s}}$, compute the representative α-scenario over the whole horizon as:

$$\mathbf{W}(s_\alpha) = \frac{\sum_{s\in\mathcal{S}_\alpha} \pi(s)\mathbf{W}^{\mathrm{s}}(s)}{\sum_{s\in\mathcal{S}_\alpha} \pi(s)}, \tag{3.21}$$

where $\mathcal{S}_\alpha = \{s \in \mathcal{S} \mid J(s) \geq \mathrm{VaR}_\alpha\}$ contains the worst-case scenarios in terms of cost, and $\pi(s)$ denotes their associated probabilities. This ensures that $\mathbf{W}(s_\alpha)$ reflects the desired risk level from a cost-minimization perspective, then set $\mathbf{W}^{\mathrm{d}} = \mathbf{W}(s_\alpha)$. The updated α-scenario is sent to the deterministic MPC stage when it becomes available.

4. **Deterministic MPC (high frequency):** At a higher frequency (e.g., every minute), solve the deterministic MPC problem in Eq. (3.13) using the full nonlinear model and the most recently received α-scenario s_α. This provides a control trajectory optimized under risk-aware conditions but with the computational efficiency of a single-scenario formulation. The deterministic MPC runs continuously with short sampling, ensuring real-time responsiveness to system dynamics.

5. **Control implementation:** Apply only the first control input from the computed trajectory, which is valid until an update is received or a new sampling step starts. The horizon recedes and the problem is re-solved at the next step.

6. **Receding horizon and updates:** Continuously update system states and uncertainty forecasts. Steps 1–3 (stochastic stage) are repeated with lower resolution, whereas steps 4–5 (deterministic stage) run in parallel with higher resolution. This hierarchical timing ensures that control remains responsive while preserving risk-awareness.

This combined MPC procedure integrates the risk-aware stochastic formulation with the high-resolution deterministic control loop. The parallelization of both stages shortens delays between invocation and application of the results, with the stochastic MPC updating the α-scenario and the deterministic MPC continuously providing updated control actions based on the latest scenario and current measurements, see schematic in Figure 3.3.

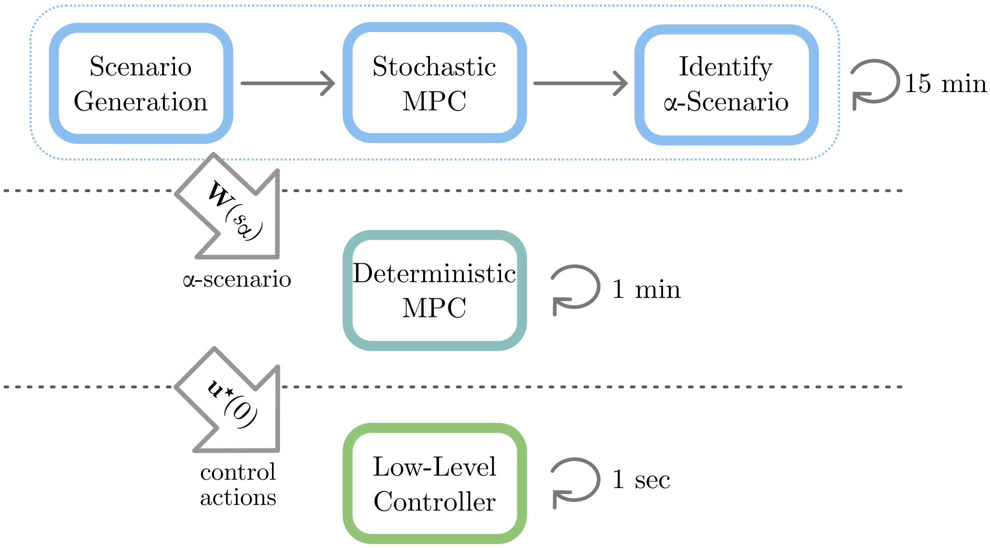

Figure 3.3: Schematic of the procedure. The two stages run in parallel; the stochastic stage (top row) is updated at a lower frequency by design, because solving the multi-scenario problem is computationally heavier than the single-scenario deterministic stage (bottom row), whose computed actions are sent to low-level controllers for execution every minute.

Section 4.2 in the next chapter is dedicated to the application of the proposed framework and the achieved results.

3.4 Power Distribution

Moving further in the control hierarchy to the power management layer, there is a need for a power distribution strategy responsible for distributing the power setpoints generated by the energy management layer to individual microgrid components. This is particularly relevant for microgrids with multiple controllable assets within the same group, as the energy management layer typically provides aggregated setpoints for each group of assets, such as storage systems, loads, and renewable generators. The power distribution strategy ensures that these aggregated setpoints are allocated to individual components, taking into account their specific characteristics and operational constraints.

This section is devoted to designing an optimization-based control algorithm for distributing the storage group power setpoint among multiple battery storage units. The concept was first introduced in our paper [21], here elaborated in the context of hierarchical control with improved solvability. The aim is to achieve a balanced distribution while considering the individual characteristics and states of each storage unit. From the viewpoint of the energy management layer—represented here by the proposed MPC framework—the group of battery storage systems should ideally behave as a single, aggregated asset. To ensure that the collective system can reliably deliver the requested power, it is essential to maintain balanced energy levels across the storage units. Further, when dealing with temperature-sensitive devices such as battery energy storage systems, effective power distribution must also account for cell temperature and the impact of control actions on thermal behavior to ensure reliable and safe operation.

The power allocation algorithm must satisfy several practical and performance-related requirements to ensure reliable and efficient operation of the battery storage group. We state the requirements:

- The total power requested by the energy management layer must be delivered at each control step.
- State of charge imbalances between units should be actively reduced.
- Temperature constraints should be respected where possible, preventing operation outside safe thermal limits.
- The amount of internal energy exchange between units should be adjusted based on configuration, where none is also an option.
- Frequent and unnecessary power transitions between units should be avoided to ensure smooth operation.
- The solution must be obtained quickly, making the method suitable for real-time implementation.

3.4.1 Related Work

The conventional approach for achieving state of charge balance when using multiple BESS units is through adaptive droop control, where droop coefficients are adjusted based on SoC values—units with higher SoC discharge at a higher rate and vice versa [10]. This approach results in synchronized states and equal power sharing, but it does not perform well in systems with different nominal capacities and output power limits. Several improved droop-based schemes and fuzzy logic strategies have been proposed to address this, but they often do not account for BESS power output limits. The intuitive approach was used in [11], where a designed priority stack controller sorts identical BESS units based on their SoC, and the units with the highest SoC are given priority to discharge, and those with the lowest SoC are given priority to charge. This is a simple solution that might be effective in small systems, but it does not consider heterogeneous parameters and additional conditions. In [97], the authors propose a power allocation algorithm for batteries with unknown parameters. However, it leads to slow balancing and tracking of the desired power reference. To avoid non-uniform battery aging, it is desirable to balance both SoC and temperature, as discussed in [98]. Still, these methods do not include the possibility of energy exchange between BESS units. In [14], a control strategy is introduced to avoid energy exchange altogether by ensuring that all units only charge or discharge. This avoids energy losses and aging due to internal energy flow, but it slows down the SoC balancing process.

Very few power allocation methods consider temperature, despite the recommended operating range for lithium-ion batteries being between 15–35 °C [99]. Since the performance of a battery pack is limited by its weakest cell, more attention has been given to temperature balancing at the cell level. In [100], the authors use a thermal model to balance temperatures, while in [101], a model predictive controller is designed to reduce both SoC and thermal imbalances while tracking the power setpoint provided by the energy management layer.

Other optimization-based methods have also been proposed. In [12], an optimization-based approach is proposed that gradually reduces SoC differences, unlike the equal division method, which may result in SoC imbalances, particularly when the batteries differ in capacity. An optimization-based method to maximize energy efficiency is presented in [102], and another addressing SoC imbalances in [103]. The authors assume that energy efficiency is mainly affected by SoC and output power, and formulate the Lagrangian equation using a piecewise linear approximation to solve the convex problem. In [13], three power allocation methods are presented: the equal allocation where power is distributed evenly, a SoC balance method, which minimizes the variance of SoC values, and a method, which considers the aging model of the batteries, including thermal effects and depth of discharge. They verified the methods in a simulation with uniform battery storages, where a single-objective multivariate non-linear optimization was executed for every time step, whose length was set to 1 minute. Another example is [15], where mixed-integer linear programming is used to allocate power between a battery and a supercapacitor to provide ancillary services. Although the approach is relevant, the study does not consider computational demands or validation on a real system, which are critical for practical applications.

Despite these advances, the reviewed approaches collectively fail to deliver a power distribution algorithm that jointly accounts for heterogeneous battery parameters (capacity, state of charge, power limits, and thermal behavior), allows controlled energy exchange between units [14], and demonstrates scalability and validation on a real system [15]. The power distribution algorithm developed in the remainder of this section addresses these gaps through a quadratic program formulation that jointly enforces individual operational and thermal limits across heterogeneous units, supports controlled inter-unit energy transfer, and is validated on a commercial multi-battery deployment.

3.4.2 Problem Formulation

The aggregated group of battery energy storage systems, denoted as $\mathcal{B} = \{1, \ldots, N_B\}$, consists of N_B individual units indexed by $i \in \mathcal{B}$, which must deliver the requested power P^{req}. Each BESS unit i is characterized by its nominal energy capacity E_i^{nom}, SoC limits $\underline{S}_i$ and $\overline{S}_i$, charging/discharging power limits $\overline{P}_i^{\text{ch}}$ and $\overline{P}_i^{\text{dch}}$, and an upper temperature limit $\overline{T}_i$. The initial state of each unit is described by the state of charge $S_{0,i}$ (ratio of current to nominal energy, given in percentage, unlike the formerly used E, which is in absolute energy units), power $P_{0,i}$ (positive for charging, negative for discharging, i.e. $P_{0,i} = P_{0,i}^{\text{ch}} - P_{0,i}^{\text{dch}}$), and cell temperature $T_{0,i}$.

3.4.2.1 Constraints

Change in SoC due to applied power P_i over sampling interval Δt is described with linear dynamics:

$$S_i = S_{0,i} + \frac{\Delta t}{E_i^{\text{nom}}} P_i, \tag{3.22}$$

for this and the following equations, $\forall i \in \mathcal{B}$ applies.

Temperature dynamics is modeled using the specific heat capacity formula:

$$T_i = T_{0,i} + \frac{\Delta t}{3600} \cdot \frac{Q_i}{m_i c_{p,i}}, \tag{3.23}$$

where m_i and $c_{p,i}$ are the battery's mass and specific heat capacity, and Q_i is the total heat flow, which consists of the heat generated by the battery cells combined with the heat flow from the HVAC system, $Q_i = Q_i^{\text{gen}} + Q_i^{\text{hvac}}$. Generated heat flow by the cells during charging and discharging processes can be approximated by fitting a quadratic polynomial function of the output power and state of charge:

$$Q_i^{\mathrm{gen}} = a_i^{\mathrm{P}} P_i^2 + b_i^{\mathrm{P}} |P_i| + a_i^{\mathrm{S}} S_i^2 + b_i^{\mathrm{S}} S_i + c_i, \tag{3.24}$$

where $a_i^{\mathrm{P}}, b_i^{\mathrm{P}}, a_i^{\mathrm{S}}, b_i^{\mathrm{S}}, c_i$ are fitted coefficients.

BESS SoC and input powers are bounded:

$$\underline{S}_i - \underline{\epsilon}_i \leq S_i \leq \bar{S}_i + \bar{\epsilon}_i, \tag{3.25a}$$

$$-\bar{P}_i^{\mathrm{dch}} \leq P_i \leq \bar{P}_i^{\mathrm{ch}}, \tag{3.25b}$$

with slack terms $\underline{\epsilon}_i, \bar{\epsilon}_i \geq 0$.

In the absence of additional constraints, energy transfer between units is not restricted, allowing charged batteries to supply power to the emptier ones. It speeds up reaching the state balance, but also overuses the battery, which might be undesirable. To have a control over this, the parameter P^{trans} is introduced to limit the maximum transfer power between the individual BESS. Additionally, two binary parameters (not optimized variables) are defined, δ^{ch} and δ^{dch}, indicating a charging or discharging request to the BESS group.

$$P^{\mathrm{req}} > 0 \Rightarrow \delta^{\mathrm{ch}} = 1,\ \delta^{\mathrm{dch}} = 0, \tag{3.26a}$$

$$P^{\mathrm{req}} < 0 \Rightarrow \delta^{\mathrm{ch}} = 0,\ \delta^{\mathrm{dch}} = 1. \tag{3.26b}$$

The following constraints prevent power transfer beyond the value of P^{trans}:

$$P_i \leq \delta^{\mathrm{ch}} \overline{P}_i^{\mathrm{ch}} + \delta^{\mathrm{dch}} P^{\mathrm{trans}}, \tag{3.27a}$$

$$-P_i \leq \delta^{\mathrm{dch}} \overline{P}_i^{\mathrm{dch}} + \delta^{\mathrm{ch}} P^{\mathrm{trans}}, \tag{3.27b}$$

$$P_i \leq |P^{\mathrm{req}}| + P^{\mathrm{trans}}, \tag{3.27c}$$

$$-P_i \leq |P^{\mathrm{req}}| + P^{\mathrm{trans}}. \tag{3.27d}$$

3.4.2.2 Objectives

The objective of the optimization problem is to determine the most appropriate power allocation for each battery unit while satisfying operational constraints and minimizing undesired effects. This is achieved through a weighted sum of quadratic penalty terms, each capturing a specific control goal or penalizing violations of physical or operational constraints.

Power Setpoint Tracking

The primary objective is to ensure that the total power delivered by the BESS group matches the requested power setpoint P^{req} from the energy management layer. This is achieved by minimizing the squared difference between the total power output and the requested power:

$$q^{\text{P}} \left(P^{\text{req}} - \sum_{i \in \mathcal{B}} P_i \right)^2 , \tag{3.28}$$

where q^{P} is a positive coefficient that weights the importance of this objective.

SoC Balancing

While delivering the requested power, the intention is to balance the state of charge across the BESS group. Instead of enforcing a uniform SoC target for all units, the approach assigns an individualized target SoC for each battery based on its operating range, ensuring fair usage and avoiding boundary saturation. With the target SoC computed as:

$$S_i^{\text{tgt}} = \frac{\sum_{j \in \mathcal{B}} E_j (\bar{S}_j - \underline{S}_j)}{\sum_{j \in \mathcal{B}} E_j (S_j - \underline{S}_j)} (\bar{S}_i - \underline{S}_i) + \underline{S}_i \, , \tag{3.29}$$

the first term in the cost function penalizes deviation from these individualized SoC targets at the next time step, weighted by a coefficient q^{S}:

$$q^{\text{S}} \sum_{i \in \mathcal{B}} \left(S_i - S_i^{\text{tgt}} \right)^2 . \tag{3.30}$$

Slack Variable Penalization

Slack variables are used to maintain feasibility in the case of conflicting constraints. These are penalized to ensure they are only used when strictly necessary:

$$q^{\epsilon} \sum_{i \in \mathcal{B}} \left(\underline{\epsilon}_i + \bar{\epsilon}_i \right) , \tag{3.31}$$

where q^{ϵ} penalizes SoC constraint violations.

Power Ramp Smoothing

To avoid abrupt changes in control actions between time steps, the following delta penalization is included:

$$q^{\Delta} \sum_{i \in \mathcal{B}} \left(P_{0,i} - P_i \right)^2 , \tag{3.32}$$

where $P_{0,i}$ is the control input from the previous step.

Power Sharing Uniformity

To encourage equitable use of the BESS units, the following term promotes uniform net power contributions:

$$q^{\mathrm{u}} \sum_{i \in \mathcal{B}} \left(P_i - \frac{P^{\mathrm{req}}}{N_B} \right)^2 . \tag{3.33}$$

Temperature-Aware Penalization

To limit thermal stress and promote the long-term health of the batteries, units operating at elevated temperatures are penalized more heavily. Individual temperature penalty coefficients are computed as:

$$c_i^{\mathrm{T}} = \begin{cases} (T_{0,i} - \overline{T}_i) + 1\,, & T_{0,i} \geq \overline{T}_i\,, \\ \dfrac{1}{(T_{0,i} - \overline{T}_i)^2 + 1}\,, & T_{0,i} < \overline{T}_i\,. \end{cases} \tag{3.34}$$

The corresponding term in the objective function is:

$$q^{\mathrm{T}} \sum_{i \in \mathcal{B}} c_i^{\mathrm{T}} P_i^2 . \tag{3.35}$$

The resulting power allocation optimization problem is defined as follows (with state S_i substituted from Eq. (3.22)):

$$\begin{aligned} \min_{\{P_i, \underline{\epsilon}_i, \overline{\epsilon}_i\}} \quad & q^{\mathrm{P}} \left(P^{\mathrm{req}} - \sum_{i \in \mathcal{B}} P_i \right)^2 \\ & + q^{\mathrm{S}} \sum_{i \in \mathcal{B}} \left(S_{0,i} + \frac{\Delta t}{E_i^{\mathrm{nom}}} P_i - S_i^{\mathrm{tgt}} \right)^2 \\ & + q^{\epsilon} \sum_{i \in \mathcal{B}} (\underline{\epsilon}_i + \overline{\epsilon}_i) \\ & + q^{\Delta} \sum_{i \in \mathcal{B}} (P_{0,i} - P_i)^2 \\ & + q^{\mathrm{u}} \sum_{i \in \mathcal{B}} \left(P_i - \frac{P^{\mathrm{req}}}{N_B} \right)^2 \\ & + q^{\mathrm{T}} \sum_{i \in \mathcal{B}} c_i^{\mathrm{T}} P_i^2 \end{aligned} \tag{3.36}$$

subject to the following constraints for all $i \in \mathcal{B}$:

$$\underline{S}_i - \underline{\epsilon}_i \leq S_{0,i} + \frac{\Delta t}{E_i^{\mathrm{nom}}} P_i \leq \overline{S}_i + \overline{\epsilon}_i \,, \tag{3.37a}$$

$$-\overline{P}_i^{\mathrm{dch}} \leq P_i \leq \overline{P}_i^{\mathrm{ch}} \,, \tag{3.37b}$$

$$P_i \leq \delta^{\mathrm{ch}} \overline{P}_i^{\mathrm{ch}} + \delta^{\mathrm{dch}} P^{\mathrm{trans}} \,, \tag{3.37c}$$

$$-P_i \leq \delta^{\mathrm{dch}} \overline{P}_i^{\mathrm{dch}} + \delta^{\mathrm{ch}} P^{\mathrm{trans}} \,, \tag{3.37d}$$

$$P_i \leq |P^{\mathrm{req}}| + P^{\mathrm{trans}} \,, \tag{3.37e}$$

$$-P_i \leq |P^{\mathrm{req}}| + P^{\mathrm{trans}} \,, \tag{3.37f}$$

$$\underline{\epsilon}_i \geq 0 \,, \tag{3.37g}$$

$$\overline{\epsilon}_i \geq 0 \,. \tag{3.37h}$$

Setpoints for each BESS unit are obtained by solving the given optimization problem at each time step. All variables and parameters are summarized in Table 3.2, categorized into decision variables and known parameters related to the battery group as a whole, individual battery units, and the controller settings.

3.4.3 Quadratic Program Formulation

The presented optimization problem is a quadratic program due to the quadratic objective function and linear constraints. To be efficiently solved using standard QP solvers, the problem is reformulated into standard form:

$$\begin{aligned} \min_{\mathbf{x}} \quad & \frac{1}{2} \mathbf{x}^\top \mathbf{H} \mathbf{x} + \mathbf{f}^\top \mathbf{x} \\ \text{s.t.} \quad & \mathbf{b}_\mathrm{l} \leq \mathbf{A} \mathbf{x} \leq \mathbf{b}_\mathrm{u} \,, \end{aligned} \tag{3.38}$$

where, in general, $\mathbf{x}$ is the vector of optimization variables, $\mathbf{H} \succeq 0$ is the matrix representing the quadratic terms, $\mathbf{f}$ is the linear term vector, and $\mathbf{A}, \mathbf{b}_\mathrm{l}, \mathbf{b}_\mathrm{u}$ define the inequality constraints.

Specifically, vector $\mathbf{x} \in \mathbb{R}^{3N_B}$ contains the charge/discharge powers P_i and auxiliary slack variables $\underline{\epsilon}_i$ and $\overline{\epsilon}_i$ for each BESS unit $i = 1, \ldots, N_B$:

$$\mathbf{x} = \begin{bmatrix} P_1 & \ldots & P_{N_B} & \underline{\epsilon}_1 & \ldots & \underline{\epsilon}_{N_B} & \overline{\epsilon}_1 & \ldots & \overline{\epsilon}_{N_B} \end{bmatrix}^\top . \tag{3.39}$$

The matrix $\mathbf{H} \in \mathbb{R}^{3N_B \times 3N_B}$ is structured as follows:

$$\mathbf{H} = \begin{bmatrix} \mathbf{H}_P & \mathbf{0} & \mathbf{0} \\ \mathbf{0} & \mathbf{H}_{\underline{\epsilon}} & \mathbf{0} \\ \mathbf{0} & \mathbf{0} & \mathbf{H}_{\overline{\epsilon}} \end{bmatrix} \tag{3.40}$$

Table 3.2: Decision variables and parameters of the power distribution optimization problem.

	Description	Unit
Decision variables		
P_i	battery power	(kW)
S_i	battery state of charge	(%)
$\underline{\epsilon}_i, \overline{\epsilon}_i$	slack variables for state of charge	(%)
Battery group		
$\mathcal{B}$	set of battery storage units	–
N_B	number of battery storage units	–
P^{req}	total requested power demand	(kW)
P^{trans}	limit for power transfer between units	(kW)
δ^{ch}, δ^{dch}	binaries indicating charging and discharging	–
Battery units		
E_i^{nom}	nominal capacity	(kWh)
$\overline{P}_i^{\text{ch}}$, $\overline{P}_i^{\text{dch}}$	maximum charging and discharging power	(kW)
$\underline{S}_i$, $\overline{S}_i$	lower and upper state of charge limits	(%)
S_i^{tgt}	target state of charge	(%)
T_i	temperature of the cells	(°C)
$\overline{T}_i$	upper temperature limit	(°C)
$Q_i, Q_i^{\text{gen}}, Q_i^{\text{hvac}}$	heat flows	(kW)
$a_i^{\text{P}}, b_i^{\text{P}}, a_i^{\text{S}}, b_i^{\text{S}}, c_i$	coefficients of the temperature model	–
c_i^{T}	temperature penalization coefficient	–
m_i	mass of the battery cells	(kg)
$c_{p,i}$	specific heat capacity of the battery cells	($\text{J}\,\text{kg}^{-1}\,\text{K}^{-1}$)
Controller		
Δt	sampling time	(h)
$q^{\text{S}}, q^{\epsilon}, q^{\Delta}, q^{\text{u}}, q^{\text{T}}$	weights	–

with:

$$[\mathbf{H}_P]_{i,i} = q^{\mathrm{P}} + q^{\Delta} + q^{\mathrm{u}} + q^{\mathrm{T}} + \frac{\Delta t^2 q^{\mathrm{S}}}{E_i^{\mathrm{nom}^2}}\,, \tag{3.41}$$

$$[\mathbf{H}_P]_{i,j} = q^{\mathrm{P}}, \quad i \neq j \tag{3.42}$$

$$[\mathbf{H}_{\underline{\epsilon}}]_{i,i} = q^{\epsilon}\,, \tag{3.43}$$

$$[\mathbf{H}_{\overline{\epsilon}}]_{i,i} = q^{\epsilon}\,. \tag{3.44}$$

The vector $\mathbf{f} \in \mathbb{R}^{3N_B}$ is defined similarly:

$$\mathbf{f}_i = \begin{cases} -2P_{0,i}q^{\Delta} - 2P^{\mathrm{req}}q^{\mathrm{P}} - 2\dfrac{q^{\mathrm{u}}P^{\mathrm{req}}}{N_B} - 2\dfrac{\Delta t q^{\mathrm{S}}}{E_i^{\mathrm{nom}}}\left(S_{0,i} - S_i^{\mathrm{tgt}}\right), & \text{if } i \leq N_B \\ 0, & \text{otherwise} \end{cases} \tag{3.45}$$

The matrix $\mathbf{A} \in \mathbb{R}^{3N_B \times 3N_B}$ is defined as:

$$\mathbf{A} = \begin{bmatrix} I & \mathbf{0} & \mathbf{0} \\ -\operatorname{diag}\left(\frac{\Delta t}{E_1^{\mathrm{nom}}}, \ldots, \frac{\Delta t}{E_N^{\mathrm{nom}}}\right) & I & \mathbf{0} \\ \operatorname{diag}\left(\frac{\Delta t}{E_1^{\mathrm{nom}}}, \ldots, \frac{\Delta t}{E_N^{\mathrm{nom}}}\right) & \mathbf{0} & I \end{bmatrix} \tag{3.46}$$

with the identity matrix I of size $N_B \times N_B$.

The corresponding lower and upper bounds are:

$$\mathbf{b}_{\mathrm{l}} = \begin{bmatrix} -\overline{P}_1^{\mathrm{dch,mod}} \\ \vdots \\ -\overline{P}_{N_B}^{\mathrm{dch,mod}} \\ \underline{S}_1 - S_{0,1} \\ \vdots \\ \underline{S}_{N_B} - S_{0,N_B} \\ S_{0,1} - \overline{S}_1 \\ \vdots \\ S_{0,N_B} - \overline{S}_{N_B} \end{bmatrix}, \qquad \mathbf{b}_{\mathrm{u}} = \begin{bmatrix} \overline{P}_1^{\mathrm{ch,mod}} \\ \vdots \\ \overline{P}_{N_B}^{\mathrm{ch,mod}} \\ +\infty \\ \vdots \\ +\infty \\ +\infty \\ \vdots \\ +\infty \end{bmatrix} \tag{3.47}$$

where $\overline{P}_i^{\mathrm{ch,mod}}$ and $\overline{P}_i^{\mathrm{dch,mod}}$ are modified charge/discharge power limits based on the allowable power transfer between individual units and on the direction and magnitude of the requested total power. Then, the tightest bound is applied:

$$\overline{P}_i^{\mathrm{ch,mod}} = \min\left(\overline{P}_i^{\mathrm{ch}},\, |P^{\mathrm{req}}| + P^{\mathrm{trans}},\, \overline{P}_i^{\mathrm{ch}} \cdot \delta^{\mathrm{ch}} + P^{\mathrm{trans}} \cdot \delta^{\mathrm{dch}}\right), \tag{3.48a}$$

$$\overline{P}_i^{\mathrm{dch,mod}} = \min\left(\overline{P}_i^{\mathrm{dch}},\, |P^{\mathrm{req}}| + P^{\mathrm{trans}},\, \overline{P}_i^{\mathrm{dch}} \cdot \delta^{\mathrm{dch}} + P^{\mathrm{trans}} \cdot \delta^{\mathrm{ch}}\right). \tag{3.48b}$$

Overall, the first N_B rows of the constraints encode limits on battery power:

$$-\overline{P}_i^{\mathrm{dch,mod}} \leq P_i \leq \overline{P}_i^{\mathrm{ch,mod}}, \quad i = 1, \ldots, N_B \tag{3.49}$$

The remaining $2N_B$ rows enforce lower bounds for SoC deviations, while leaving upper bounds unbounded to enable soft constraint relaxation via slack variables.

3.5 Optimal Component Sizing

Before any control strategy can be deployed in a microgrid, fundamental design decisions must be made—most notably, determining the appropriate size of key components. In the proposed hierarchical control framework, this is the responsibility of the business layer, which operates offline and sets the long-term goals and possibly also the parameters of the microgrid. Usually, the microgrid's fundamental composition is predetermined, but open to extension. The frequent question to be answered is what size of the battery storage is optimal for a given microgrid. Sometimes, the problem is supplemented with the optimal sizing of renewable energy sources, such as photovoltaic systems, but the focus here remains on the storage technologies.

So, the objective of optimal sizing is to determine the ideal storage power and energy capacity that maximizes economic performance, given the microgrid's structure, already decided operational goals, and available historical data. An undersized battery may not provide sufficient benefits to the system, while an oversized battery increases capital expenditures without proportionate returns. As such, sizing is a trade-off problem, seeking to balance investment costs with potential long-term savings or revenues.

Although the sizing task precedes the actual deployment of the control system, it closely builds on the same optimization foundations used in the model predictive control technique described earlier. The key idea of the proposed methodology is to extend the short-term optimization horizon of the MPC to a full year, using historical data on electricity prices, weather conditions, and load profiles to simulate microgrid operation over an extended period. Instead of computing daily control decisions for a fixed storage system, in the sizing problem the battery's power and capacity are the decision variables, optimizing their values to minimize total operational costs over the storage lifetime.

The model, objective function, and most constraints are shared with the MPC formulation; only minor modifications and the inclusion of the sizing variables are necessary. Unlike in the short-term control problem, uncertainties in forecasts are not explicitly assumed, as the long-term effects of variability tend to average out over the evaluation horizon. Due to the long time horizon, the problem scale is large, but the computation is performed offline and only once, meaning that the solving time is not a limiting factor.

The resulting methodology enables informed investment decisions using the same predictive optimization tools later applied in operation. It connects strategic planning with operational control to ensure that promised benefits will be realized in practice, because they are driven by the same modeling and optimization principles.

3.5.1 Related Work

Optimal sizing is a key design task in microgrids, and it has therefore received considerable attention in the literature. The techniques and methods do not differ much from those applied in short-term control problems, they are also based on mathematical optimization, most commonly linear programming or mixed-integer linear programming [104, 105], and then heuristic or artificial intelligence methods, such as fuzzy expert systems, genetic algorithms, and particle swarm optimization [106, 17].

Of particular importance are the criteria used to determine the optimal size of the battery. The performance indicators can be broadly classified into three categories: financial, technical, and their hybrid combination [107]. The greatest motivation for investment into storage technologies is indeed the financial return. Expressing all criteria in terms of monetary value makes comparison easier, but still there are several indicators used to evaluate the financial performance of the battery storage system. The most common is the net present value (NPV) or net present cost (NPC), which is the difference between the present value of all cash inflows and outflows over the lifetime of the battery. As in [108], the NPV may include the initial costs, maintenance and operation costs, replacement costs of the BESS and PV, and the NPV of electricity, while considering interest rates, discounting, and project lifespan. Next is the levelized cost of electricity (LCOE), which reflects the average cost of electricity over the lifetime of the system. Other financial indicators include the payback period (PP), which represents the number of years until the capital costs are paid back; the annualized profit/cost, defined as the difference between the annual savings and the annual costs of the components; and the internal rate of return (IRR), an interest rate at which the NPV of all cash flows is zero [109].

Technical indicators are more case-specific and depend on the microgrid's operational goals. In the optimization problem, they are either included in the constraints or represent the single objective goal. The usual technical targets that should be achieved or improved using the battery storage are the autonomy of the microgrid system, reliability in terms of loss of load expectation (LOLE), avoiding outages and loss of power supply, minimizing curtailed energy, carbon emissions, or improving customer satisfaction [109]. Often a combination of financial and technical indicators is used, when the objective is to minimize the investment and operational costs while the target LOLE is included as a constraint [110].

Despite these advances, the reviewed approaches collectively fail to deliver a battery sizing methodology that uses an evaluation horizon long enough to capture seasonal and inter-annual variability of microgrid operation, sizes storage in both the energy and power dimensions independently rather than fixing the ratio a priori, and transfers the resulting sizes to the actual control policy that will operate the storage. Most studies validate their methods on single representative days or up to one week of data [16, 17, 18], with [111] a rare long-horizon exception. The sizing methodology developed in the remainder of this section addresses these gaps through a long-horizon optimization formulated over the full project lifetime at minute-level resolution, independent decision variables for energy capacity and power rating, and direct integration of the MPC operating policy into the sizing loop.

3.5.2 Problem Formulation

Building upon the short-horizon MPC formulation introduced previously, we now extend the optimization framework to support long-term strategic planning over a multi-year horizon. While the MPC problem focuses on operational decisions within a receding prediction window with fixed system parameters, this investment-level formulation aims to determine the optimal design of key energy system components alongside their operation over the entire project lifetime.

The core structure of the optimization problem remains similar—minimizing costs subject to system dynamics and operational constraints that model the microgrid behavior. However, several fundamental differences are introduced:

- **Horizon length:** The optimization is extended over a long-term horizon (e.g., 15 years). Unlike the receding-horizon approach in MPC, this formulation is solved as a single offline problem, where the optimal investment and operational plan is determined once and applied over the entire project duration.

- **Decision variables:** While the control variables $\mathbf{U}$, states $\mathbf{X}$, costs $\mathbf{C}$, slack variables $\mathbf{E}$, and penalty weights $\mathbf{Q}$ are retained (from Eqs. (3.10)–(3.11)), the uncertainties from $\mathbf{W}$ are now treated as known parameters based on historical data. Binary variables $\mathbf{B}$ are omitted in order to stay in the LP domain, with post-checking of the complementarity conditions.

  Some parameters previously included in $\mathbf{P}$ are now relaxed as optimization variables, forming a new vector $\mathbf{Z}$. Specifically, the battery design parameters—nominal energy capacity E_{nom} and inverter power rating P_{inv} (setting the bounds for both charging and discharging: $P_{\text{inv}} = \overline{P}_{\text{ch}} = \overline{P}_{\text{dch}}$)—are introduced as decision variables. Optionally, other microgrid design parameters such as the grid import limit $\overline{P}_{\text{imp}}$ or the size of other components may also be optimized, providing guidance on sizing the grid connection or additional renewable energy sources.

- **Objective:** The goal is to minimize the net present cost of the system over its lifetime. The NPC consists of two main components: capital expenditures (CAPEX) and operational expenditures (OPEX). CAPEX accounts for the upfront investment costs in the battery storage system, while OPEX represents the yearly operating costs of the system, including energy purchases and demand charges, discounted to present value.

The optimization thus identifies the most cost-effective configuration of the energy system over its entire operational life, taking into account technical constraints, component degradation, and economic factors such as projected electricity price inflation. In addition, it provides an operational strategy and expected power profiles. The full objective is defined as:

$$\min_{\mathbf{X},\mathbf{U},\mathbf{E},\mathbf{Z}} \text{NPC} = \text{CAPEX} + \sum_{y=1}^{N_Y} \frac{1}{(1+r)^{y-1}} \cdot \text{OPEX}^y, \tag{3.50}$$

where r is the discount rate, N_Y is the number of years in the planning horizon, and years are indexed $y \in \{1, \ldots, N_Y\}$ with $y = 1$ denoting the first year of operation, so that the $y-1$ exponent leaves the first-year cost undiscounted.

The capital cost component is expressed as:

$$\text{CAPEX} = c_{\text{E}} \cdot E_{\text{nom}} + c_{\text{P}} \cdot P_{\text{inv}} + c_{\text{F}}, \tag{3.51}$$

where c_{E} and c_{P} are the unit costs of battery energy capacity and power rating, respectively, and c_{F} represents fixed installation costs (e.g., commissioning, infrastructure, battery management system).

The operational cost for year y is defined as:

$$\mathrm{OPEX}^y = C_\mathrm{O}^y + C_\mathrm{M}^y, \tag{3.52}$$

where C_O^y denotes the optimized microgrid operating cost for year y, consistent with the MPC cost formulation (Eq. (3.12)). It typically includes energy procurement costs, demand charges, imbalance penalties or remuneration, renewable incentives, and other operational expenses that are applicable for a particular microgrid. The term C_M^y represents annual maintenance costs of the battery system, scaling linearly with the size of the planned installation. Demand charges are included in the operational costs and are computed based on the optimized maximum power draw from the grid ($\overline{P}_\mathrm{imp}$), multiplied by a fixed demand charge rate (c_D). Battery replacement costs are already included in the operational costs, similarly as they are applied in the MPC formulation.

BESS and PV degradation is modeled via constraints as an annual reduction in usable capacity or power output, and thus implicitly affects the operation and performance of the system. The lifetime of the PV power plant is 20–25 years, but production is expected to decline over time due to degradation. This degradation is modeled as a linear annual decrease in production potential, given by:

$$P_\mathrm{PV}^y = P_\mathrm{PV}^0 \cdot (1 - d_\mathrm{PV})^{y-1}, \tag{3.53}$$

where P_PV^0 is the known PV production in the past year and d_PV is the annual degradation rate, typically $\approx 0.5\%$.

Electricity prices are assumed to follow an inflation rate. The inflation-adjusted price in year y is modeled as:

$$c^y = c^0 \cdot (1 + i)^{y-1}, \tag{3.54}$$

where c^0 is the price level in the past year and i is the assumed annual inflation rate, targeted to be in the range of 2–3%.

Battery aging is modeled through a declining state of health (S_oH), representing the ratio of current usable capacity to nominal capacity. The battery is guaranteed for N_cycles full cycles when the recommended DoD is maintained (with higher DoD one can expect a lower number of life cycles and vice versa), before reaching its end of life. Given a total project lifetime of N_Y years, the maximum allowable number of full cycles per year is:

$$\overline{N}_\mathrm{cyc} = \frac{N_\mathrm{cycles}}{N_Y}, \tag{3.55}$$

which imposes a constraint to ensure that the total number of full equivalent cycles performed in each year does not exceed this limit:

$$N_\mathrm{cyc}^y \leq \overline{N}_\mathrm{cyc}, \quad \forall y \in \{1, \ldots, N_Y\}. \tag{3.56}$$

The number of cycles in year y is calculated from the battery throughput divided by the usable capacity:

$$N_{\mathrm{cyc}}^{y} = \frac{1}{2\, S_{\mathrm{oH}}^{y} \cdot E_{\mathrm{nom}}} \sum_{k=1}^{N} \big(|P_{\mathrm{ch}}(k)| + |P_{\mathrm{dch}}(k)|\big) \cdot \Delta t, \tag{3.57}$$

where N is the number of time steps in year y with duration Δt given in hours. The SoH is modeled as a decreasing exponential function of the number of years passed:

$$S_{\mathrm{oH}}^{y} = (1 - d_{\mathrm{bat}})^{y-1}, \tag{3.58}$$

where d_{bat} is the annual degradation rate of the battery capacity. To determine the appropriate value of d_{bat}, we assume that the battery reaches its end of life when its capacity drops to a defined threshold $S_{\mathrm{oH}}^{\mathrm{EoL}}$ (typically 70–80%) after N_Y years of use. The degradation rate is then computed by solving:

$$(1 - d_{\mathrm{bat}})^{N_Y - 1} = S_{\mathrm{oH}}^{\mathrm{EoL}} \tag{3.59}$$

and for d_{bat} we obtain:

$$d_{\mathrm{bat}} = 1 - \exp\left(\frac{\ln(S_{\mathrm{oH}}^{\mathrm{EoL}})}{N_Y - 1}\right). \tag{3.60}$$

This approach ensures that the battery operation remains within safe usage limits and avoids aggressive cycling.

In the next chapter dedicated to the application of the proposed energy management system, the problem of optimal sizing is demonstrated using a real case study of a commercial microgrid (Section 4.4).

Chapter 4

Application

This chapter presents the results from the application and practical aspects of the proposed energy management system. While previous chapters were devoted to the theoretical foundations of microgrid systems and the methodology of the hierarchical control framework, this chapter focuses on the evaluation and demonstration of the designed methods. Results and data obtained from real-world implementations are complemented by simulation results to demonstrate performance under controlled conditions when necessary.

4.1 Overview

The EMS with hierarchical control was deployed and operated in several real-world microgrid setups, including mid- to large-scale commercial and industrial facilities. This chapter includes a detailed description of the selected microgrid setup, the implementation of the proposed control strategies, and an evaluation of their performance. Over its lifetime, the EMS was deployed in several different configurations, starting with a pilot project and subsequently expanding to other commercial and industrial microgrids across multiple countries. Table 4.1 provides an overview of the microgrid entities where the EMS was implemented, including their composition, functionalities provided by the EMS, and timeframes of operation. The projects vary in size and complexity, ranging from commercial buildings with photovoltaic systems and battery energy storage to industrial parks with multiple energy assets. The depicted functionalities indicate those with the highest relevance; however, in practice, priorities often change and evolve over the lifetime of a project. This further emphasizes the importance of flexibility and adaptability of the EMS, which supports reconfiguration to meet changing microgrid requirements. As a reminder, the aims, goals, and motivations of each microgrid are determined by an external entity, represented in the hierarchical control framework by the uppermost business layer.

Table 4.1: Overview of microgrid projects where the EMS was implemented, including their composition, functionalities (IO: Imbalance Optimization, PA: Price Arbitrage, PS: Peak Shaving, SS: Self-Sustainability, PD: Power Distribution), and timeframes of operation.

ID	Facility	Composition	IO	PA	PS	SS	PD	Timeframe
1	Commercial building	PV (220 kWp), BESS (184 kW/558 kWh), EV chargers (200 kW)	✓		✓			Aug 2024 – Nov 2024
2	Commercial building	PV (150 kWp), BESS (50 kW/151 kWh), EV chargers (132 kW)		✓	✓			Nov 2022 – Nov 2024
3	Industrial park	PV (500 kWp), BESS (92 kW/151 kWh)			✓	✓		Jun 2023 – Nov 2024
4	Industrial park	PV (600 kWp), BESS (200 kW/302 kWh), Heat pumps	✓		✓		✓	Apr 2023 – Nov 2024
5	Industrial park	PV (280 kWp), BESS (100 kW/151 kWh), Heat pumps	✓					Oct 2023 – Nov 2024
6	Industrial park	PV (500 kWp), BESS (80 kW/130 kWh)		✓		✓		Sep 2021 – Aug 2022
7	Industrial park	PV (500 kWp), BESS (150 kW/302 kWh)		✓	✓		✓	Mar 2022 – Dec 2023
8	Mountain resort	PV (800 kWp), BESS (184 kW/558 kWh)			✓	✓		Jun 2024 – Nov 2024
9	Utility BESS	BESS (21 MW/53 MWh)					✓	Mar 2024 – Nov 2024

Note that not every microgrid project employs all layers of the proposed hierarchical control framework. For example, microgrids with a single battery storage system do not require the power distribution algorithm within the power management layer; however, the layer is still present and simplified to a basic power setpoint validation. While the energy management layer is almost exclusively represented by the proposed MPC framework, there is a case where only the power distribution algorithm was required and the energy management layer was outsourced to a third-party system (microgrid project with ID 9). This further highlights the flexibility and modularity of the proposed hierarchical control framework.

4.2 Case Study: Model Predictive Control

One of the setups where the proposed EMS was deployed is the microgrid at a commercial building in the Netherlands (project ID 1 in Table 4.1). This site serves as a representative example due to its combination of diverse controllable assets and participation in real market operations. The system includes a rooftop photovoltaic installation rated at 220 kWp, a battery energy storage system with a rated power of 180 kW and a usable capacity of 558 kWh, a set of electric vehicle chargers with 200 kW available for demand control, while the remaining building consumption belongs to non-controllable electrical loads.

The microgrid is connected to the Dutch distribution grid, with fixed import and export power limits defined contractually. A third-party energy supplier acts as the market interface, responsible for handling electricity trading on the day-ahead market (DAM). This supplier also provides the daily reference schedule (known as the day-ahead diagram), which the EMS uses to guide its short-term planning. Any deviation from this planned schedule—whether due to forecast inaccuracies or operational adjustments—is settled based on real-time market imbalance prices, which introduces both risk and opportunity.

4.2.1 Business Layer and Objectives

The main goal defined by the microgrid owner is to reduce energy-related costs while maintaining reliable and predictable operation. These cost-saving measures are pursued through several EMS-driven functions, including participation in imbalance settlement, utilization of on-site PV, and active limitation of grid exchanges when these are economically disadvantageous.

Among all cost components within the EMS's control, imbalance charges are the most financially significant. When real-time consumption or generation deviates from the day-ahead commitment, the resulting imbalance can either incur a penalty or yield a profit, depending on prevailing imbalance prices. To influence this outcome, the EMS controls the BESS and EV chargers and curtails PV generation when necessary.

The control objectives and actions the EMS is designed to achieve can be summarized as follows:

- Minimizing imbalance charges by aligning operation with the day-ahead schedule, while deliberately deviating from it when opportunities arise to capitalize on favorable real-time market conditions.
- Maximizing utilization of on-site PV generation, particularly when exporting is financially unattractive, while actively curtailing PV output when grid export is not viable.
- Respecting import and export power limits imposed by the distribution network operator by performing peak shaving to avoid penalties, with a preference for supply-side management (e.g., battery discharge) over demand-side management (e.g., EV charging reduction).

Furthermore, the business layer is responsible for determining the acceptable level of risk tolerance. The EMS supports risk-aware control decisions through the CVaR-based formulation, where risk aversion is parameterized by α and configured according to user preferences.

4.2.2 Model Parametrization

For this application, the MPC was configured with a 24-hour prediction horizon, reflecting the daily repetition of consumption and generation patterns. The control interval ΔT was set to 15 minutes, aligned with standard market billing periods, leading to a total of $N = 96$ time steps. However, practice has shown that assuming constant power over 15-minute intervals is not realistic. Therefore, the optimal control actions from the energy management layer are updated every 1 minute, with real-time adjustments handled at the power management layer. This approach has proven to be the best trade-off between computational tractability, available computational resources, and responsiveness to changing conditions.

The forecasted uncertainties in $\mathbf{w}$ include PV generation and load demand. These are modeled using confidence intervals generated from historical data. Day-ahead electricity prices are known in advance and are therefore included directly in the cost vector $\mathbf{c}$. For imbalance prices, only the current value is known in real time; future values are estimated based on historical patterns.

The control inputs $\mathbf{u}$ determined by the MPC include:

- Battery power flow (charging and discharging),
- Curtailment of PV power,
- Controllable EV charging load,
- Power exchange with the external grid,
- Deviation from the day-ahead schedule.

Note that these control inputs are not independent; for example, deviation from the day-ahead schedule is a consequence of the applied control actions. Nevertheless, it is explicitly represented as a decision variable in the optimization problem.

Each action is associated with a corresponding cost. Battery cycling incurs degradation, which is modeled using a penalty proportional to usage. PV curtailment represents a loss of renewable energy. Reducing EV charging may impact user satisfaction due to longer charging times, which is reflected through an associated cost component. These costs, together with other fixed parameters, are summarized in Table 4.2.

4.2.3 Imbalance Price Characterization

Due to their significant influence on operational decisions, imbalance prices were analyzed in more detail. Figure 4.1 shows the distribution of real-time imbalance prices on the Dutch market over September 2024. Prices ranged between -1000 €/MWh and 1850 €/MWh, with median values of 67.0 €/MWh (long) and 79.2 €/MWh (short). The imbalance pricing mechanism depends on the amount of ancillary services required to maintain grid balance; therefore, prices are highly volatile. These prices provide indirect incentives for adjusting the microgrid's balance profile according to the real-time state of the utility grid. The EMS responds to the dual pricing mechanism as follows:

- When both long and short prices are positive, energy deficits are penalized and surpluses are rewarded.

Table 4.2: Microgrid parameters and their values.

Parameter description		**Symbol**	**Value**
Battery nominal energy capacity	(kWh)	E_{nom}	558.0
Battery state of health	(%)	S_{oH}	99.6
Min. state of charge	(%)	$\underline{S}$	10.0
Max. state of charge	(%)	$\overline{S}$	95.0
Charging efficiency	(%)	η_{ch}	95.0
Discharging efficiency	(%)	η_{dch}	95.0
Max. charging power	(kW)	$\overline{P}_{\text{ch}}$	180.0
Max. discharging power	(kW)	$\overline{P}_{\text{dch}}$	180.0
Max. import power	(kW)	$\overline{P}_{\text{imp}}$	49.0
Max. export power	(kW)	$\overline{P}_{\text{exp}}$	150.0
Cost of imported energy	(€/MWh)	c_{imp}	100.0
Cost of exported energy	(€/MWh)	c_{exp}	1.5
Cost of charging	(€/MWh)	c_{ch}	0.0
Cost of discharging	(€/MWh)	c_{dch}	25.0
Cost of PV curtailment	(€/MWh)	c_{curt}	5.0
Cost of load adjustment	(€/MWh)	c_{adj}	600.0
Penalty for exceeding lower SoC limit	(€/kWh)	$\underline{q}_{\text{E}}$	1×10^6
Penalty for exceeding upper SoC limit	(€/kWh)	$\overline{q}_{\text{E}}$	1×10^6
Penalty for exceeding import limit	(€/kW)	q_{imp}	1×10^5
Penalty for exceeding export limit	(€/kW)	q_{exp}	1×10^5

- When both prices are negative, surpluses incur penalties.
- When prices differ in sign, any deviation from the scheduled balance leads to a financial loss.

The most common state is when both long and short prices are equal at a given time. Alternatively, the long price may exceed the short price, but never the opposite.

4.2.4 Risk Aversion Analysis

The level of risk aversion is determined by the parameter α, which reflects how conservatively the controller should behave with respect to uncertainty. This parameter is adjusted by the user or operator based on risk preferences. To assess its impact on operational performance and to support informed decisions regarding the trade-off between profit and risk, simulations were conducted for varying values of α.

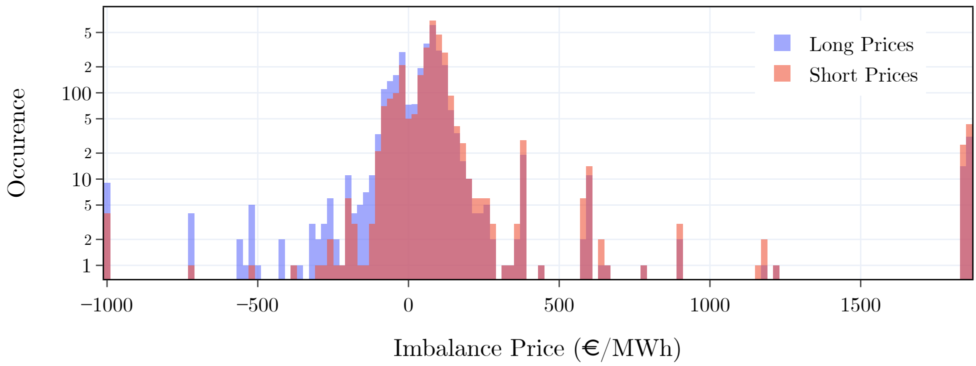

Figure 4.1: Distribution of Dutch imbalance prices (occurrence on a logarithmic scale), with typical values around 70–80 €/MWh and rarer but significant occurrences of extreme prices.

The parameter α defines how cautious or risk-seeking the controller is. Lower values of α lead to more conservative behavior—favoring robustness over potential gains—while higher values encourage more aggressive strategies, prioritizing performance under expected conditions but exposing the system to higher risk. For example, with a low α, the controller plans for more extreme future scenarios, possibly charging the battery during expensive hours to ensure sufficient reserve capacity. In contrast, a high α implies that the system assumes more optimistic forecasts, using storage more opportunistically for revenue-generating services, even if this increases exposure to forecast errors or operational constraints.

To evaluate the real-world implications of different risk profiles, a closed-loop simulation was performed using historical forecast and measurement data. One hundred different realizations of uncertain parameters were randomly generated to simulate possible future microgrid conditions. For each realization, the proposed MPC framework was executed with identical parameters except for varying α values, ranging from 0% (most conservative) to 100% (most aggressive) in increments of 25%. Figure 4.2 presents the results. For each value of α, profit distributions are illustrated using key percentiles, highlighting performance in both typical and tail cases.

As expected, conservative settings such as $\alpha = 0\%$ limit the potential for large losses, offering the strongest protection in worst-case outcomes, but underperform under normal conditions. At the other extreme, the fully aggressive setting ($\alpha = 100\%$) performs well in favorable scenarios but does not protect against losses when reality diverges from forecasts. The results indicate that moderate levels of risk aversion, such as $\alpha = 25\%$ or 50%, provide a balanced outcome.

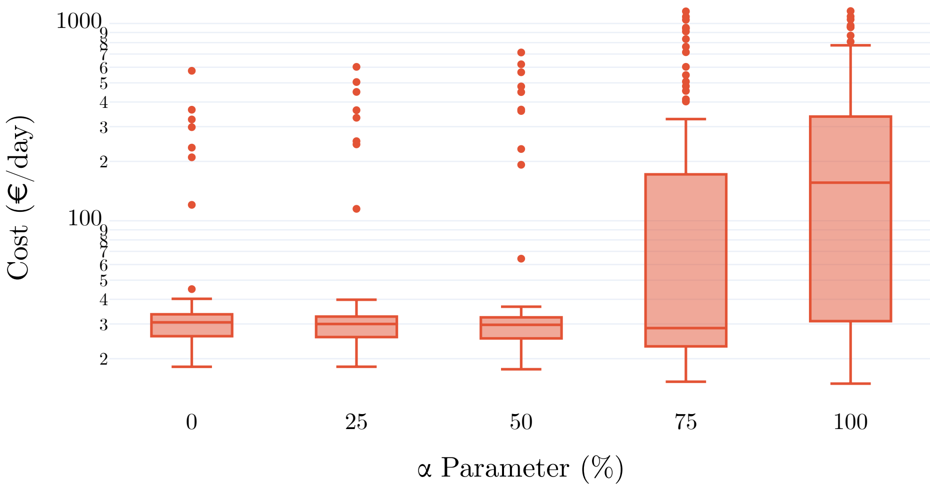

Figure 4.2: Box plots of the cost distribution (100 runs) for each α value. The lowest cost was obtained with $\alpha = 100\%$, and the best median cost was obtained with $\alpha = 75\%$; however, these choices also come with several high-cost outcomes.

The influence of α is further illustrated in Figure 4.3, which shows an example of 25 possible realizations of daily power consumption generated within the depicted confidence interval, along with the selected scenario corresponding to a given α. The α-scenario is computed from the cost distribution as the average of the worst $\alpha\%$ scenarios. At high α values, the selected scenario closely tracks the nominal forecast, whereas at lower values it shifts toward the less favorable confidence bound. The algorithm naturally identifies whether greater caution is required toward the upper or lower bound, independently for each uncertain parameter.

The choice of α also depends on the quality of the forecasting models and the reliability

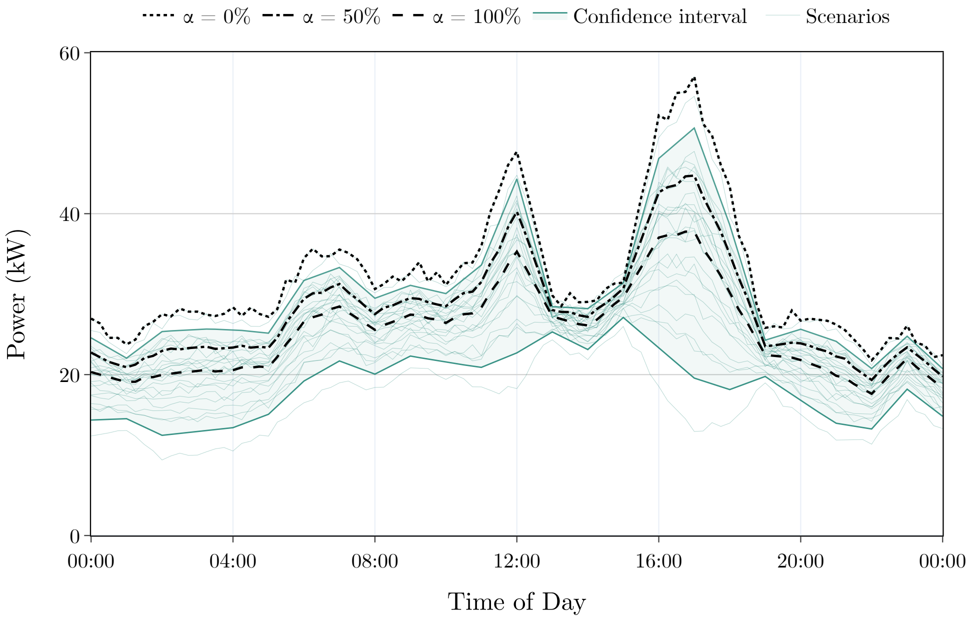

Figure 4.3: Output from the forecasting model for daily consumption P_{cons} (90% confidence intervals), including an example of 25 generated scenarios and the computed α-scenario for different values of α.

of their outputs. It may further depend on user preferences, the type of objectives, the presence of backup options, and other contextual factors. In this specific case, a value of $\alpha = 30\%$ was selected as a good compromise between risk and performance.

4.2.5 Performance Evaluation

In this particular microgrid, the EMS had been running since September 2024 for a period of three months. Its operation is illustrated in Figure 4.4 using data from October 8$^{\text{th}}$, a representative weekday with typical variability in PV generation and electricity demand. The plot compares the actual power exchange with the grid to a hypothetical scenario in which no control actions are applied. This reference is reconstructed by removing the recorded control signals and estimating the corresponding power flow using the system's balance equation.

Grid import is limited to 49 kW, as indicated by the dashed line. Several instances occurred during the day when demand exceeded the combined output of PV generation and the allowed grid import. During these periods, battery discharging compensated for the deficit, keeping the system within its power limits. An hourly breakdown of operational revenues and costs for this day is depicted in Figure 4.5. The evaluated total daily cost without active EMS control would have been 12.1 €, whereas optimal power flow management reduced costs to −3.0 €, resulting in a net profit. While absolute values are less relevant, the difference of 15.1 € for this day represents the EMS yield.

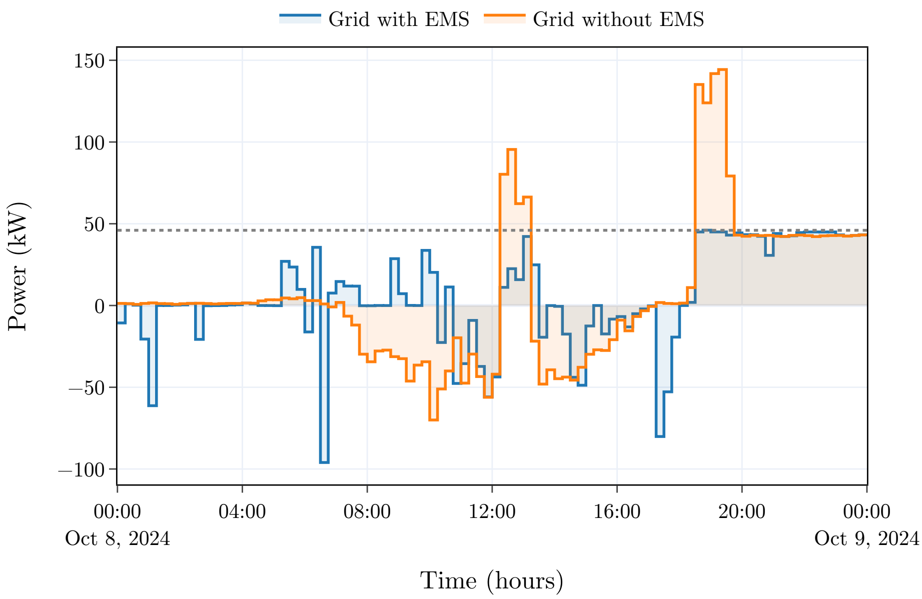

Figure 4.4: Power exchange with the grid on a representative day (negative values indicate exports to the grid). Actual operation (blue line) is compared with a reconstructed no-control case (orange line). The dashed line indicates the maximum grid import limit.

To visualize longer-term performance, Figure 4.6 shows power flows of generation, consumption, and storage over an entire month. PV production exhibits expected diurnal patterns, while consumption is less regular, with occasional high-demand events. Storage acts as the most flexible asset, responding to instantaneous conditions

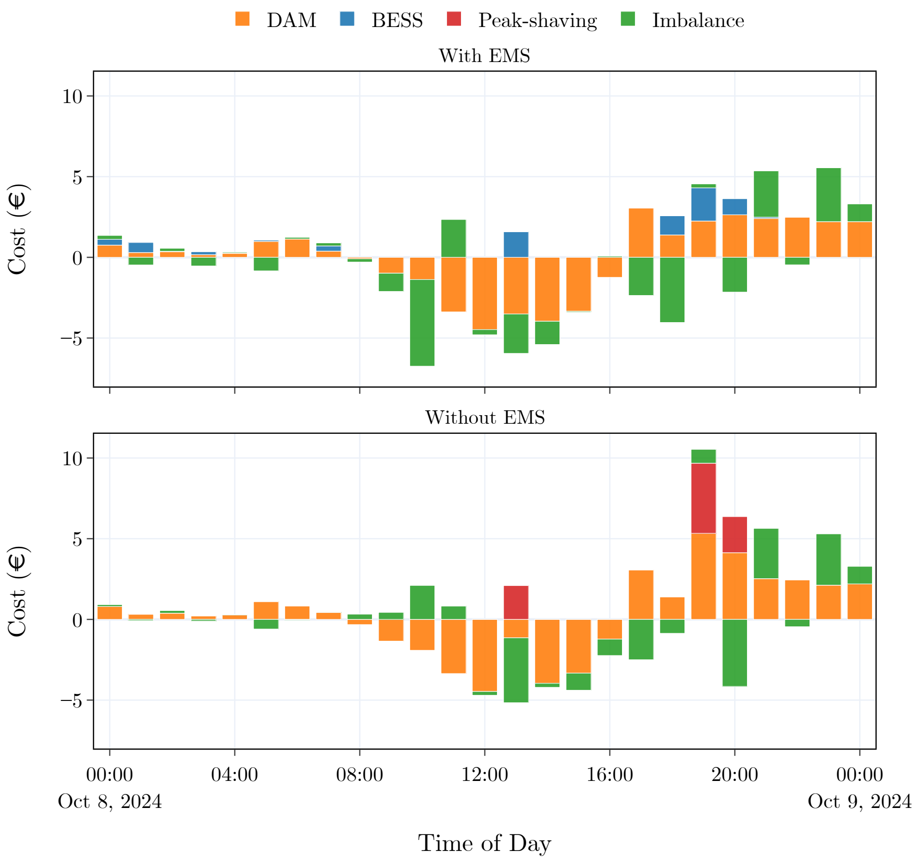

Figure 4.5: Hourly breakdown of operational revenues and costs on a representative day. The EMS avoided penalties and shifted operation toward profitable periods. As a result, total costs were -3.0 €/day compared to 12.1 €/day without EMS control.

while considering forecasts several hours ahead. As a result, battery charging occurred primarily during periods of energy abundance or favorable imbalance prices, while discharging aligned with periods of higher demand or elevated market prices. The EMS, capable of accounting for multiple objectives, components, and operating conditions, ensures that storage and other assets are positioned optimally with respect to the defined control goals.

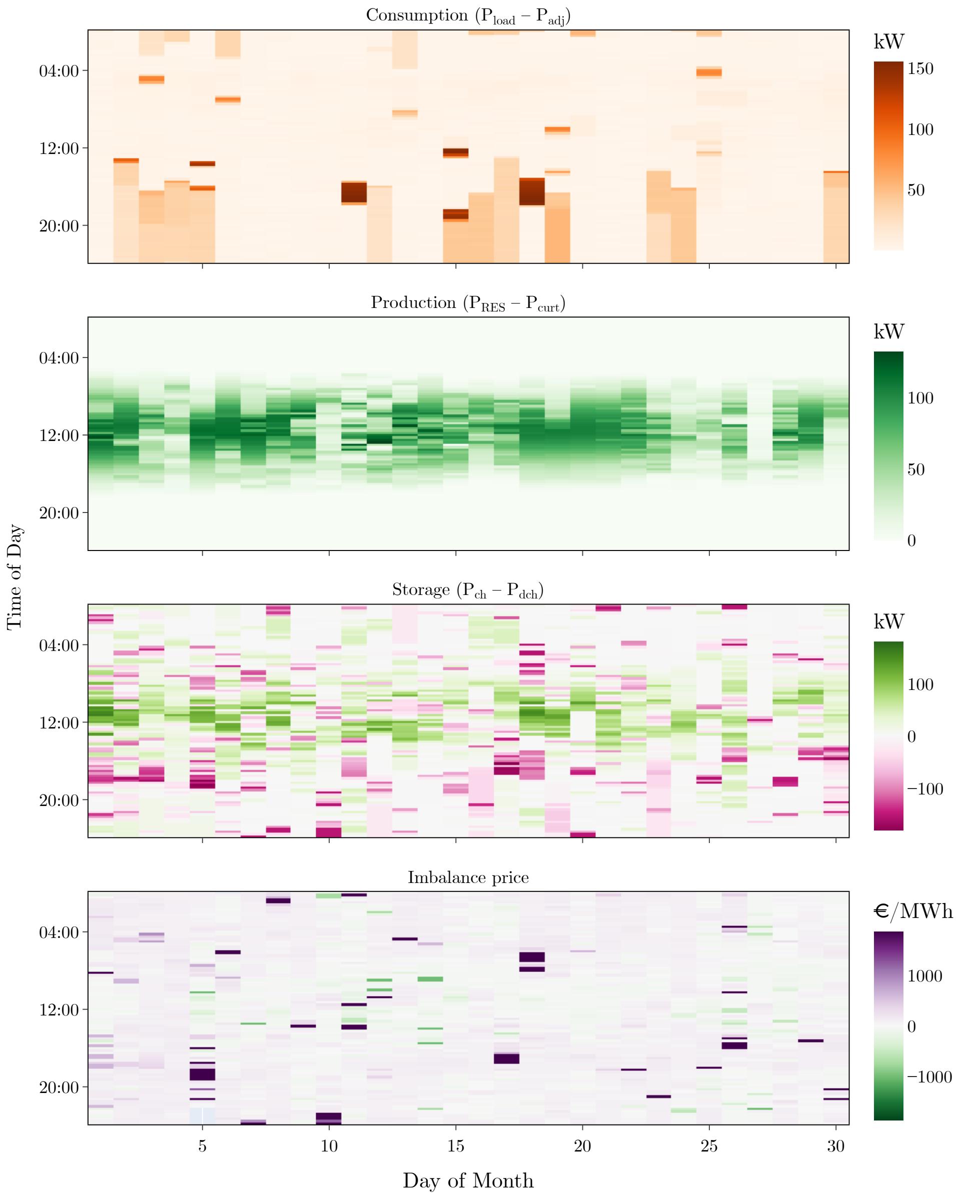

Figure 4.6: Monthly power profiles for consumption, generation, and storage. The bottom plot shows the imbalance price.

A detailed summary of revenues and costs over the examined month is provided in Table 4.3. Without any control, the microgrid would have incurred significant imbalance penalties of 600.4 € and peak-shaving violations amounting to 267.0 €. With EMS control, the imbalance position was actively managed, resulting in negative costs of −2471.1 €, in other words, positive revenue. Active battery usage incurred additional expenses reflecting degradation costs, estimated at 210.0 €. Expenses related to the day-ahead market slightly increased due to higher traded volumes; however, overall benefits outweighed the costs. This led to a total profit of 1855.8 € for the month, compared to a cost of 1193.6 € without EMS control. The monthly profit alone exceeds the site's baseline monthly electricity cost, putting the magnitude of the savings in perspective for a commercial building of this scale.

Table 4.3: Breakdown of operational revenues and costs over one month, with and without EMS. Positive values represent costs; negative values represent revenue.

Revenue/Cost Component		**Without EMS**	**With EMS**
Imbalance market	(€)	600.4	−2471.1
Day-ahead market	(€)	326.2	405.3
Battery degradation	(€)	0.0	210.0
Peak shaving	(€)	267.0	0.0
Total Cost	(€)	1193.6	−1855.8

The actual benefit of the EMS service is the difference between the total costs with and without EMS control, amounting to 3049.4 € for the month. This value represents the added benefit generated by the EMS through cost savings and revenue creation enabled by optimized operation of microgrid assets. As this value depends on the size of the microgrid and its assets, it is useful to normalize the profit to the rated power of the battery storage system, which is common practice in the industry when comparing different installations. To facilitate interpretation, Table 4.4 reports the total profit relative to the battery's rated power. The profit for the examined month was 17 €/kW, with an estimated annual profit of 159 €/kW.

Results are microgrid-specific, as they depend on system composition, size, operational conditions, and, most importantly, the set of services and functionalities provided by the EMS. However, observations from other microgrid projects indicate that an expected annual profit exceeding 150 €/kW is achievable for microgrids participating in the imbalance market and equipped with battery storage systems with a C-rate of up to 0.5C.

Table 4.4: Profit from operation over one month and one year, normalized to battery rated power.

		1 Month	1 Year*
Total Profit	(€)	3049	28 700
Profit per kW	(€/kW)	17	159

* Annualized based on three months of EMS operation.

4.2.6 Discourse on EMS Economy

Achieved return of 159 €/kW/year compares favorably with published benchmarks. According to [112], a revenue of approximately 145 €/kW/year is typically sufficient to reach a 10% internal rate of return. The achievable revenue is highly dependent on the markets in which the microgrid operates. A direct comparison with studies focusing on imbalance market participation is limited. In [8], the theoretical revenue potential of a BESS operating on the Belgian imbalance market was evaluated on a monthly basis. Two months with extreme price behavior were selected: one with the lowest average imbalance price of 33 €/MWh and another with the highest average price of 216 €/MWh. In a simulated environment, the resulting monthly BESS revenue was 5.3 €/kW for the low-price month and 21.8 €/kW for the high-price month, indicating that expected returns lie between these values. During our test period, the average monthly imbalance price ranged between 67 and 79 €/MWh, which can be considered typical. Under these conditions, the EMS achieved a profit of 17 €/kW, placing the result well within the expected range. For a directly comparable real-experimental study, [3] reports energy-arbitrage savings of up to 50 £/day on a 240 kW/180 kWh battery integrated with photovoltaic generation and flexible buildings in the UK, equivalent to roughly 85 €/kW/year. The higher result achieved here reflects the broader revenue stack exploited by the proposed EMS, including imbalance-market participation that is not addressed in [3].

This addresses the economics of microgrid operation, but not the economics of the EMS itself. The business model for energy management systems is often underexamined in the literature, even though it is essential to their long-term viability. Although microgrids can benefit from lower operating costs and additional revenue streams, the EMS provider incurs ongoing costs associated with system operation, maintenance, monitoring, and customer support. For the service to be sustainable, the EMS must generate sufficient revenue to cover these costs and enable continued development. When the control system is provided as a service—referred to here as Energy

Management-as-a-Service—a clearly defined billing model is therefore required.

In this analysis, the EMS provider receives a share of the profit generated by the EMS, commonly referred to as a “success fee,” with values between 10% and 20% considered acceptable in practice. This model aligns incentives between the microgrid owner and the EMS provider, as the provider’s revenue is directly linked to the performance improvements delivered by the EMS.

The EMS operates as a cloud-based EMaaS solution, relying on external computing resources and incurring recurring monthly costs. The leading cloud service providers by market share include Amazon Web Services (AWS), Microsoft Azure, and Google Cloud Platform. For the cost analysis, Amazon EC2 On-Demand pricing as of June 2025 was used. A general-purpose medium-sized virtual CPU (vCPU) instance with one core and 4 GiB of memory was selected as a representative unit. Its cost is 0.0694 \$/hour, corresponding to approximately 49.97 \$/month (42.63 €/month). The EMS solution is constructed by stacking such vCPU units.

The total cloud infrastructure cost of running the EMS consists of fixed expenses that are independent of the number of microgrids in the portfolio, and variable expenses that scale with the number of managed microgrids. Fixed costs include database hosting, the web interface, and other supporting services, which are handled by shared vCPU resources. Computational resources for running the MPC are allocated separately for each microgrid project, as these scale approximately linearly with the number of microgrids. Table 4.5 summarizes the estimated number of vCPUs allocated to each service.

Table 4.5: Number of vCPUs allocated for each EMS service.

Service	**vCPUs**
Database	4
Web interface	2
Other services	1
MPC computation	$N_M \times 1$

This straightforwardly sets the minimum monthly revenue required per microgrid to cover the variable costs (c_v), which correspond to the price of one vCPU (c_1), i.e., 42.63 €/month. This threshold establishes a practical criterion for deciding whether to include a new microgrid project in the EMS portfolio. The fixed costs (c_f) are shared among all managed microgrids (N_M), meaning that the cost per microgrid decreases as the portfolio grows. On the revenue side, the EMS provider earns a share of the total economic benefit generated for the microgrid owner, denoted by r. The total costs and total revenues can therefore be expressed as:

$$C(N_M) = c_f + c_v \cdot N_M, \tag{4.1a}$$

$$R(N_M) = r \cdot N_M. \tag{4.1b}$$

The break-even point for the EMS provider is reached when the total revenue equals the total cost of operating the EMS, i.e., $C(N_M) = R(N_M)$. Solving this condition yields the minimum number of microgrids N_M^{BE} required for the service to become profitable:

$$N_M^{\mathrm{BE}} = \frac{c_f}{r - c_v}. \tag{4.2}$$

This expression illustrates the importance of minimizing variable costs: if the variable cost per microgrid approaches the revenue per microgrid (r), the break-even point shifts toward an impractically large portfolio size. Consequently, careful consideration of algorithmic complexity and computational requirements is necessary to ensure cost efficiency and long-term financial viability of an EMaaS offering.

Our previous analysis in [23] provided guidance on selecting alternative cloud computing paradigms for MPC execution, including event-driven serverless computing (e.g., AWS Lambda) and containerized computing (e.g., AWS Fargate). That study identified conditions under which it becomes cost-efficient to replace on-demand vCPUs with serverless solutions, depending on the scale and runtime of the optimization problem. In particular, serverless computing was shown to be more economical when the optimization runtime can be reduced below approximately 12 seconds.

The current EMS deployment was evaluated accordingly, with fixed costs $c_f = 7c_1$ and variable costs $c_v = c_1$. The revenue share was conservatively set to $r = 10\%$ of the total profit generated for the microgrid owner. Assuming the achieved profit from the previous analysis of the exemplary microgrid, and assuming an average mid-scale battery storage system with a rated power of 125 kW, the break-even point was calculated as $N_M^{\mathrm{BE}} = 2.4$ microgrids. The resulting break-even behavior is illustrated in Figure 4.7, where the total EMS profit is plotted against the number of microgrids in the portfolio.

The break-even point is reached when total revenue exceeds total costs; in this case, at least three microgrids are required for profitability. However, this value represents a necessary minimum, as the analysis considers only the operational costs of running the EMS and does not account for development, deployment, and ongoing maintenance expenses. In practice, the EMS provider should therefore aim for a larger portfolio to ensure robust profitability and long-term sustainability of the service.

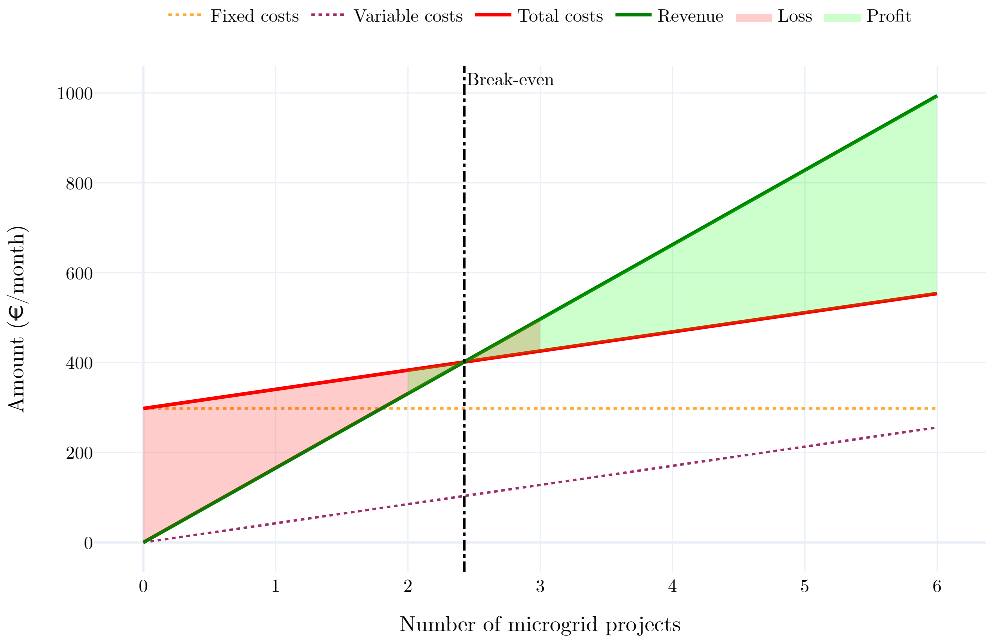

Figure 4.7: Economics of the EMS as a function of the number of microgrids in the portfolio. The break-even point is reached when total revenue exceeds total operating costs.

4.2.7 Computational Complexity

Stochastic MPC is computationally demanding, particularly for large-scale systems with multiple assets and uncertain inputs. Achieving sufficiently fast solution times for real-time deployment using free and open-source software was the primary motivation for developing the proposed time-reduction technique. The computational time required to solve the optimization problem increases with the prediction horizon N, the number of scenarios N_S, the number of control variables, parameters, and the number of constraints. Among these factors, the number of scenarios N_S is both the most influential and the most adjustable, while the remaining dimensions are largely dictated by the microgrid configuration.

The scaling of the optimization problem—measured in terms of continuous and binary decision variables, parameters, and constraints—as a function of the number of scenarios is summarized in Table 4.6. As expected, all quantities grow approximately linearly with N_S, resulting in a rapid increase in problem size for larger scenario sets.

Table 4.6: Problem size for varying number of scenarios.

N_S	**Continuous Var.**	**Binary Var.**	**Parameters**	**Constraints**
1	2310	192	2799	3068
5	11 546	960	5487	15 348
10	23 091	1920	8847	30 698
25	57 726	4800	18 927	76 748
50	115 451	9600	35 727	153 498
100	230 901	19 200	69 327	306 998

The motivation for conducting a detailed computational time analysis was twofold. First, it aims to quantify the computational savings achieved by the proposed time-reduction technique in comparison to a full stochastic MPC formulation. Second, it seeks to characterize the relationship between the number of scenarios and the resulting computational time. This relationship provides practical guidance for selecting an appropriate number of scenarios for a given microgrid setup and available computational resources, such that real-time operation remains feasible.

All experiments were conducted on a MacBook Air M2 equipped with an 8-core CPU, 24 GB RAM, and a 512 GB SSD. The optimization problem was formulated in Python using the `pyomo` library and solved with the `GLPK` solver. Computational times were measured for the same microgrid configuration as described in the previous sections, using a prediction horizon of $N = 96$ and varying the number of scenarios N_S from 1 to 100. Table 4.7 compares the runtimes of the full stochastic MPC formulation and the proposed relaxed formulation. Reported values are averaged over 50 runs, with maximum observed runtimes also indicated.

While the scale of the optimization problem in terms of the number of decision variables grows linearly with the number of scenarios, the computational time grows exponentially. As a result, relying on the original sMPC formulation quickly becomes intractable for real-time operation, as the solver runtime exceeds the desired limit of one minute. The proposed LP relaxation technique significantly reduces the computational time, making it feasible to solve the problem in real time even for a larger number of scenarios.

This reduction comes at the cost of relaxing complementarity constraints. To ensure

Table 4.7: Computational time for solving the optimization problem with varying number of scenarios N_S, comparing full and relaxed sMPC formulations. Results are averaged over 50 runs. The symbol † indicates a solver timeout after 60 minutes.

N_S	Full sMPC (s)		Relaxed sMPC (s)	
	Max. Runtime	**Avg. Runtime**	**Max. Runtime**	**Avg. Runtime**
1	2.2	1.8	1.9	1.6
5	345.7	274.6	5.9	3.6
10	1820.4	1811.8	9.7	7.7
25	†	†	37.5	34.6
50	†	†	157.1	126.7
100	†	†	761.9	577.6

feasibility with respect to the original non-linear formulation, the relaxed sMPC must therefore be supplemented with a consecutive dMPC stage. However, the dMPC is not computationally demanding: its solving time is comparable to that of the full sMPC with a single scenario. Consequently, the inclusion of dMPC does not significantly affect the overall runtime of the control procedure.

While measuring runtime in simulation provides an evaluation under controlled conditions and is well suited for benchmarking, runtime measured during real-world operation offers a more realistic perspective. In practice, deviations from expected runtimes may occur due to external factors such as server load, database load, network latency, communication delays, temporary outages, and other operational conditions. The measured runtime from real-world deployment therefore includes the complete execution chain, from triggering the MPC computation to receiving the optimal control actions, including data retrieval, scenario generation, sMPC and dMPC execution, and data pre- and post-processing. As such, it reflects the end-to-end performance rather than the solver time alone.

The measured runtime for the showcase microgrid is visualized in Figure 4.8. For this microgrid, the number of scenarios was set to $N_S = 20$, selected to satisfy the following conditions: an average runtime below 10 seconds and a worst-case runtime below 60 seconds, given the available computational resources. The figure presents runtime data over a one-month period with a one-minute resolution, along with a zoomed-in view of an 8-hour window for closer inspection.

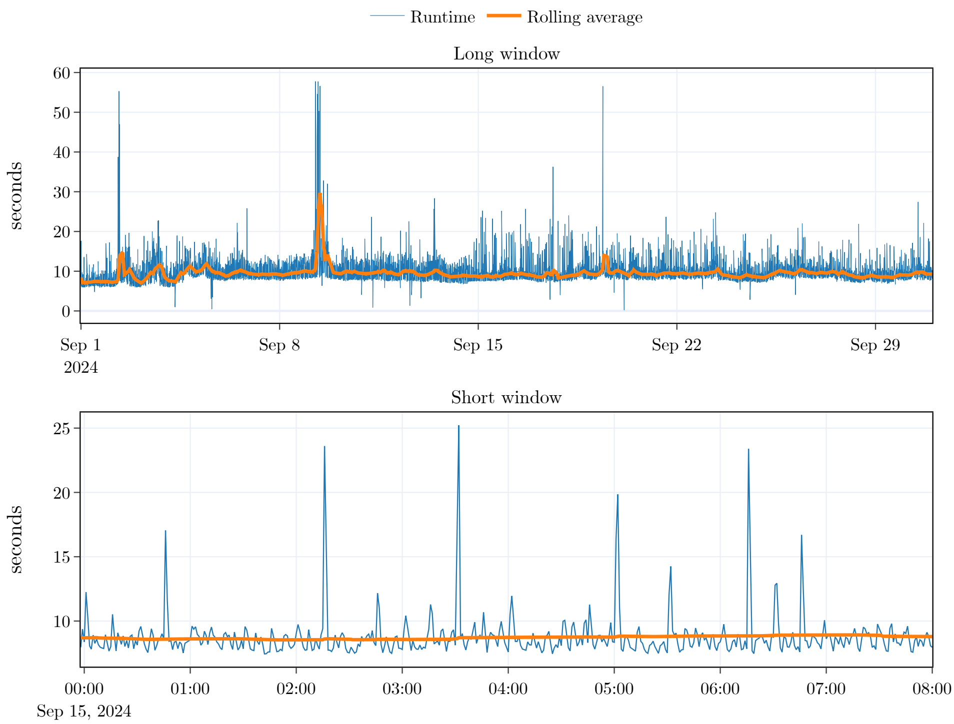

Figure 4.8: Measured runtime of the full MPC procedure during real-world operation. The bottom plot provides a zoomed-in view, showing occasional deviations from the 4-hour rolling average.

The average runtime over the month was 9.4 seconds, with a maximum observed runtime of 57.8 seconds, which is consistent with the real-time requirements. The availability of the MPC service—defined as the share of successful calls for which a response was received within the required time frame—was monitored throughout the operational period. For the presented microgrid and the examined period of September 2024, the availability reached 99.86%, indicating that the EMS reliably delivered control actions in nearly all cases.

4.3 Case Study: Power Distribution

The second case study shifts the focus further down the hierarchical control framework to the power management layer, which is responsible for real-time power distribution among controllable assets. The functionality and performance of the proposed algorithm are first demonstrated in a simulation environment, followed by results from real-world microgrid operation. For this case study, microgrid project with ID 7 from Table 4.1 was selected, as it contains two independent battery energy storage systems.

4.3.1 Simulation Environment

A closed-loop simulation was conducted to evaluate the performance of the proposed algorithm in distributing a requested power setpoint among multiple battery storage systems. The simulation environment included three batteries with distinct parameters and initial conditions, as summarized in Table 4.8. The maximum charging and discharging power for each battery was set as $\overline{P}_i^{\mathrm{ch}} = \overline{P}_i^{\mathrm{dch}} = \overline{P}_i$. The batteries were allowed to exchange power up to $P^{\mathrm{trans}} = 70\,\mathrm{kW}$, and a temperature penalty was applied when the temperature exceeded $\overline{T} = 30\,°\mathrm{C}$. Additionally, an HVAC cooling power of $2\,\mathrm{kW}$ was applied whenever the temperature rose above $23\,°\mathrm{C}$.

The simulation was performed over a 90-minute horizon with a time step of $\Delta t = 1\,\mathrm{s}$, and the total power setpoint P^{req} was updated every 15 minutes.

Table 4.8: BESS parameters and initial conditions used in the simulation.

i	E_i^{nom} (kWh)	$\overline{P}_i$ (kW)	$\underline{S}_i$ (%)	$\overline{S}_i$ (%)	$S_{0,i}$ (%)	$T_{0,i}$ (°C)
1	120	90	10	90	90	25
2	150	140	10	90	65	33
3	180	150	10	90	19	23

The simulation results are presented in Figure 4.9. The first row illustrates the requested total power setpoint P^{req} and the actual power delivery $\sum_i P_i$. The second row shows the individual battery power contributions P_i. The third row depicts the energy states of each battery, with the target state of charge S_i^{tgt} indicated by the red dashed line (which is uniform across batteries in this case due to identical SoC limits; otherwise, it may differ among units). The fourth row presents the temperature profiles of each battery.

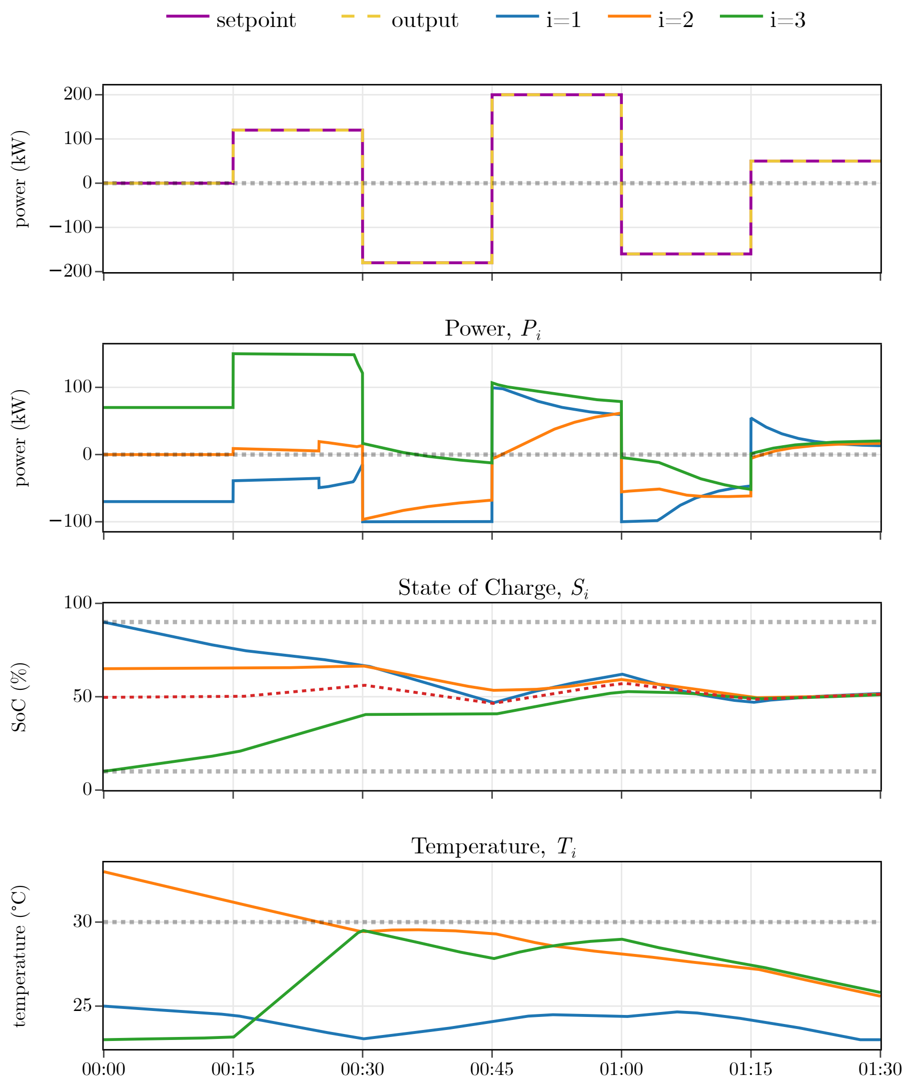

Figure 4.9: Results of the closed-loop simulation. First row: requested total power setpoint P^{req} and actual power delivery $\sum_i P_i$; second row: individual battery power contributions; third row: energy states with the target state of charge S_i^{tgt} indicated by the red dashed line; fourth row: battery temperature profiles, with the dotted line marking the 30 °C threshold—one battery starts above the threshold and is idled until it cools below it.

The simulation was performed to demonstrate the effectiveness of the proposed algorithm in distributing the requested power setpoint among the available battery energy storage systems. The algorithm successfully satisfied the power request at every time step—the total delivered power was equal to the requested setpoint—while respecting the individual limits of each battery. Initially unbalanced battery states converged toward equilibrium, and temperatures were stabilized below the desired limit. The overheated battery unit remained idle until its temperature dropped below the threshold, while the other two batteries continued to deliver the requested power. A non-zero value of P^{trans} allowed batteries to exchange power—one battery charging while another was discharging—even when the total power request was zero, enabling faster convergence toward a balanced state.

The algorithm is designed to be always feasible, even in situations where the power demand cannot be fully delivered by the available batteries due to their limits, for example when the batteries are depleted or when the requested power exceeds the sum of their maximum power ratings. In such cases, the algorithm distributes the maximum feasible power, and the requesting entity is informed about the remaining unmet power.

The algorithm was developed with scalability in mind, allowing it to manage systems with a large number of battery units. To evaluate its scalability, a runtime analysis was conducted to determine the theoretical limit on the number of batteries the algorithm can handle in real time. The computational time was measured for varying numbers of batteries with randomly assigned parameters. The analysis was performed on a MacBook Air M2 with an 8-core CPU, 24 GB RAM, and a 512 GB SSD. The QP problem was solved using DAQP [113], a dual active-set solver interfaced with Python. The average and maximum computation times obtained from 100 runs are reported in Table 4.9.

The results indicate that the algorithm is computationally efficient, with an average solving time below 30 ms for up to 100 batteries, which covers the majority of practical microgrid applications. The maximum runtime remains below 40 ms, well within the requirements for real-time operation. As the computational time grows rapidly with the number of batteries, systems with more than approximately 200 batteries would require partitioning the storage fleet into smaller clusters, with each cluster managed independently by the algorithm, to ensure efficient and reliable real-time execution.

Table 4.9: Computational time for solving the power distribution problem with varying numbers of batteries. The results are averaged over 100 runs.

N_B	**Avg. Runtime (ms)**	**Max. Runtime (ms)**
2	0.06	0.15
5	0.09	0.11
10	0.20	0.24
20	0.63	0.66
50	4.57	5.17
75	13.56	23.51
100	27.64	39.54
200	189.16	218.23
500	2784.93	3302.47

4.3.2 Field Operation

After validation in the simulated environment, the algorithm was integrated into the EMS of an existing microgrid. The facility is a manufacturing plant equipped with a rooftop photovoltaic system that utilizes battery storage for peak shaving, price arbitrage, and storing renewable energy when power production exceeds consumption. The microgrid, in addition to other energy assets, contains two independent lithium-ion NMC chemistry battery storage systems with distinct parameters.

Different power output limits complicate the maintenance of balanced battery states, as higher requested power levels inevitably lead to state divergence. The first BESS has maximum charging and discharging power limits of $\overline{P}_1^{\mathrm{ch}} = \overline{P}_1^{\mathrm{dch}} = \overline{P}_1 = 50\,\mathrm{kW}$ and a nominal energy capacity of $E_1^{\mathrm{nom}} = 151\,\mathrm{kWh}$. The second BESS has a rated power of 100 kW and the same nominal capacity of 151 kWh. A photograph of the latter system is shown in Fig. 4.10.

Due to the recommended depth of discharge of 80 %, both batteries are operated within the SoC range of 10 % to 90 %. The main parameters of the two storage systems are summarized in Table 4.10. An HVAC system is also present at the site, but it is not under direct control of the algorithm. In fact, a suboptimally designed HVAC system with insufficient cooling capacity was one of the motivations for explicitly considering thermal effects in the power distribution algorithm.

The battery storage systems have been seamlessly controlled by the proposed algorithms

Figure 4.10: Battery container of the 100 kW/151 kWh system. On the left-hand side, battery cells are organized into ten modules; on the right-hand side, the power conversion system (PCS) is located, consisting of two 50 kW inverters and a control panel with the battery management system and switchgear.

Table 4.10: Parameters of the two BESS units installed in the microgrid.

i	E_i^{nom} (kWh)	$\overline{P}_i$ (kW)	$\underline{S}_i$ (%)	$\overline{S}_i$ (%)	$\overline{T}_i$ (°C)
1	151	50	10	90	28
2	151	100	10	90	28

for several months. A comprehensive visualization of one month of operation is presented in Fig. 4.11. Over this period, the batteries consistently delivered power as requested by the grid operator, maintained balanced states of charge, and operated within the desired temperature limits.

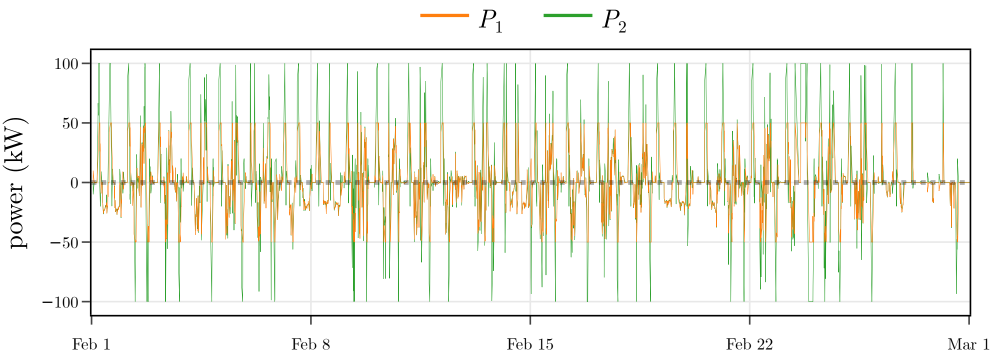

Figure 4.11: Monthly operation of two battery energy storage systems. The plot illustrates the actual power delivery of both units.

To provide a more detailed perspective, a two-hour window was selected for closer examination. The resulting power and state profiles during this period are depicted in Fig. 4.12. The observed behavior aligns with the expected and desired outcomes. The total power demand was met at every time step, with a sampling interval of 5 s. During periods of maximum power demand, when the requested total power P^{req} reached 150 kW, both batteries operated at their respective maximum power limits. This inevitably led to a temporary imbalance in their states of charge, as the battery with the higher power rating charged or discharged more rapidly. When the power demand decreased, the optimal power allocation strategy ensured that the energy states of the batteries returned to balance as quickly as possible. To prevent overuse and excessive cycling, the algorithm limited the energy transfer between the batteries to a maximum of $P^{\text{trans}} = 20\,\text{kW}$. This controlled energy exchange allowed the fuller battery to support the emptier one, promoting balanced utilization while adhering to operational constraints.

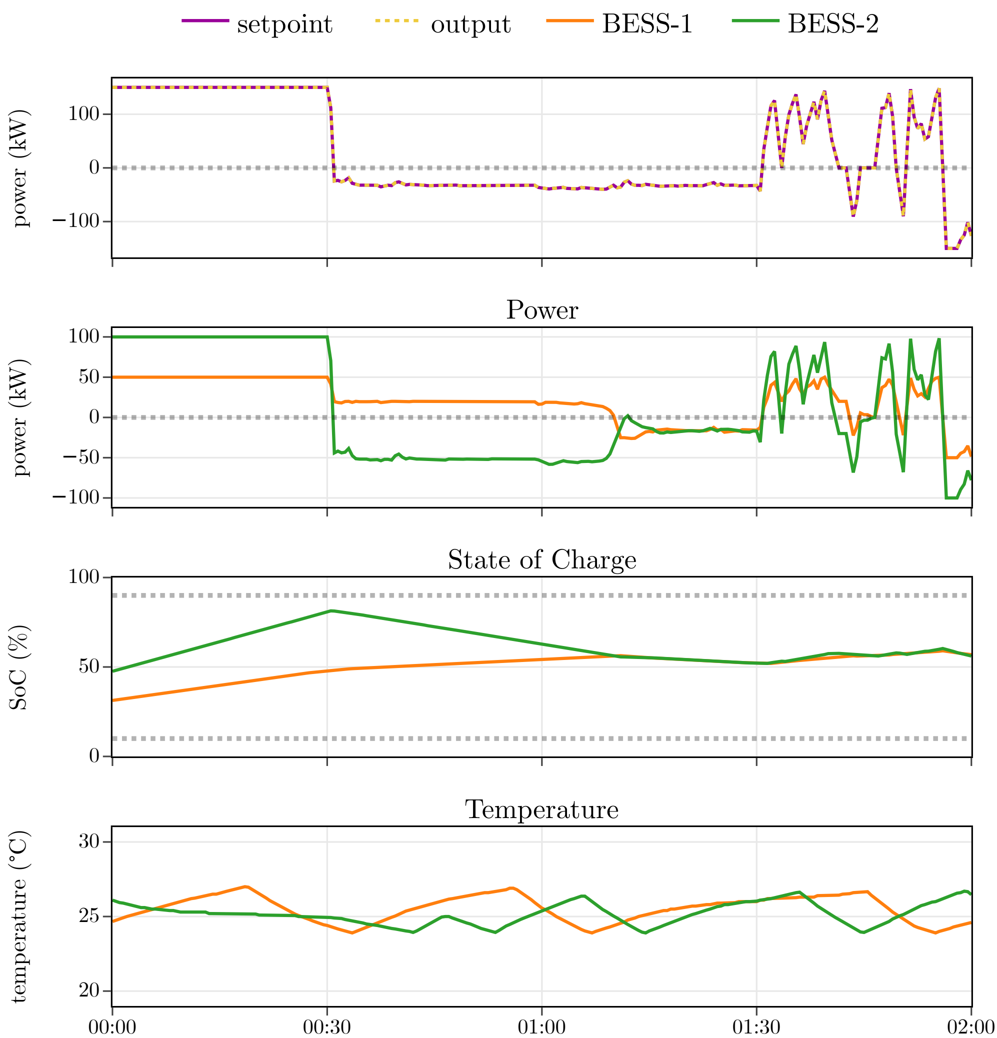

Figure 4.12: Short-term operation of two battery energy storage systems. First row: requested total power setpoint P^{req} and actual power delivery $\sum P_i$; second row: individual power contributions from each battery; third row: state of charge profiles; fourth row: temperature profiles.

4.4 Case Study: Component Sizing

This case study illustrates the application of the optimization framework for component sizing. The analysis belongs to the business layer of the hierarchical control framework, which is responsible for long-term strategic decisions, including the selection of control objectives, optimal configuration of the microgrid system, sizing of energy assets, and investment planning.

The aim of this case study is to determine the optimal dimensions of the battery energy storage system for microgrid project with ID 7, listed in Table 4.1. This type of analysis was conducted prior to the actual realization of the project and served as a key input for the investment planning and technical design phases. Here, the same analysis is presented using the most recent data collected during operation.

The main goals of the analysis are:

1. Identify the economically optimal nominal energy capacity (E_{nom} [kWh]) and inverter power rating of the BESS (P_{inv} [kW]).
2. Quantify the achievable reduction in the reserved grid import capacity (denoted as $\overline{P}^{y}_{\text{imp}}$), which directly influences demand charges and grid connection requirements.
3. Evaluate the net present cost and other economic indicators over the project lifetime, providing the expected financial performance for the microgrid owner.

The optimal BESS dimensions are computed such that they minimize the total NPC over the system's expected operational lifetime, considering both capital expenditures and discounted operational costs. The resulting BESS dimensions therefore represent a trade-off between investment in storage and the achievable savings in grid-related charges and energy procurement.

4.4.1 Setup and Input Data

The microgrid is a manufacturing plant located in Slovakia, connected to the distribution grid at the 22 kV voltage level, which is operated by the company VDS a.s., whose rules and tariffs apply. It is an energy-intensive facility with high power consumption, which is partially covered by a rooftop photovoltaic system with a nominal power of 500 kWp. The panels have an east–west orientation with an expected yearly yield of 996 kWh per kWp installed, which is typical for this region. No additional energy generation assets are planned in the near future.

The facility aims to reduce energy costs and increase the utilization of its installed renewable energy source. Currently, a portion of renewable energy is wasted due to necessary curtailment, primarily during weekends when consumption is low. The facility is not allowed to export energy to the grid due to limitations imposed by the distribution operator. To address this, the facility plans to invest in a battery energy storage system to store excess energy for later use. Given the high investment costs, determining the optimal size of the BESS is critical to ensure the project's economic viability. A single-function battery storage system would not provide sufficient return on investment; therefore, it is essential to combine multiple revenue streams.

The facility is charged dynamic electricity tariffs based on day-ahead market prices and also pays grid connection fees (demand charges) determined by the maximum annual power import. The battery storage system is expected to deliver multiple functionalities: peak shaving, price arbitrage, and renewable energy utilization. These functionalities are considered in the sizing analysis.

The analysis uses real operational data collected over the full calendar year of 2023, with a 1-minute resolution. For the sizing analysis, the data were aggregated to 15-minute intervals, as this is the standard billing period and relevant for demand charges, which are based on the maximum power consumption averaged over 15 minutes. The dataset includes day-ahead electricity prices from the Slovakian market, measured active power consumption, and measured photovoltaic production. Since the actual PV production was curtailed during operation, in these periods the expected power output was estimated using irradiance data. The data used for the optimization problem are visualized in Figure 4.13.

Photovoltaic production exhibits a typical seasonal pattern, with the highest production during the summer months and the lowest during winter. The measured consumption profile shows a clear daily pattern, with peaks during working hours and lower consumption during nights, weekends, and holidays. The highest power demand usually occurs in the morning hours, before PV production starts. Although a weekly pattern is distinguishable, deviations are present. Planned shutdowns with a duration of one week occur twice a year, in mid-summer and at the end of the year, when the facility is closed for maintenance.

Day-ahead market prices exhibit a typical daily pattern, with two peaks—morning and evening—and the lowest prices during the night. Negative prices are present but

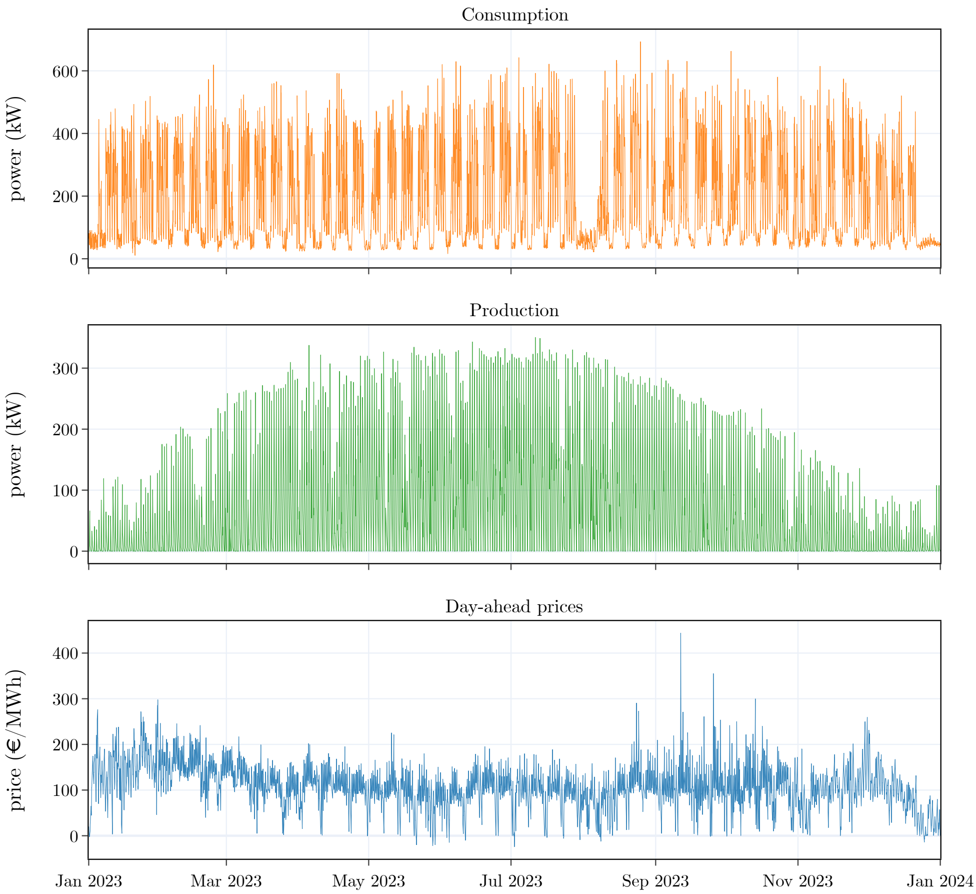

Figure 4.13: Power and price profiles over the year. First row: measured active power consumption; second row: measured and reconstructed photovoltaic production; third row: market prices.

rare and usually occur in summer months when PV production is high and demand is low. There are occasional periods with prices well above the average. This behavior is not uncommon, and extreme events are also expected in upcoming years due to increasing shares of renewable energy sources in the generation mix.

Annual electricity consumption of the facility in 2023 was 1646 MWh, and the annual PV production is estimated at 482 MWh, of which only 307 MWh was utilized (resulting in a 64% utilization rate), the remainder was curtailed due to grid connection limitations. Other key metrics of the microgrid power profile are summarized in Table 4.11.

Table 4.11: Key metrics of microgrid power profile and market prices.

Parameter		Minimum	Maximum	Average
Consumption	(kW)	10.5	693.4	187.9
PV production	(kW)	0.0	350.6	55.1
Energy market price	(€/MWh)	−24.4	444.0	104.7

According to these key metrics, the microgrid belongs to the mid-scale commercial/industrial category. It is reasonable to expect the optimal BESS size to be larger than residential systems (5–50 kW), but below utility-scale installations (1 MW and above).

4.4.2 Parametrization

The analysis is conducted over a 12-year period. Predictions over such a long horizon are subject to uncertainty. In the case of electricity consumption, the best estimate is to assume that it remains at the current level, as the facility does not plan any significant expansion or reduction of production. Electricity production from the photovoltaic system is expected to decline at a linear rate of $d_{\mathrm{PV}} = 0.5\%$ per year. Prices—both on the energy market and demand charges for the grid connection—are assumed to increase with an inflation rate of $i = 2\%$.

The investment cost of the battery is divided into two components: the unit cost per installed energy capacity, c_{E} (€/kWh), and the unit cost per installed power capacity, c_{P} (€/kW). These costs vary depending on battery chemistry, manufacturer, and market conditions, and they exhibit a long-term declining trend. According to projections in [114], battery costs for utility-scale, four-hour lithium-ion systems in 2025 range from 260 to 420 €/kWh (including the power conversion system). Besides costs scaling with the BESS size, fixed installation costs c_{F} (e.g., commissioning, infrastructure, battery management system) are included separately in the capital expenditure model, as defined in Eq. (3.51).

The optimal sizing of the battery depends on several additional parameters, such as maintenance costs, technical lifetime, state of health at end of life, allowable depth of discharge, maximum number of full cycles, and degradation behavior. These parameters directly influence the usable capacity over time and constrain the maximum yearly energy throughput, thereby affecting the overall economic performance. The values used in this sizing analysis are summarized in Table 4.12.

Table 4.12: Parameters used in the optimal sizing problem and their representative values.

Parameter description		**Symbol**	**Value**
Project duration	(years)	N_Y	12
Discount rate	(%)	r	5
Electricity price inflation	(%/year)	i	2
Annual PV degradation rate	(%/year)	d_{PV}	0.5
Annual BESS degradation rate	(%/year)	d_{bat}	3.2
State of health at EoL	(%)	$S_{\mathrm{oH}}^{\mathrm{EoL}}$	70
Depth of discharge	(%)	–	80
Charging and discharging efficiency	(%)	$\eta_{\mathrm{ch}}, \eta_{\mathrm{dch}}$	95
Max. full cycles over lifetime	(-)	N_{cycles}	6000
Battery replacement cost	(€/MWh)	c_{dch}	10
Demand charge rate	(€/kW/year)	c_{D}	77.0
Unit cost of energy capacity	(€/kWh)	c_{E}	350
Unit cost of power capacity	(€/kW)	c_{P}	100
Fixed installation cost	(€)	c_{F}	10 000
Annual maintenance cost	(% of CAPEX/year)	C_{M}	0.5

The parameter values assumed in this analysis are representative of commercial battery storage systems installed today and provide a reasonable estimate of expected costs and performance. The discount rate used in the net present cost calculation reflects both the time value of money and the risk associated with the investment. Reported values in the literature for BESS sizing problems vary widely, ranging from 2% [115] to 10% [116]. In this work, a moderate value of 5% is selected as the baseline, with a sensitivity analysis performed to evaluate the impact of this parameter.

4.4.3 Computational Complexity

While in real-time, short-term optimal control the computational complexity was the limiting factor—the available time window for solving the optimization problem is short and the choice of high-performance solvers is limited—this is not the case for component sizing. In the sizing problem, high-performance solvers capable of handling large-scale optimization problems can be used, and the solution time is not a limiting factor.

The problem was solved using the Gurobi solver; however, it still needed to be formulated as a linear program to keep the computational requirements within the limits of the available resources. Feasibility with respect to the nonlinear complementarity constraints was verified after obtaining the optimal solution. In this particular case, the complementarity constraint was satisfied due to the formulation of the cost function (i.e., simultaneous charging and discharging would increase the objective value).

To illustrate the computational complexity of the problem, the model consists of approximately 2.5×10^6 variables, 4.9×10^5 parameters, and 3.8×10^6 constraints when the horizon is set to 12 years. The time required to solve the problem to optimality varies with the parametrization. Based on all runs from the sensitivity analysis (see Sec. 4.4.5), the runtime ranged from 402 to 885 seconds, with an average of 617 seconds. Approximately 77% of this time was spent on solving the optimization problem, while the remainder was consumed by model construction and translation.

4.4.4 Results

The optimal BESS dimensions resulting from the proposed optimization framework were determined as:

$$\begin{aligned} E_{\text{nom}} &= 325.9 \text{ kWh}, \\ P_{\text{inv}} &= 171.2 \text{ kW}. \end{aligned}$$

These values represent the most cost-effective balance between investment and operational savings over the 12-year project horizon. The actually installed BESS in this microgrid project (commissioned in 2022) was sized at 301 kWh and 150 kW, which is close to the identified optimum and satisfies the operational requirements of the microgrid.

In addition to battery sizing, the model recommends reducing the reserved grid import capacity from the original value of $\overline{P}_{\text{imp}} = 590$ kW to $\overline{P}^{1}_{\text{imp}} = 419$ kW in year 1 and gradually increasing it to $\overline{P}^{15}_{\text{imp}} = 448$ kW in the final year. These limits are recalculated annually based on the maximum 15-minute power draw, and their reduction results in additional savings through lower demand charges paid to the distribution operator.

Net Present Cost

The NPC is minimized in the objective function of the optimization problem, Eq. (3.50). The net present cost of the optimal solution over the 12-year project lifetime is 2.055 million €, of which 141 189 € represents capital expenditures. In comparison, a baseline scenario without any storage investment results in an NPC of 2.110 million €.

Annual savings

Annual cost savings are computed as the difference between the baseline operational expenditures ($\mathrm{OPEX}^y_{\mathrm{base}}$) and the operational expenditures with optimal storage (OPEX^y). The percentage savings are defined as:

$$\mathrm{AS}^y = \frac{\mathrm{OPEX}^y_{\mathrm{base}} - \mathrm{OPEX}^y}{\mathrm{OPEX}^y_{\mathrm{base}}} \cdot 100\%. \tag{4.3}$$

Evaluated annually, the optimal BESS reduces total microgrid operational costs by 10.3% in the first year and by 8.1% in the final year, with an average reduction of 9.3% over the project lifetime. The gradual decrease in savings is caused by the expected degradation of the battery system, which reduces its usable capacity over time.

Normalized profit

The normalized profit is defined as the average annual savings generated by the battery storage divided by its installed power capacity. It provides a normalized measure of economic performance in €/kW:

$$\mathrm{NP} = \frac{\frac{1}{N_Y}\sum_{y=1}^{N_Y}\left(\mathrm{OPEX}^y_{\mathrm{base}} - \mathrm{OPEX}^y\right)}{P_{\mathrm{inv}}} = 123\ \text{€/kW/year}. \tag{4.4}$$

This metric enables comparison across different BESS installations by normalizing the achieved savings with respect to system size.

Net Present Value

The net present value measures the value created by the investment and is defined as the difference between the discounted operational savings and the initial capital expenditure:

$$\mathrm{NPV} = \sum_{y=1}^{N_Y} \frac{\mathrm{OPEX}^y_{\mathrm{base}} - \mathrm{OPEX}^y}{(1+r)^{y-1}} - \mathrm{CAPEX} = 54\,928\ \text{€}. \tag{4.5}$$

A positive NPV indicates that the operational savings exceed the investment cost, and therefore the storage investment is financially beneficial.

Internal Rate of Return

The IRR is defined as the discount rate r^{IRR} at which the net present value equals zero. It represents the effective break-even rate of return of the investment over its lifetime and is obtained by solving:

$$\sum_{y=1}^{N_Y} \frac{\mathrm{OPEX}_{\mathrm{base}}^{y} - \mathrm{OPEX}^{y}}{(1 + r^{\mathrm{IRR}})^{y-1}} - \mathrm{CAPEX} = 0. \tag{4.6}$$

The resulting IRR for the proposed battery investment is 10.3%. Since this exceeds typical thresholds for industrial investments (e.g., 8–10%), the project can be considered economically attractive.

Payback Period

The payback period represents the number of years required for cumulative cost savings to recover the initial investment. It is calculated as:

$$\mathrm{PP} = \frac{\mathrm{CAPEX}}{\frac{1}{N_Y} \sum_{y=1}^{N_Y} (\mathrm{OPEX}_{\mathrm{base}}^{y} - \mathrm{OPEX}^{y})} = 6.7 \text{ years}. \tag{4.7}$$

For a battery storage investment to be considered economically reasonable, the payback period should be shorter than the expected lifetime of the battery system, which is 12 years in this case. This condition is satisfied by the obtained solution.

A summary of the economic performance indicators of the battery storage investment is presented in Table 4.13.

Table 4.13: Summary of economic performance of the battery storage investment.

Parameter	**Value**
Net Present Cost	2 055 860 €
Net Present Value	54 928 €
Capital Expenditures	141 189 €
Internal Rate of Return	10.3%
Average Annual Savings	9.3%
Average Normalized Profit	123 €/kW/year
Payback Period	6.7 years

All evaluated economic indicators consistently show that the optimally sized battery energy storage system is financially viable and leads to a measurable improvement in the overall economic performance of the microgrid.

4.4.5 Sensitivity Analysis

While the recommended BESS size is based on best estimates of the model parameters, assessing the sensitivity of the results to variations in these parameters provides valuable insight into the robustness of the investment decision. The sensitivity analysis was therefore conducted by varying selected key parameters within reasonable ranges and observing their impact on the optimal BESS dimensions and economic indicators.

Three parameters were selected for the sensitivity analysis due to their strong influence on economic outcomes and inherent uncertainty in their estimation:

- **Discount rate (r)**: A higher discount rate reduces the present value of future cash flows, thereby lowering the NPV, and vice versa. The discount rate was varied between 2% and 10%.
- **Project lifetime (N_Y)**: This parameter reflects the assumed operational lifetime of the battery system and the duration over which benefits are accrued. Values between 10 and 15 years were considered.
- **Battery energy capacity cost ($c_{\mathbf{E}}$)**: The unit investment cost per kWh of nominal energy capacity, which depends on market conditions, manufacturer, and technology, and exhibits a declining long-term trend. A range of 250–400 €/kWh was analyzed.

Each parameter was varied independently, while all other parameters were kept at their default values. In addition to the optimal BESS dimensions, key economic metrics were evaluated for each scenario, namely the net present value and internal rate of return. The results of the sensitivity analysis are summarized in Table 4.14.

The discount rate has a significant influence on investment attractiveness. Higher discount rates reduce both the optimal BESS size and the NPV, as future savings are discounted more heavily. The IRR, however, increases slightly with smaller storage systems that recover capital more quickly.

Extending the assumed project lifetime allows more time to recover the initial investment, which leads to larger optimal storage sizes and higher NPV values, while the IRR remains relatively stable across the examined range.

Battery energy capacity cost has the strongest impact on sizing decisions. Lower unit costs justify larger storage systems and result in substantially higher NPV and

Table 4.14: Sensitivity analysis of optimal BESS sizing, NPV, and IRR under different assumptions.

Parameter	**Value**	**BESS** (kW/kWh)	**NPV** (€)	**IRR** (%)
Discount rate (%)	2	196/452	86 849	8.4
	3	195/438	73 808	8.6
	4	186/388	63 286	9.3
	5	171/327	54 910	10.3
	6	160/284	47 740	11.2
	7	154/258	41 074	11.7
	8	151/246	34 846	12.0
	9	144/225	29 546	12.5
	10	142/216	24 570	12.7
Storage lifetime (years)	10	148/235	35 127	10.1
	11	156/267	45 234	10.6
	12	171/327	54 922	10.3
	13	188/399	65 127	10.0
	14	195/438	76 653	10.1
	15	196/452	88 459	10.5
Battery cost (€/kWh)	250	201/518	96 599	13.4
	275	198/483	84 348	12.2
	300	196/452	72 878	11.1
	325	194/425	62 059	10.1
	350	171/327	54 920	10.3
	375	157/271	48 940	10.3
	400	151/246	42 885	9.7

IRR values. Conversely, higher battery costs reduce the optimal size and investment returns.

Overall, the results demonstrate that the battery investment remains financially viable across all tested scenarios, providing confidence that the proposed BESS sizing methodology is robust with respect to reasonable variations in key economic and technical parameters.

Chapter 5

Conclusions

This thesis has proposed and demonstrated a framework for optimal energy management in microgrids with renewable sources and energy storage. It contributes both methodological and practical advances. Drawing on direct experience deploying and operating real-world systems at industry scale, the work is informed by practical insights—particularly the economic viability of control strategies and the limitations of computational resources.

Central to the thesis is the energy management system, which integrates three control frameworks, each operating at a different layer of the proposed hierarchy. Each framework is developed with detailed methodology, validated through simulations and real-world applications, and designed to be modular, scalable, and adaptable to different microgrid configurations. Together they form a complete solution delivered as "Energy Management-as-a-Service".

The first contribution improves economic model predictive control for daily operational planning. It minimizes energy costs, maximizes renewable self-consumption, and provides grid services such as peak shaving and price arbitrage. A novel two-stage formulation combines the computational efficiency of deterministic MPC with the robustness of the stochastic formulation, and uncertainty is handled with a risk-aware approach reflecting end-user aversion to losses from rare events. The method has been deployed at several commercial and industrial sites, delivering measurable economic benefits over long-term operation.

The second contribution extends the MPC framework to support strategic decision-making for long-term planning—specifically, the optimal sizing of battery storage systems. This sizing methodology utilizes the same optimization model used for operational control, modified to incorporate key economic indicators and scaled over multi-year horizons, using historical data to simulate future performance and determine cost-optimal storage dimensions. The results demonstrate that using the same underlying model for both operation and design ensures consistency and delivers economically sound investment recommendations. The analysis confirms that battery storage with proper dimensions and a proper control strategy is nowadays a financially attractive investment.

At shorter timescales (on the order of seconds), the task of distributing power setpoints among heterogeneous battery storage units—while balancing state of charge and respecting thermal constraints—is addressed through a dedicated optimization-based algorithm. Formulated as a quadratic program for fast execution, the algorithm integrates seamlessly with the EMS and has been validated in simulation and in real-world deployment at a mid-scale battery storage installation.

Across three detailed case studies, the practical applicability of the proposed energy management system was demonstrated. The long-term planning case study showed that optimal battery sizing based on real operational data can yield internal rates of return exceeding 10% and reduce energy costs by up to 10%. While the exact results are system-specific, the underlying methodology is general and transferable to other microgrid configurations. The case study of daily operational control confirmed substantial economic benefits of the MPC-based approach, exceeding expectations by achieving annual revenues above 150 €/kW of installed battery power.

In summary, the proposed hierarchical energy management system supports the full spectrum of microgrid control tasks—from long-term investment planning to fast real-time operation. Beyond delivering direct economic value, it also contributes to the broader transformation of the energy system toward a more sustainable future by facilitating the integration of renewable energy sources and supporting the balance and stability of the electricity grid as a whole.

Two natural directions extend the proposed framework beyond the present scope. The first is a risk-aware extension of the sizing methodology, coupling the long-term sizing optimization with a stochastic operating layer to yield investment decisions hedged against worst-case operational scenarios. The second is coordinated operation across the portfolio of microgrids managed under EMaaS, where storage capacity, demand flexibility, and market participation are pooled at the provider level—a setting that opens connections to peer-to-peer energy trading and distributed, potentially privacy-preserving MPC across geographically separated sites.

Appendix A

Author's Publications

Articles in Journal

- **T. Ábelová** – M. Wadinger – M. Kvasnica: Predictive risk-aware control for microgrids: Operation of a revenue-generating energy management system. *Sustainable Energy, Grids and Networks*, vol. 44, 2025. `doi:10.1016/j.segan.2025.102028`
  Citations: WoS 2, Scopus 1, Google Scholar 2.

Articles in Conference Proceedings

- **T. Ábelová** – R. Kohút – K. Fedorová – M. Kvasnica: Risk-Aware Stochastic Energy Management of Microgrid with Battery Storage and Renewables. In *IFAC World Congress 2023*, Yokohama, Japan, 2023. `doi:10.1016/j.ifacol.2023.10.1042`
  Citations: WoS 3, Scopus 4, Google Scholar 5.

- **T. Ábelová** – K. Fedorová – M. Kvasnica: Optimization-Based Power Distribution Method for State-of-Charge Balancing of Battery Storage Systems. In *Proceedings of the 24th International Conference on Process Control*, IEEE, Slovak University of Technology in Bratislava, 2023. `doi:10.1109/PC58330.2023.10217738`
  Citations: WoS 0, Scopus 0, Google Scholar 0.

- K. Fedorová – **T. Ábelová** – M. Kvasnica: Dynamic Power Purchase Agreement. In *Proceedings of the 24th International Conference on Process Control*, IEEE, Slovak University of Technology in Bratislava, 2023. `doi:10.1109/PC58330.2023.10217697`
  Citations: WoS 1, Scopus 4, Google Scholar 6.

- **T. Ábelová** – M. Kvasnica: Modelling of Battery Energy Storage Systems for Predictive Control in Microgrid Applications. In *2022 Cybernetics & Informatics (K&I)*, 2022. `doi:10.1109/KI55792.2022.9925957`
  Citations: WoS 0, Scopus 2, Google Scholar 2.
- R. Kohút – L. Galčíková – K. Fedorová – **T. Ábelová** – M. Bakošová – M. Kvasnica: Hidden Markov Model-based Warm-start of Active Set Method in Model Predictive Control. In *Proceedings of the 23rd International Conference on Process Control*, IEEE, Slovak University of Technology in Bratislava, 2021. `doi:10.1109/PC52310.2021.9447506`
  Citations: WoS 6, Scopus 8, Google Scholar 9.

As of May 31, 2026, the publications have accumulated a total of 12 citations in Web of Science, 19 in Scopus, and 24 in Google Scholar.

Appendix B

Curriculum Vitae

Personal Information

Name:	Tereza Ábelová
Year of birth:	1996
Nationality:	Slovak
Email:	tereza.abelova@stuba.sk
ORCID iD:	0000-0002-4692-0174

Education

2020–present	**Ph.D.** Slovak University of Technology in Bratislava Study Program: Process Control
2017–2020	**M.Sc.** Slovak University of Technology in Bratislava Study Program: Automation and Information Engineering in Chemistry and Food Industry
2014–2017	**B.Sc.** Slovak University of Technology in Bratislava Study Program: Biotechnology and Food Technology

Work Experience

2025–present	**Technical Lead** *Wattstor, s.r.o.* Technical product owner responsible for optimal control, machine learning, and energy trading solutions.
2020–2025	**Data Scientist** *TESLA Group, a.s.* Development and deployment of EMS for microgrids. Responsible for optimal asset control and data analytics.
2019–2020	**Data Analyst** *ProGridTech, a.s.* Data analysis, modeling, simulations, and scientific computations for energy and power systems.
2018–2020	**Control Engineer** *STUBA Green Team* Design and development of control systems for an autonomous electric racing car.

International Visits and Study Stays

2023	**EECI International Graduate School on Control** Learning-based Model Predictive Control, Zurich, Switzerland
2022	**EECI International Graduate School on Control** Control and Optimization of Autonomous Power Systems, Stockholm, Sweden
2018	**Erasmus+ Study Stay** University of Ljubljana, Slovenia

Appendix C

Resumé

C.1 Mikrosiete a batériové úložiská

Prvá kapitola je venovaná uvedeniu lokálnej energetickej siete, tzv. mikrosiete, a prostrediu, v ktorom pôsobí a ktoré vplýva na jej činnosť. Mikrosiete predstavujú moderné, lokálne energetické systémy, ktoré integrujú obnoviteľné zdroje, úložisko a riaditeľnú spotrebu a môžu fungovať autonómne alebo v prepojení s distribučnou sieťou. Ich cieľom je optimalizovať tok energie v rámci vlastnej elektrickej siete s dôrazom na spoľahlivosť, stabilitu a ekonomickú efektívnosť. Riadenie mikrosietí si vyžaduje pokročilé systémy energetického manažmentu (EMS), ktoré reagujú na prevádzkové a trhové signály a vykonávajú viacero funkcionalít (napr. cenová arbitráž, znižovanie špičiek, využívanie energie z obnoviteľných zdrojov, práca s odchýlkou).

Komponenty, z ktorých je mikrosieť zložená je možné zaradiť do štyroch hlavných skupín: zdroje energie (preferované sú obnoviteľné), záťaže (riaditeľné a neriaditeľné), úložiská energie a prepojenie s distribučnou sieťou. Výroba a spotreba energie musí byť v každom momente v rovnováhe. Osobitná pozornosť je venovaná PV systémom, z ktorých výroba energie je nestála a závislá od počasia – preto je nevyhnutná presná predikcia výkonu pomocou fyzikálnych alebo dátovo-orientovaných modelov. Tieto predikcie tvoria vstupy pre optimalizované riadenie spotreby a výroby v rámci EMS.

Úložiská energie zohrávajú kľúčovú úlohu pri vyvažovaní výroby a spotreby v mikrosieťach, z mnohých typov technológií v mikrosieťach dominujú batériové systémy (BESS) pre ich vysokú hustotu energie, rýchlu odozvu, životnosť a účinnosť pri zohľadnení nákladov. Časť práce sa detailne venuje parametrom batérií vrátane kapacity, výkonu, stavu nabitia (SoC), stavu zdravia (SoH), hĺbky vybitia (DoD) a celkovej účinnosti, pre neskoršie využitie pri návrhu riadiaceho systému. Diskutované sú tiež matematické modely používané na predikciu a riadenie správania úložiska – od nelineárnych modelov po zjednodušené lineárne a kombinované prístupy. Výber konkrétneho modelu závisí od požiadaviek na presnosť a výpočtovú náročnosť v riadiacom systéme.

C.2 Riadiaci systém energetického manažmentu

Nasleduje kapitola venovaná návrhu komplexného riadiaceho systému pre mikrosiete, založenému na hierarchickej architektúre so štyrmi úrovňami: biznis vrstva, vrstva energetického manažmentu, vrstva riadenia výkonu a vykonávacia vrstva. Každá vrstva má vlastnú časovú škálu, úroveň abstrakcie a ciele – od strategického plánovania po reálne vykonávanie výkonových príkazov. Predstavený je koncept Energy Management-as-a-Service (EMaaS), v ktorom je EMS poskytovaný ako služba zákazníkom – vlastníkom mikrosietí. Návrh zohľadňuje nielen technickú, ale aj ekonomickú stránku prevádzky EMS poskytovateľa, ktorá je kľúčová pre dlhodobú prevádzkovateľnosť EMS riešení. Model založený na delení úspor motivuje obidve strany a vyžaduje škálovateľné a nákladovo efektívne riešenie.

Časť práce sa zameriava na návrh prediktívneho riadenia (MPC) vhodného pre energetický manažment mikrosietí. MPC optimalizuje energetické toky medzi zdrojmi, ako sú batériové úložiská, obnoviteľné zdroje a riaditeľné záťaže, pričom zohľadňuje viacero cieľov, obmedzení a neistôt. Za najvhodnejší bol zvolený typ stochastického MPC regulátora zohľadňujúceho riziko, ktorý umožňuje balansovať medzi výkonnosťou a robustnosťou voči neurčitostiam. Navrhovaná metóda využíva dvojstupňové riadenie MPC: prvý stupeň rieši stochastický problém so zjednodušeným modelom, zatiaľ čo druhý stupeň realizuje deterministické MPC s plným modelom pre zvolený scenár. Deterministická formulácia poskytuje rýchle a presné riadenie pre konkrétny scenár, zatiaľ čo stochastické MPC integruje rôzne možné realizácie neistôt a zabezpečuje odolnosť voči extrémnym situáciám. Využíva pritom ukazovateľ podmienenej hodnoty v riziku (CVaR). Výhodou je tiež flexibilita parametrizácie (napr. výber počtu scenárov alebo úroveň rizikovej averzie), vďaka ktorej je možné prispôsobiť riadiaci algoritmus konkrétnym potrebám prevádzkovateľa. Kombináciou oboch prístupov do dvojstupňového algoritmu sa dosahuje rovnováha medzi výpočtovou náročnosťou a kvalitou rozhodnutí. V práci je podrobne sformulovaný optimalizačný model, vrátane ohraničení a účelovej funkcie. Cieľom MPC je maximalizácia ekonomického prínosu mikrosiete prostredníctvom viacerých funkcií vrátane cenovej arbitráže, znižovania špičiek a maximalizácie vlastnej spotreby.

V rámci vrstvy riadenia výkonu bola navrhnutá optimalizačná metóda pre alokáciu výkonu medzi viaceré batériové úložiská v skupine, ktorej cieľom je zabezpečiť rovnomerné vyťažovanie jednotlivých jednotiek pri splnení požiadavky na celkový výkon generovanej energetickým manažmentom. Navrhnutý algoritmus zohľadňuje odlišné kapacity a výkonové limity batérií, obmedzenia stavu nabitia, ako aj ich aktuálnu teplotu a vplyv riadiacich zásahov na teplotnú dynamiku. Súčasťou návrhu je aj mechanizmus ovládania možného prestupu energie medzi batériami, ktorého povolenie či obmedzenie ovplyvňuje rýchlosť vyrovnávania SoC, ale aj mieru ich opotrebovania. Formulovaný problém je riešený ako kvadratický program (QP), ktorý umožňuje efektívne riešenie v reálnom čase. Účelová funkcia pozostáva zo súčtu kvadratických penalizačných členov reprezentujúcich jednotlivé požiadavky: dodržanie výkonovej požiadavky, vyrovnávanie stavu nabitia, rešpektovanie teplotných obmedzení, a rovnomerné rozdelenie záťaže.

Tretím významným príspevkom dizertačnej práce je metodológia optimálneho dimenzovania komponentov, najmä batériových úložísk, ktorá je súčasťou najvyššej – biznisovej vrstvy navrhnutej hierarchickej architektúry riadenia. Táto vrstva má za úlohu definovať dlhodobé investičné ciele a parametre systému ešte pred samotným nasadením riadiacich stratégií. Optimalizačná úloha sa zameriava na určenie ideálnej veľkosti batériového úložiska, konkrétne jeho nominálnej kapacity a výkonu meniča, ktorá zabezpečí najlepšiu ekonomickú návratnosť počas celého životného cyklu projektu. Využíva sa pritom predikčné optimalizačné jadro vyvinuté pre MPC, ktoré je v tomto prípade aplikované na viacročný horizont. Navrhnutý prístup optimalizuje ekonomický ukazovateľ čistých súčasných nákladov (NPC)–diskontované prevádzkové náklady vrátane počiatočnej investície, pričom rešpektuje dlhodobé obmedzenia ako degradáciu batérií a fotovoltických systémov, limity životnosti či obmedzenie počtu cyklov. Výsledky poskytujú nielen optimálne dimenzovanie pre investičné rozhodnutia, ale aj očakávaný operačný profil systému, čím zabezpečuje prepojenie medzi návrhom a prevádzkou mikrosiete.

C.3 Praktické nasadenie a prípadové štúdie

Posledná kapitola dizertačnej práce prezentuje dosiahnuté výsledky a predstavuje praktické nasadenie navrhnutého systému energetického manažmentu v reálnych projektoch. Obsahuje tri prípadové štúdie, pričom každá sa zameriava na jednu z metód vyvinutých v predchádzajúcich častiach práce – prediktívne riadenie energetických tokov, optimalizácia distribúcie výkonu a dlhodobé investičné plánovanie. Vytvorený EMS systém bol nasadený a prevádzkovaný vo viacerých odlišných (zložením aj funkciami) komerčných a priemyselných mikrosieťach potrebujúcich energetický manažment. Práca vychádza z reálnych dát zo systémov, ktoré boli v prevádzke niekoľko mesiacov až rokov, čím je zabezpečená relevancia a overiteľnosť navrhovaných metód.

Prvá prípadová štúdia sa zameriava na výsledky prediktívneho riadenia, pre demonštráciu ktorých bol vybraný jeden z projektov pre jeho reprezentatívnu kombináciu riaditeľných zdrojov a poskytovaných funkcionalít. Nasadený systém energetického manažmentu využíval navrhovaný prístup prediktívneho riadenia na koordináciu batériového úložiska, fotovoltického systému a nabíjania elektromobilov v súlade s dennými harmonogramami a dynamickými trhmi s energiou. Hlavné prevádzkové ciele zahŕňali optimalizáciu odchýlok, maximalizáciu využitia lokálne vyrobenej energie a dodržiavanie sieťových obmedzení výkonu. EMS pracoval s plánovacím rozlíšením 15 minút a jednou aktualizáciou za minútu v reálnom čase, čo si vyžadovalo vyvinutie techniky časovej redukcie pri zachovaní scenárového prístupu. Vyhodnotenie pomocou historických údajov potvrdilo, že EMS konzistentne znižoval prevádzkové náklady a v niektorých prípadoch generoval zisk vďaka využívaniu priaznivých trhových podmienok, pričom zaznamenaný mesačný finančný prínos presiahol 3000 €. Vyhodnotená bola aj ekonomická stránka samotného EMS poskytovaného ako cloudová služba, zdôrazňujúc dôležitosť škálovateľnosti a modulárnosti.

Druhá prípadová štúdia sa zameriava na algoritmus pre distribúciu výkonu medzi viaceré batériové úložiská. Navrhnuté riešenie bolo najprv overené v simulácii, kde úspešne zabezpečilo rovnomerné rozdelenie požadovaného výkonu medzi tri batérie s rozdielnymi počiatočnými stavmi a parametrami, pričom boli dodržané všetky obmedzenia a zároveň boli teploty udržiavané pod kritickou hranicou. Následne bol algoritmus nasadený do reálnej prevádzky v priemyselnej mikrosieti s dvoma batériami a fotovoltikou, kde spoľahlivo zabezpečoval požadovaný výkon, vyvažoval stavy nabitia a rešpektoval teplotné limity. Škálovateľnosť bola overená v simulácii, kde výpočtový čas ostal pod 30 ms aj pre systémy so 100 batériami.

V tretej prípadovej štúdii sa optimalizačný rámec využil na dimenzovanie batériového úložiska pre konkrétny priemyselný projekt na Slovensku. Cieľom analýzy bolo určiť ekonomicky optimálnu kapacitu batérie a výkon meniča tak, aby sa maximalizovali úspory prostredníctvom redukcie rezervovanej kapacity, využitia prebytočnej fotovoltickej energie a cenovej arbitráže na trhu s elektrinou. Model využil reálne dáta za celý rok 2023 a zohľadnil technické, ekonomické a prevádzkové parametre vrátane degradácie batérie, cien, taríf a investičných nákladov. Analyzovaná bola aj výpočtová náročnosť pri uvažovaní až 12-ročného horizontu so štvrťhodinovými intervalmi. Výsledkom simulácie je odporúčaná veľkosť úložiska 326 kWh/171 kW, ktorá prináša kladnú čistú súčasnú hodnotu (NPV) vo výške 54 928 €, vnútorné výnosové percento (IRR) 10,3% a dobu návratnosti 6,7 roka. Citlivostná analýza ukázala, že investícia ostáva ekonomicky výhodná aj pri rôznych predpokladoch o dĺžke projektu, diskontnej sadzbe či cene batérie, čo potvrdzuje robustnosť navrhovaného prístupu.

Bibliography

[1] Martín A Alarcón, Rodrigo G Alarcón, Alejandro H González, and Antonio Ferramosca. Economic model predictive control for energy management of a microgrid connected to the main electrical grid. *Journal of Process Control*, 117:40–51, 2022.

[2] Ricardo Silva, Clara Gouveia, Leonel Carvalho, and Jorge Pereira. Improved battery storage systems modeling for predictive energy management applications. In *2022 IEEE PES Innovative Smart Grid Technologies Conference Europe (ISGT-Europe)*, pages 1–5. IEEE, 2022.

[3] Alberto Bolzoni, Alessandra Parisio, Rebecca Todd, and Andrew Forsyth. Model predictive control for optimizing the flexibility of sustainable energy assets: An experimental case study. *International Journal of Electrical Power & Energy Systems*, 129:106822, 2021.

[4] Yan Zhang, Fanlin Meng, Rui Wang, Wanlu Zhu, and Xiao-Jun Zeng. A stochastic mpc based approach to integrated energy management in microgrids. *Sustainable cities and society*, 41:349–362, 2018.

[5] Zhongwen Li, Chuanzhi Zang, Peng Zeng, Haibin Yu, and Hepeng Li. Two-stage stochastic programming based model predictive control strategy for microgrid energy management under uncertainties. In *2016 International Conference on Probabilistic Methods Applied to Power Systems (PMAPS)*, pages 1–6. IEEE, 2016.

[6] Vahid Hamdipoor, Hoai Nam Nguyen, Bouchra Mekhaldi, Johan Parra, Jordi Badosa, and Fausto Calderon Obaldia. Experimental validation of scenario-based stochastic model predictive control of nanogrids. *Control Engineering Practice*, 157:106249, 2025.

[7] Raheleh Khodabakhsh and Shahin Sirouspour. Optimal control of energy storage

in a microgrid by minimizing conditional value-at-risk. *IEEE Transactions on Sustainable Energy*, 7(3):1264–1273, 2016.

[8] Ruben Smets, Kenneth Bruninx, Jérémie Bottieau, Jean-François Toubeau, and Erik Delarue. Strategic implicit balancing with energy storage systems via stochastic model predictive control. *IEEE Transactions on Energy Markets, Policy and Regulation*, 1(4):373–385, 2023.

[9] Lars Herre. Risk-averse aggregator of controllable loads as virtual battery providing multiple services. In *2020 17th International Conference on the European Energy Market (EEM)*, pages 1–6. IEEE, 2020.

[10] Khanh Duc Hoang and Hong-Hee Lee. Accurate power sharing with balanced battery state of charge in distributed dc microgrid. *IEEE Transactions on Industrial Electronics*, 66(3):1883–1893, 2018.

[11] Mazen Elsaadany, Mads R Almassalkhi, and Simon H Tindemans. Linear model of aggregated homogeneous energy storage elements with realizable dispatch guarantees. *arXiv preprint arXiv:2501.04508*, 2025.

[12] Liu Gege. Optimal power distribution method for energy storage system based on available capacity. *International Journal of Low-Carbon Technologies*, 16(1):45–49, 2021.

[13] Shu Wang, Shuran Liu, Fan Yang, Xiaohui Bai, Shuo Wang, and Chengyan Yue. Novel power allocation approach in a battery storage power station for aging minimization. *Frontiers in Energy Research*, 7:166, 2020.

[14] Thomas Morstyn, Andrey V Savkin, Branislav Hredzak, and Vassilios G Agelidis. Multi-agent sliding mode control for state of charge balancing between battery energy storage systems distributed in a dc microgrid. *IEEE Transactions on smart grid*, 9(5):4735–4743, 2017.

[15] Jianwei Li, Weitao Zou, Qingqing Yang, Fengyan Yi, Yunfei Bai, Zhongbao Wei, and Hongwen He. Size optimization and power allocation of a hybrid energy storage system for frequency service. *International Journal of Electrical Power & Energy Systems*, 141:108165, 2022.

[16] Hirotaka Takano, Ryosuke Hayashi, Hiroshi Asano, and Tadahiro Goda. Optimal sizing of battery energy storage systems considering cooperative operation with microgrid components. *Energies*, 14(21):7442, 2021.

[17] Rahmat Khezri, Amin Mahmoudi, and Mohammed H Haque. Optimal capacity of solar pv and battery storage for australian grid-connected households. *IEEE Transactions on Industry Applications*, 56(5):5319–5329, 2020.

[18] Jirawat Wongyai, Thavatchai Tayjasanant, and Taisuke Masuta. Optimal scheduling and sizing of battery energy storage system in an industrial microgrid. In *2024 21st International Conference on Harmonics and Quality of Power (ICHQP)*, pages 132–136. IEEE, 2024.

[19] Yu-Wen Chen and J Morris Chang. Emaas: Cloud-based energy management service for distributed renewable energy integration. *IEEE Transactions on Smart Grid*, 6(6):2816–2824, 2015.

[20] Tereza Ábelová and Michal Kvasnica. Modelling of battery energy storage systems for predictive control in microgrid applications. In *2022 Cybernetics & Informatics (K&I)*, pages 1–6. IEEE, 2022.

[21] Tereza Ábelová, Kristína Fedorová, and Michal Kvasnica. Optimization-based power distribution method for state of charge balancing of battery storage systems. In *2023 24th International Conference on Process Control (PC)*, pages 144–149. IEEE, 2023.

[22] Tereza Ábelová, Roman Kohút, Kristína Fedorová, and Michal Kvasnica. Risk-aware stochastic energy management of microgrid with battery storage and renewables. *ifac-Papersonline*, 56(2):8445–8450, 2023.

[23] Tereza Ábelová, Marek Wadinger, and Michal Kvasnica. Predictive risk-aware control for microgrids: Operation of a revenue-generating energy management system. *Sustainable Energy, Grids and Networks*, page 102028, 2025.

[24] N. Hatziargyriou. *Microgrids: Architectures and Control*. Wiley-IEEE Press, 2014.

[25] Abhishek Kumar, Ramesh C Bansal, Deng Yan, and Praveen Kumar. *Microgrid handbook: Planning to practices*. CRC Press, 2025.

[26] Muhammad Fahad Zia, Elhoussin Elbouchikhi, and Mohamed Benbouzid. Microgrids energy management systems: A critical review on methods, solutions, and prospects. *Applied energy*, 222:1033–1055, 2018.

[27] Abbas Zare Ghaleh Seyyedi, Mohsen Gitizadeh, Mahan Fakhrooeian, and Mehdi Jabareh Nasero. Achieving the goals of energy arbitrage, peak-shaving, and pv self-consumption using pv-btm bess microgrids coupled with a distribution network. *Journal of Energy Storage*, 112:115479, 2025.

[28] European Commission. Commission regulation (eu) 2017/2195 of 23 november 2017 establishing a guideline on electricity balancing, 2017. Text with EEA relevance.

[29] Devnath Shah and Saibal Chatterjee. A comprehensive review on day-ahead electricity market and important features of world's major electric power exchanges. *International Transactions on Electrical Energy Systems*, 30(7):e12360, 2020.

[30] Jinqi Liu, Jihong Wang, and Joel Cardinal. Evolution and reform of uk electricity market. *Renewable and Sustainable Energy Reviews*, 161, 2022.

[31] Fouad El Gohary, Britt Stikvoort, and Cajsa Bartusch. Evaluating demand charges as instruments for managing peak-demand. *Renewable and Sustainable Energy Reviews*, 188:113876, 2023.

[32] Yang Zhou and Carl Ngai-Man Ho. A review on microgrid architectures and control methods. In *2016 IEEE 8th international power electronics and motion control conference (IPEMC-ECCE Asia)*, pages 3149–3156. IEEE, 2016.

[33] N Jungbluth, M Stucki, R Frischknecht, and S Buesser. Photovoltaics. *Sachbilanzen von Energiesystemen: Grundlagen für den ökologischen Vergleich von Energiesystemen und den Einbezug von Energiesystemen in Ökobilanzen für die Schweiz. ecoinvent report*, (6-XII):16–69, 2009.

[34] Mugdha V Dambhare, Bhavana Butey, and SV Moharil. Solar photovoltaic technology: A review of different types of solar cells and its future trends. In *Journal of Physics: Conference Series*, volume 1913, page 012053. IOP Publishing, 2021.

[35] Antonio Ricardo Zanatta. The shockley–queisser limit and the conversion efficiency of silicon-based solar cells. *Results in optics*, 9:100320, 2022.

[36] Elisa Skoplaki and John A Palyvos. On the temperature dependence of photovoltaic module electrical performance: A review of efficiency/power correlations. *Solar energy*, 83(5):614–624, 2009.

[37] Fouzia Brihmat and Said Mekhtoub. Pv cell temperature/pv power output relationships homer methodology calculation. In *Conférence Internationale des Energies Renouvelables" CIER*, volume 13, pages 0–0, 2014.

[38] Javier Antonanzas, Natalia Osorio, Rodrigo Escobar, Ruben Urraca, Francisco J Martinez-de Pison, and Fernando Antonanzas-Torres. Review of photovoltaic power forecasting. *Solar energy*, 136:78–111, 2016.

[39] Alfredo Nespoli, Emanuele Ogliari, S. Leva, Alessandro Massi Pavan, Adel Mellit, Vanni Lughi, and Alberto Dolara. Day-ahead photovoltaic forecasting: A comparison of the most effective techniques. *Energies*, 12:1621, 04 2019.

[40] Ramy Georgious, Rovan Refaat, Jorge Garcia, and Ahmed A Daoud. Review on energy storage systems in microgrids. *Electronics*, 10(17):2134, 2021.

[41] Gaurav Chaudhary, Jacob J Lamb, Odne S Burheim, and Bjørn Austbø. Review of energy storage and energy management system control strategies in microgrids. *Energies*, 14(16):4929, 2021.

[42] Haisheng Chen, Thang Ngoc Cong, Wei Yang, Chunqing Tan, Yongliang Li, and Yulong Ding. Progress in electrical energy storage system: A critical review. *Progress in natural science*, 19(3):291–312, 2009.

[43] Masood Ul Hassan, Sajeeb Saha, Md Enamul Haque, Shama Islam, Apel Mahmud, and Nishad Mendis. A comprehensive review of battery state of charge estimation techniques. *Sustainable Energy Technologies and Assessments*, 54:102801, 2022.

[44] Chang Wen-Yeau. The state of charge estimating methods for battery: A review. *International Scholarly Research Notices*, 2013:7, 2013.

[45] Matúš Danko, Juraj Adamec, Michal Taraba, and Peter Drgona. Overview of batteries state of charge estimation methods. *Transportation Research Procedia*, 40:186–192, 2019.

[46] Jason Porzio and Corinne D Scown. Life-cycle assessment considerations for batteries and battery materials. *Advanced Energy Materials*, 11(33):2100771, 2021.

[47] Sunil K Pradhan and Basab Chakraborty. Battery management strategies: An essential review for battery state of health monitoring techniques. *Journal of energy storage*, 51:104427, 2022.

[48] Yanqiu Xiao, Jishu Wen, Lei Yao, Jie Zheng, Zhanpeng Fang, and Yongpeng Shen. A comprehensive review of the lithium-ion battery state of health prognosis methods combining aging mechanism analysis. *Journal of Energy Storage*, 65:107347, 2023.

[49] Seon Hyeog Kim and Yong-June Shin. Optimize the operating range for improving the cycle life of battery energy storage systems under uncertainty by managing the depth of discharge. *Journal of Energy Storage*, 73:109144, 2023.

[50] V Bobanac, H Bašić, and H Pandžić. A method for deriving battery one-way efficiencies. *Journal of energy storage*, 73:108815, 2023.

[51] Yuejiu Zheng, Hang Wu, Wei Yi, Xin Lai, Haifeng Dai, Xuebing Han, and Minggao Ouyang. A novel classification method of commercial lithium-ion battery cells based on fast and economic detection of self-discharge rate. *Journal of power sources*, 478:229039, 2020.

[52] David Pozo, Javier Contreras, and Enzo E Sauma. Unit commitment with ideal and generic energy storage units. *IEEE Transactions on Power Systems*, 29(6):2974–2984, 2014.

[53] Ramteen Sioshansi, Paul Denholm, Juan Arteaga, Sarah Awara, Shubhrajit Bhattacharjee, Audun Botterud, Wesley Cole, Andres Cortés, Anderson De Queiroz, Joseph DeCarolis, et al. Energy-storage modeling: State-of-the-art and future research directions. *IEEE transactions on power systems*, 37(2):860–875, 2021.

[54] Ha-Lim Lee and Yeong-Han Chun. Using piecewise linearization method to pcs input/output-efficiency curve for a stand-alone microgrid unit commitment. *Energies*, 11(9):2468, 2018.

[55] Alexander Murray, Timm Faulwasser, and Veit Hagenmeyer. Mixed-integer vs. real-valued formulations of battery scheduling problems. *IFAC-PapersOnLine*, 51(28):350–355, 2018.

[56] Alberto Bemporad and Manfred Morari. Control of systems integrating logic, dynamics, and constraints. *Automatica*, 35(3):407–427, 1999.

[57] David Pozo. Linear battery models for power systems analysis. *Electric Power Systems Research*, 212:108565, 2022.

[58] Nawaf Nazir and Mads Almassalkhi. Guaranteeing a physically realizable battery dispatch without charge-discharge complementarity constraints. *IEEE Transactions on Smart Grid*, 14(3):2473–2476, 2021.

[59] Sumit K Rathor and Dipti Saxena. Energy management system for smart grid: An overview and key issues. *International Journal of Energy Research*, 44(6):4067–4109, 2020.

[60] Abdellatif Elmouatamid, Radouane Ouladsine, Mohamed Bakhouya, Najib El Kamoun, Mohammed Khaidar, and Khalid Zine-Dine. Review of control and energy management approaches in micro-grid systems. *Energies*, 14(1):168, 2020.

[61] Gokul Sidarth Thirunavukkarasu, Mehdi Seyedmahmoudian, Elmira Jamei, Ben Horan, Saad Mekhilef, and Alex Stojcevski. Role of optimization techniques in microgrid energy management systems—a review. *Energy Strategy Reviews*, 43:100899, 2022.

[62] Mehdi Ahmadi Jirdehi, Vahid Sohrabi Tabar, Saeid Ghassemzadeh, and Sajjad Tohidi. Different aspects of microgrid management: A comprehensive review. *Journal of Energy Storage*, 30:101457, 2020.

[63] Zia Ullah, Shoarong Wang, Guoan Wu, Mengmeng Xiao, Jinmu Lai, and Mohamed R Elkadeem. Advanced energy management strategy for microgrid using real-time monitoring interface. *Journal of Energy Storage*, 52:104814, 2022.

[64] Mohammad Hossein Amrollahi and Seyyed Mohammad Taghi Bathaee. Techno-economic optimization of hybrid photovoltaic/wind generation together with energy storage system in a stand-alone micro-grid subjected to demand response. *Applied energy*, 202:66–77, 2017.

[65] Ionela Prodan and Enrico Zio. A model predictive control framework for reliable microgrid energy management. *International Journal of Electrical Power & Energy Systems*, 61:399–409, 2014.

[66] Sandeep Vuddanti and Surender Reddy Salkuti. Review of energy management system approaches in microgrids. *Energies*, 14(17):5459, 2021.

[67] Vasileios Boglou, Christos-Spyridon Karavas, Athanasios Karlis, and Konstantinos Arvanitis. An intelligent decentralized energy management strategy for the optimal electric vehicles' charging in low-voltage islanded microgrids. *International journal of energy research*, 46(3):2988–3016, 2022.

[68] Sane Lei Lei Wynn, Terapong Boonraksa, Promphak Boonraksa, Watcharakorn Pinthurat, and Boonruang Marungsri. Decentralized energy management system in microgrid considering uncertainty and demand response. *Electronics*, 12(1):237, 2023.

[69] Razieh Darshi, Saeed Shamaghdari, Aliakbar Jalali, and Hamidreza Arasteh. Decentralized energy management system for smart microgrids using reinforcement learning. *IET Generation, Transmission & Distribution*, 17(9):2142–2155, 2023.

[70] Saad Ahmad, Md Shafiullah, Chokri Belhaj Ahmed, and Maad Alowaifeer. A review of microgrid energy management and control strategies. *IEEE Access*, 11:21729–21757, 2023.

[71] Tian Liu, Xiaoqi Tan, Bo Sun, Yuan Wu, and Danny HK Tsang. Energy management of cooperative microgrids: A distributed optimization approach. *International Journal of Electrical Power & Energy Systems*, 96:335–346, 2018.

[72] Paulo RC Mendes, Julio E Normey-Rico, and Carlos Bordons. Distributed energy management system for v2g networked microgrids. In *2017 IEEE PES innovative smart grid technologies conference-Latin America (ISGT Latin America)*, pages 1–6. IEEE, 2017.

[73] Seyyed Ali Ghorashi Khalil Abadi, Seyed Iman Habibi, Tohid Khalili, and Ali Bidram. A model predictive control strategy for performance improvement of

hybrid energy storage systems in dc microgrids. *IEEE Access*, 10:25400–25421, 2022.

[74] David Q Mayne, James B Rawlings, Christopher V Rao, and Pierre OM Scokaert. Constrained model predictive control: Stability and optimality. *Automatica*, 36(6):789–814, 2000.

[75] Matthew Ellis, Jinfeng Liu, and Panagiotis D Christofides. Economic model predictive control. *Springer*, 5(7):65, 2017.

[76] Alberto Bemporad and Manfred Morari. Robust model predictive control: A survey. In *Robustness in identification and control*, pages 207–226. Springer, 2007.

[77] Wilbur Langson, Ioannis Chryssochoos, SV Raković, and David Q Mayne. Robust model predictive control using tubes. *Automatica*, 40(1):125–133, 2004.

[78] Ali Mesbah. Stochastic model predictive control: An overview and perspectives for future research. *IEEE Control Systems Magazine*, 36(6):30–44, 2016.

[79] Giuseppe Carlo Calafiore and Marco C Campi. The scenario approach to robust control design. *IEEE Transactions on automatic control*, 51(5):742–753, 2006.

[80] Marco C Campi, Simone Garatti, and Maria Prandini. The scenario approach for systems and control design. *Annual Reviews in Control*, 33(2):149–157, 2009.

[81] Yin-Lam Chow and Marco Pavone. A framework for time-consistent, risk-averse model predictive control: Theory and algorithms. In *2014 American Control Conference*, pages 4204–4211. IEEE, 2014.

[82] Tana Siqin, Shan He, Bing Hu, and Xiaochao Fan. Shared energy storage-multi-microgrid operation strategy based on multi-stage robust optimization. *Journal of Energy Storage*, 97:112785, 2024.

[83] Weilin Yang, Haojie Fang, Dezhi Xu, Bin Jiang, and Peng Shi. A stochastic model predictive control based energy management approach for microgrids with electric vehicles. *IEEE Transactions on Transportation Electrification*, 2024.

[84] Stefano Raimondi Cominesi, Marcello Farina, Luca Giulioni, Bruno Picasso, and Riccardo Scattolini. A two-layer stochastic model predictive control scheme for microgrids. *IEEE Transactions on Control Systems Technology*, 26(1):1–13, 2017.

[85] Zhiping Cheng, Dongqiang Jia, Zhongwen Li, Shuai Xu, Changyi Zhi, and Long Wu. Multi-time scale energy management of microgrid considering the uncertainties in both supply and demand. *Energy Reports*, 8:10372–10384, 2022.

[86] Lars Herre. Impact of imbalance settlement system design on risk-averse energy storage. In *2020 17th International Conference on the European Energy Market (EEM)*, pages 1–6. IEEE, 2020.

[87] Yiqian Wu, Bolun Xu, and James Anderson. Energy storage arbitrage under price uncertainty: Market risks and opportunities. *arXiv preprint arXiv:2501.08472*, 2025.

[88] Marta Fochesato, Christian Peter, Lisa Morandi, and John Lygeros. Peak shaving with hydrogen energy storage: From stochastic control to experiments on a 4 mwh facility. *Applied Energy*, 376:123965, 2024.

[89] Syed Rafayal, Aliaa Alnaggar, and Mucahit Cevik. Optimizing electricity peak shaving through stochastic programming and probabilistic time series forecasting. *Journal of Building Engineering*, 88:109163, 2024.

[90] Silvana Matrone, Andrea Pozzi, Emanuele Ogliari, and Sonia Leva. Deep learning-based predictive control for optimal battery management in microgrids. *IEEE Access*, 2024.

[91] Vincenzo Trovato and Bharath Kantharaj. Energy storage behind-the-meter with renewable generators: Techno-economic value of optimal imbalance management. *International Journal of Electrical Power & Energy Systems*, 118:105813, 2020.

[92] Hong Fan, Qianqian Yuan, and Haozhong Cheng. Multi-objective stochastic optimal operation of a grid-connected microgrid considering an energy storage system. *Applied Sciences*, 8(12):2560, 2018.

[93] Abbas Khosravi, Saeid Nahavandi, Doug Creighton, and Amir F Atiya. Lower upper bound estimation method for construction of neural network-based prediction intervals. *IEEE transactions on neural networks*, 22(3):337–346, 2010.

[94] Qiang Ni, Shengxian Zhuang, Hanming Sheng, Gaoqiang Kang, and Jian Xiao. An ensemble prediction intervals approach for short-term pv power forecasting. *Solar Energy*, 155:1072–1083, 2017.

[95] Pablo Velarde, L Valverde, Jose Maria Maestre, Carlos Ocampo-Martínez, and C Bordons. On the comparison of stochastic model predictive control strategies applied to a hydrogen-based microgrid. *Journal of Power Sources*, 343:161–173, 2017.

[96] R Tyrrell Rockafellar, Stanislav Uryasev, et al. Optimization of conditional value-at-risk. *Journal of risk*, 2:21–42, 2000.

[97] Tingyang Meng, Zongli Lin, Yan Wan, and Yacov A Shamash. State-of-charge balancing for battery energy storage systems in dc microgrids by distributed adaptive power distribution. *IEEE Control Systems Letters*, 6:512–517, 2021.

[98] Faisal Altaf, Lars Johannesson, and Bo Egardt. Simultaneous thermal and state-of-charge balancing of batteries: A review. In *2014 IEEE Vehicle Power and Propulsion Conference (VPPC)*, pages 1–7. IEEE, 2014.

[99] Shuai Ma, Modi Jiang, Peng Tao, Chengyi Song, Jianbo Wu, Jun Wang, Tao Deng, and Wen Shang. Temperature effect and thermal impact in lithium-ion batteries: A review. *Progress in Natural Science: Materials International*, 28(6):653–666, 2018.

[100] Jan Kleiner, Lorenz Lechermann, Lidiya Komsiyska, Gordon Elger, and Christian Endisch. Thermal behavior of intelligent automotive lithium-ion batteries: Operating strategies for adaptive thermal balancing by reconfiguration. *Journal of energy storage*, 40:102686, 2021.

[101] Ricardo de Castro and Rui Esteves Araujo. Model predictive power allocation for hybrid battery balancing systems. In *2019 IEEE Vehicle Power and Propulsion Conference (VPPC)*, pages 1–5. IEEE, 2019.

[102] Qing Xie, Yanzhi Wang, Younghyun Kim, Naehyuck Chang, and Massoud Pedram. Charge allocation for hybrid electrical energy storage systems. In *Proceedings of the seventh IEEE/ACM/IFIP international conference on Hardware/software codesign and system synthesis*, pages 277–284, 2011.

[103] Jin-Young Choi, In-Sun Choi, Geon-Ho Ahn, and Dong-Jun Won. Advanced power sharing method to improve the energy efficiency of multiple battery energy storages system. *IEEE Transactions on Smart Grid*, 9(2):1292–1300, 2016.

[104] Ibrahim Alsaidan, Amin Khodaei, and Wenzhong Gao. A comprehensive battery energy storage optimal sizing model for microgrid applications. *IEEE Transactions on Power Systems*, 33(4):3968–3980, 2017.

[105] Tarek Medalel Masaud and Ehab F El-Saadany. Correlating optimal size, cycle life estimation, and technology selection of batteries: A two-stage approach for microgrid applications. *IEEE Transactions on Sustainable Energy*, 11(3):1257–1267, 2019.

[106] Juan P Fossati, Ainhoa Galarza, Ander Martín-Villate, and Luis Fontan. A method for optimal sizing energy storage systems for microgrids. *Renewable Energy*, 77:539–549, 2015.

[107] Yuqing Yang, Stephen Bremner, Chris Menictas, and Merlinde Kay. Battery energy storage system size determination in renewable energy systems: A review. *Renewable and Sustainable Energy Reviews*, 91:109–125, 2018.

[108] Mina Najafi Ashtiani, Ashkan Toopshekan, Fatemeh Razi Astaraei, Hossein Yousefi, and Akbar Maleki. Techno-economic analysis of a grid-connected pv/battery system using the teaching-learning-based optimization algorithm. *Solar Energy*, 203:69–82, 2020.

[109] Rahmat Khezri, Amin Mahmoudi, and Hirohisa Aki. Optimal planning of solar photovoltaic and battery storage systems for grid-connected residential sector: Review, challenges and new perspectives. *Renewable and Sustainable Energy Reviews*, 153:111763, 2022.

[110] Shaghayegh Bahramirad, Wanda Reder, and Amin Khodaei. Reliability-constrained optimal sizing of energy storage system in a microgrid. *IEEE Transactions on Smart Grid*, 3(4):2056–2062, 2012.

[111] Tay Son Le, Tuan Ngoc Nguyen, Dac-Khuong Bui, and Tuan Duc Ngo. Optimal sizing of renewable energy storage: A techno-economic analysis of hydrogen, battery and hybrid systems considering degradation and seasonal storage. *Applied Energy*, 336:120817, 2023.

[112] Yu Hu, Miguel Armada, and María Jesús Sánchez. Potential utilization of battery energy storage systems (bess) in the major european electricity markets. *Applied Energy*, 322:119512, 2022.

[113] Daniel Arnström, Alberto Bemporad, and Daniel Axehill. A dual active-set solver for embedded quadratic programming using recursive LDL^T updates. *IEEE Transactions on Automatic Control*, 67(8):4362–4369, 2022.

[114] Wesley Cole, A Will Frazier, and Chad Augustine. Cost projections for utility-scale battery storage: 2021 update. Technical report, National Renewable Energy Lab.(NREL), Golden, CO (United States), 2021.

[115] Yang Zhang, Anders Lundblad, Pietro Elia Campana, F Benavente, and Jinyue Yan. Battery sizing and rule-based operation of grid-connected photovoltaic-battery system: A case study in sweden. *Energy conversion and management*, 133:249–263, 2017.

[116] Brantyo Laksahapsoro, Max Bird, Salvador Acha, and Nilay Shah. Optimisation of photovoltaic and battery systems for cost-effective energy solutions in commercial buildings. *Applied Energy*, 392:125907, 2025.